Fall 2016

Addressing the influence of carbon monoxide on the behavior of an HCCI engine

Allen Charles Ernst

Department:

ADDRESSING THE INFLUENCE OF CARBON MONOXIDE ON THE BEHAVIOR OF AN HCCI ENGINE

by

ALLEN CHARLES ERNST

A THESIS

Presented to the Faculty of the Graduate School of the

MISSOURI UNIVERSITY OF SCIENCE AND TECHNOLOGY

In Partial Fulfillment of the Requirements for the Degree

MASTER OF SCIENCE IN MECHANICAL ENGINEERING

2016

Approved by

James A. Drallmeier, Advisor
Kelly O. Homan
Kakkattukuzhy M. Isaac

ABSTRACT

Homogeneous Charge Compression Ignition (HCCI) may be the next leap of improvement to internal combustion engines due to its decreased emissions and improved engine efficiencies. However, such a jump possesses challenges owing to its strict reliance on the inherent physics that dictate start of combustion and limit the reach of stable operation. This work investigates the role and fundamental influence of carbon monoxide on the cycle-to-cycle combustion dynamics present in the region of incomplete combustion that frames the limited HCCI operating region. An improved understanding will open doors to enhanced control methodologies and an expanded stable operating envelope. A constant volume chemical kinetics simulation was developed utilizing an established skeletal PRF mechanism in order to predict product species evolution in an HCCI engine under incomplete combustion conditions. The predicted product species amounts were harnessed to determine internally trapped residual carbon monoxide mass amounts that would be carried to the next engine cycle. These amounts became the basis for an experimental investigation on a single cylinder HCCI engine running on a high octane primary reference fuel. Cyclically resolved, in-cylinder active-specie injections were employed at partial burn operation to explore the effects of carbon monoxide on engine performance and its resultant cyclic dynamics. Observations made through detailed cyclic performance data, return maps, and symbol sequencing analysis help to expose a significant impact of carbon monoxide on HCCI combustion development and the potential it may possess to drive HCCI combustion as a future dynamic control mechanism.

ACKNOWLEDGMENTS

First, I would like to express my sincere gratitude to my advisor, Dr. James Drallmeier, for his patient supervision and valuable guidance during this long road to completion. He provided me the opportunity to pursue this research initially, and despite the unconventional journey, he never faltered in his support of me achieving my goal of completion. Additionally, I would like to thank my other committee members, Dr. Kelly Homan and Dr. Kakkattukuzhy Isaac, for their time, guidance, and kind support.

Thanks are also due to Dr. Charlie Westbrook for taking time out of his busy schedule to assist a simple graduate student in model verification. Furthermore, I owe a note of appreciation to the aid and companionship of my fellow graduate students in the lab. Cory Huck, Aaron Attebery, Avinash Singh, Krishawn Ridenhour, Zahra Sadeghizadeh, and Mahdi Ghareh Baygloo, among others, added a daily dose of witty banter, good conversation, and sharp minds for collaboration. Along with these, I am indebted to Jim Hoff for aid in troubleshooting his RGI masterpiece.

Additionally, I would like to thank my parents and family for their encouragement in all things to this point in life. I owe a great deal of thanks especially to those family and friends who have supported my efforts in these final months by helping me to dedicate the necessary time to finishing this work.

And finally, I would like to recognize the foundation of my support, my wife, Rebecca. Words cannot express the amount of backing that she has provided throughout my completion of this degree. I honestly could not have wrapped up this final effort without her unconditional Love. Thank you.

TABLE OF CONTENTS

Page

LIST OF ILLUSTRATIONS

Figure Page

LIST OF TABLES

NOMENCLATURE

Symbol	Description
HCCI	Homogeneous Charge Compression Ignition
NVH	Noise, Vibration, and Harshness
PRR	Pressure Rise Rate
uHC	Unburned Hydrocarbons
CO	Carbon Monoxide
EGR	Exhaust Gas Residuals
SOC	Start of Combustion
CA10	Crank angle at 10% heat release
CA50	Crank angle at 50% heat release
RGI	Residual Gas Injector
OF	Overlap Factor
OI	Octane Index
ON	Octane Number
PRF	Primary Reference Fuel
TDC	Top Dead Center
BDC	Bottom Dead Center
ATDC	After Top Dead Center
BTDC	Before Top Dead Center
EVO	Exhaust Valve Open
EVC	Exhaust Valve Close
IVO	Intake Valve Open
IVC	Intake Valve Close
CAD	Crank Angle Degrees
COV	Coefficient of Variation
IMEP	Indicated Mean Effective Pressure
LHV	Lower Heating Value

1. INTRODUCTION

Homogeneous Charge Compression Ignition (HCCI) engines present a single approach to addressing several of the problems plaguing internal combustion engines today. HCCI engine operation is a low temperature combustion (LTC) mode that, when successfully executed, results in a system with relatively high efficiencies and low emissions in regards to nitrogen oxides (NOx) and particulate matter (PM) formation [1]. These qualities make HCCI an attractive alternative to currently marketed IC engines, especially when considering the increasingly stricter regulation of engine fuel efficiency and emissions in the automotive industry. HCCI is accomplished by inducting a premixed, homogeneous charge into the engine cylinder and compressing this mixture until it auto-ignites. Such an auto-ignition combustion method causes the energy release event to happen quite quickly and often under near volumetric conditions, resulting in less time for energy to dissipate through heat transfer and, therefore, a more thermally efficient process. However, as potentially beneficial as HCCI may be, it is not without its challenges and shortcomings.

One of the key obstacles of HCCI is based in the fact that, unlike traditional spark and compression ignition (diesel) engines, HCCI lacks a combustion triggering mechanism to initiate combustion and control phasing, resulting in difficulty controlling engine operation. Instead, HCCI relies on the chemical kinetics of the initial mixture to auto-ignite as the inducted charge is compressed within the cylinder [1]. This auto-ignition combustion phasing is dictated by the boundary conditions and initial conditions

of the air/fuel charge, such as charge temperature, dilution, and chemical composition, at intake valve close (IVC) [2].

Another inherent difficulty associated with this mode of combustion is its limited operating range [1]. Within the stable range of the HCCI operating regime, complete combustion is typical and results in consistent, ideal engine performance. However, on the outskirts of this region, the engine begins to encroach on undesirable operating set-points. The operating envelope of an HCCI engine is illustrated in Figure 1.1 below.

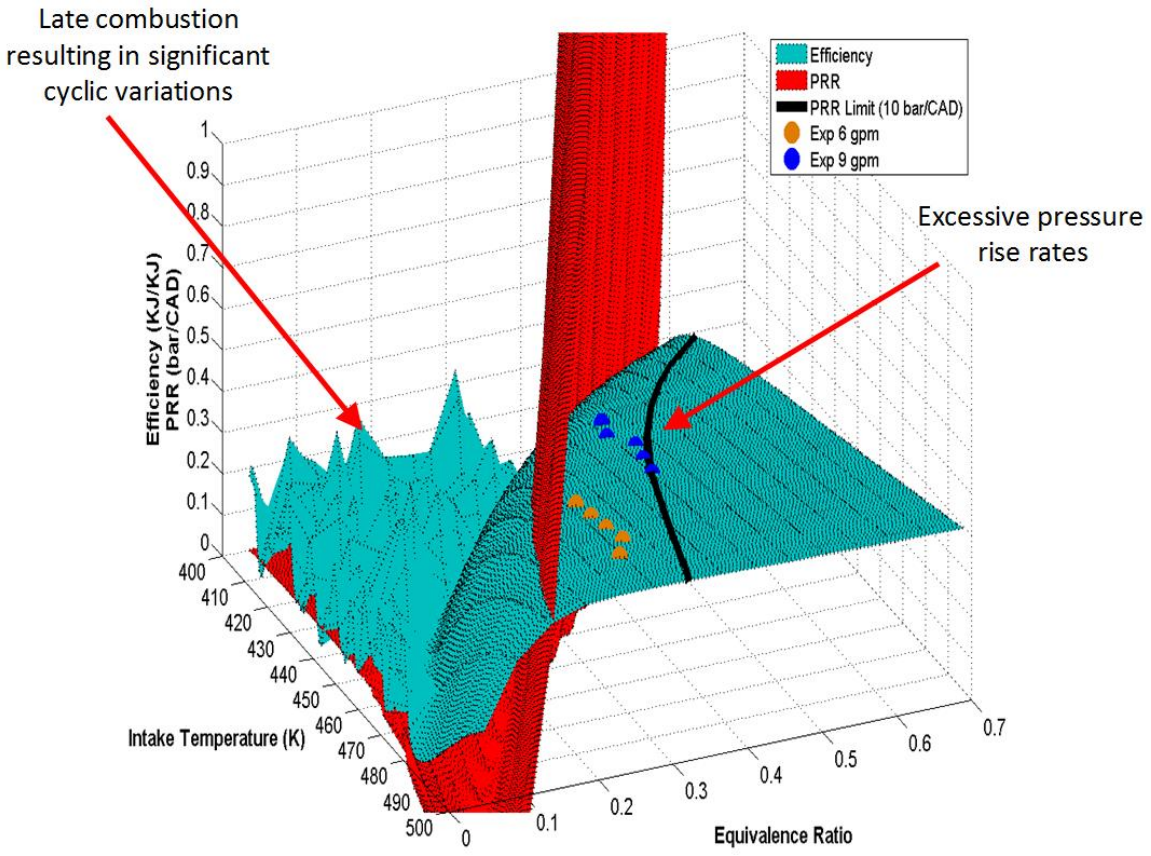

Figure 1.1. Waterfall Plot: HCCI operating regime.

The stable operating range of an HCCI engine is represented in Figure 1.1 as the plateau region on the plot of efficiency vs. intake temperature vs. equivalence ratio. This stable engine operation becomes limited at the most advanced combustion phasing by excessive pressure rise rates (PRR) that contribute to high levels of noise vibration and harshness (NVH), which can be damaging to the engine structure. A PRR of 10 bar/CAD, a typically assumed upper limit for PRR, is projected onto the operating efficiency map of Figure 1.1 to depict the engine's upper range of operation. Conversely, HCCI is limited on the edge of the plateau of stable operation, at its most retarded combustion phasing, by the presence of cycle-to-cycle combustion instability and large cyclic variations in engine performance. These variations present themselves in the form of the 'waterfall' drop-off in efficiencies on Figure 1.1 followed by a zone of highly erratic efficiencies. At these set-points, incomplete combustion and misfires exist, feeding instability, decreasing efficiency, and increasing carbon monoxide (CO) and unburned hydrocarbon (uHC) emissions [1]. This unstable operation has been shown to be governed by deterministic tendencies from one cycle to the next. Additionally, the lack of a combustion actuator means that control becomes extremely difficult when trying to navigate the regions at the edge of the operational envelope.

At partial burn operation, incomplete combustion leads to the increased production of chemical species that are not seen in significant amounts during complete combustion conditions, such as CO and uHC. These specie's concentrations may be playing a key role in the cyclic dynamics exhibited during partial burn. Exhaust gas residuals (EGR) that are carried from one engine cycle to the next have been linked to

impacting next cycle combustion during incomplete burn through the presence of deterministic behavior in HCCI operation [3]. These residuals consist of the heated exhaust products of previous combustion events and mix with the newly inducted air/fuel charge to impact the start of combustion (SOC) and rate of heat release (RHR) of the next combustion event.

In order to successfully apply HCCI technology to commercial utilization, it is most feasible to couple it with another mode of engine operation as a means of extending the engine's reach to the unattainable zones of pure HCCI. However, when doing this, transition between engine modes, which occurs in or near the partial burn regime, becomes an issue due to a lack of robust control methods. One potential method of controlling LTC within these regimes involves the introduction of synthesis gas, syn-gas (comprised primarily of H_2, CO, and N_2), produced on-board from the primary fuel, to the combustion process. The addition of these chemically active reformate gases to engine combustion has been shown on a cycle average basis to be able to alter combustion development [4-9]. In fact, evidence indicates that combustion phasing can be either advanced or retarded depending on the initial gas temperatures, but these effects remain unexplored in the partial burn regime.

In general, a more detailed understanding of the feed-forward mechanism of HCCI is necessary before additional progress can truly be made. This is especially true for engine operation around the partial burn regime, which still remains relatively unexplored. An increased understanding of the HCCI combustion process could be

utilized in order to develop more robust control schemes for HCCI operation, to navigate the partial burn zone, and to better comprehend the effects of syn-gas addition.

Due to the possible presence of CO in exhaust gas during partial combustion, and its presence in partially reformed hydrocarbon syn-gas, it is one of the key species under investigation in the current study. Prior research has shown that CO is a probable species in incomplete combustion and, furthermore, it has been demonstrated that CO may possess the potential to impact SOC and heat release characteristics under HCCI conditions [4-10]. The work at hand will focus on coupling the presence of this chemical species, and others, during incomplete combustion to being a kinetic variable in next cycle combustion evolution, through internally trapped residual gases. Chemical kinetic simulations are to be used under constant volume conditions and will emulate incomplete combustion as a means of predicting the likely species concentrations after a partial burn combustion event. Internally trapped residuals and engine geometry will then determine the feed-forward amounts of these species that could mix with the next cycle charge. Next, a set of cyclically resolved experimental tests, based carefully on the results of the chemical kinetics simulations, will be run in order to explore the sensitivity of HCCI combustion performance to the presence of these chemical species. Through this, the cycle-to-cycle dynamics in HCCI combustion will be linked to product species carryover through internally trapped residuals. This will present an insight into the variables impacting next cycle combustion within the partial burn regime of HCCI operation and

will give a better understanding to the effects that syn-gas addition can have as a means of HCCI control. In the end, the knowledge gained can be utilized to develop more robust control schemes that may lift HCCI to becoming the future standard in IC engines.

2. REVIEW OF THE LITERATURE

Understanding the deterministic behavior that becomes magnified during partial burn operation is a crucial step to the utilization of HCCI as a robust mode of engine operation. The combustion event that occurs within an HCCI engine is directly dependent upon the temperature, dilution, and chemical makeup of the cylinder mixture at IVC. This mixture is partially composed of the internally trapped residuals that are carried from the completion of one engine cycle to the start of the next and includes the thermal, chemical, and dilutive properties of that trapped EGR. Therefore, it is necessary to understand how each aspect of the trapped EGR impacts next cycle combustion.

The cycle-to-cycle coupling that forms the foundation for this research has been the focal point of multiple investigators. Through the use of a dual-mode SI-HCCI engine, Wagner et al. performed an experimental investigation in an effort to demonstrate the existence of deterministic behavior that can be exploited for the development of improved control algorithms which may expand the stable HCCI operational range [3]. In this study, statistical methods were employed to analyze the engine performance through the full range of engine mode transitions and dual mode operation. The result was that in the multi-mode engine, the cycle-to-cycle dynamics in the mode-transition zone, which coincides with the partial burn zone, were dominated by nonlinear, nonrandom processes which may be the result of nonlinear residual feedback from successive combustion reactions. Bifurcation diagrams, heat release return maps, symbol statistics, and temporal heat release data were all employed and

support the premise of non-random oscillations occurring in heat release output. This deterministic behavior, which is present to some degree at all engine operating points, experiences a nonlinear amplification as the engine crosses from stable operation into a partial-burn state. During SI-HCCI mode transition, engine behavior shifts from a stochastic condition at pure SI behavior, to noticeably deterministic patterns in the transition to HCCI, which occurs in a regime characteristic of partial burn. As the engine mode continues to progress toward a stable, fully HCCI operating point, the engine again becomes dominated by its stochastic tendencies. Additionally, Wagner et al. indicated that the forward and reverse transition between the two operating modes may follow different paths through the partial burn zone, testifying to the highly complex nature of these dynamics [3].

In exploratory efforts of the cycle-to-cycle variations that occur in a multi-mode engine, Chen et al. noted that dynamics present themselves in significantly different degrees of severity from one engine parameter to the next, such as the variation in IMEP vs in cylinder peak pressures [11]. These investigators attempted to characterize the engine dynamics based on pressure rise rate and heat release behavior of multi-mode engine guided by variable valve actuation. They noted the vast difference in the severity of cyclic variations that characterize the two engine modes, even at the transition between them. Along the same lines, other researchers have recently investigated the development of robust control methods in order to reduce these large cyclic variations in combustion [12]. Specifically, they also addressed these cyclic variations through the use of variable valve timing. Through these efforts, it has been

shown that in controlling exhaust valve timing, the cyclic variations can be significantly reduced in combustion, resulting in an expanded engine operating regime.

The works of others, including Shahakhti and Koch, supports the observation that there are non-random, deterministic oscillations in engine heat release behavior during the intermediate conditions between the stable SI and HCCI operating regimes [13]. These investigators observed normal cyclic variations, periodic cyclic variations, and weak/misfired cyclic variations. The distinct patterns go to show that HCCI cyclic dynamics are not always a random phenomenon.

Nonrandom cyclic variability has been further revealed to depend on the feed forward mechanisms of multiple engine cycles. One group of investigators documented such behavior in an HCCI engine when identifying the symbol-sequence statistical probabilities of data points at the same operating condition. It was found that as the Air/Fuel ratio decreases, the determinism in ignition timing increases [14]. Through this work, it was revealed that the signature of the engine, that is the history of previous engine cycles, lasts for a minimum of three cycles. Therefore, the output of any given engine cycle is a function of the resultant variables of at least the previous three engine cycles.

Recent work at Missouri S&T has been performed regarding the feed-forward mechanisms associated with cyclic dynamics in the partial burn regime. Through experimental investigations of HCCI operation within the partial burn regime, Attebery [15] has demonstrated a lack of dependency of next-cycle SOC on the previous cycle exhaust gas temperature. By using a fast response thermocouple near the exhaust

valve, the investigator was able to closely track the temperature profile of the exhaust gases after EVO under various partial burn conditions. While slight determinism appeared to be present in SOC with regards to previous cycle exhaust temperatures, it seemed to be quite limited, and, therefore, not sufficient enough to explain the strong cyclic coupling that is seen when combustion phasing is severely retarded during HCCI operation. This work supported efforts by Daw et al. in their investigation of spark assisted HCCI operating characteristics [16]. It was determined that variations in exhaust temperature tend to be slower and have less of an immediate impact on a cycle-to-cycle basis than variations in residual gases. Both of these investigations support the idea that another variable, such as chemical kinetics, is a more prominent factor impacting next cycle SOC and RHR.

When reviewing literature, it appears that many have explored the use of EGR as a method of extending the operating limits of HCCI, however, very few of these look into the specific chemical impact resulting from the individual residual species. Typically, investigators will generalize EGR as a composition of N_2, H_2O, and CO_2, the ideal products of combustion. This, however, does not address the region of partial burn combustion in question since EGR during incomplete combustion can consist of a significantly different chemical composition. Additionally, most researchers do not delve fully into the partial burn regime when looking at cycle-to-cycle effects. Instead, they tend to stay in areas of stable operation. As a result, this work will attempt to gain a clearer understanding into these phenomena by looking at the chemical kinetic impact of internally trapped residuals on combustion at the partial burn limit. The first step in

this process involves understanding the possible species present during incomplete combustion at partial burn conditions in HCCI and then looking into whether these species possess the ability to kinetically impact HCCI combustion. A review of previous literature around these conditions follows.

2.1. SPECIES PRODUCTION UNDER PARTIAL COMBUSTION

As it has been shown that temperature of exhaust gases may not be a primary variable impacting next-cycle combustion characteristics during incomplete combustion, the chemical kinetics due to the presence of critical species may prove to be this key factor. Since product species concentrations exist in quantities different than what is seen during complete and near complete combustion, it is possible that these residual compositions are playing a major role in the cyclic dynamics. Under stoichiometric conditions, ideal combustion of a hydrocarbon fuel with air will result primarily in the products of CO_2, H_2O, and N_2 [17]. However, as the mixture is taken to a lean state and incomplete combustion is introduced, additional species begin to present themselves in notable concentrations within the products. Dissociation of the major species will occur and various reactions among the dissociation products will lead to production of different species. Typical equilibrium assumptions for combustion may not be applicable to partial burn conditions, considering that, since combustion is not yet fully complete, species may not exist in perfect chemical equilibrium. Therefore, equilibrium predictions may be an inaccurate representation of incomplete combustion species evolution. Before fully understanding the chemical kinetics that impact next cycle

combustion in HCCI partial burn, it is first essential to understand the critical species that can be produced when operating in the partial burn regime.

As incomplete combustion occurs, it is only natural to realize that a portion of the fuel remains unburned, or more likely, only partially oxidized. Therefore, uHC's begin to come into play as a product of incomplete combustion. More specifically, it has been demonstrated that uHC levels increase linearly with later ignition timing [18]. Therefore, since the partial burn regime is associated with late combustion, uHC levels increase as the engine falls toward later, less complete combustion.

While NOx is typically not a considered a product of HCCI operation, there have been multiple investigators that have shown both experimentally and through the use of detailed kinetic simulations that there is a presence of these species in very small quantities during standard HCCI operation [18,19]. These are typically more prominent at higher equivalence ratios during complete combustion. This results from the idea that, as more fuel is introduced into the cylinder, the peak cylinder temperatures during combustion begin to climb, and, since NOx requires high temperatures to form, it naturally begins to present itself in larger quantities. However, when considering that partial burn generally has lower peak combustion temperatures, NOx is not expected to be generated in large amounts when operating near these instability limits.

One species of particular interest in this study is carbon monoxide (CO). CO is well known to exist in significant quantities during incomplete hydrocarbon combustion in rich mixtures, where insignificant amounts of oxidizer react with the fuel. This differs from the incomplete combustion seen in SI in the fact that HCCI operates under

extremely lean conditions. As a result, the concentration amount of CO in the products is a greater question under these circumstances than when considering rich incomplete combustion conditions.

In a study by Sjöberg et al. [20] it was shown both experimentally and through modeling that there exists a rapid rise in CO emissions as engine operation dropped beneath a certain fueling rate. They demonstrated that CO oxidation is dominated by the reaction CO+OH => CO_2+H, and that since OH levels fall quickly with decreasing combustion temperature, there eventually becomes a point where the OH amounts are insufficient to oxidize the remaining CO. Specifically, the CO oxidation does not go to completion when peak temperatures remain under 1500K due to the lack of OH present and, as a result, is seen as a prevalent exhaust species under these circumstances. CO concentrations began to drastically increase around equivalence ratios of 0.3, until they peaked to amounts of greater than 60% of supplied fuel carbon ending up as carbon monoxide. They demonstrated the commonality of CO production during incomplete combustion at lean operation over a wide range of n-heptane/isooctane fuel mixtures. This resulted from lower peak temperatures that do not reach the temperatures necessary to fully oxidize all of the CO and HC in the vicinity. Therefore, at low load conditions, the presence of CO and uHC's begins to result from the incomplete bulk-gas reactions. Another source of the CO production originates from the crevices and boundary layer, where a high surface-to-volume ratio and heat loss to the boundaries stop combustion early [3]. These crevice effects were explored in detail through a multi-zone KIVA3V code.

Similarly, on a route of controlling HCCI through changing the inlet temperature, Bhave et al. [19] have demonstrated that the inlet temperature to the engine strongly influences the emissions of CO and uHC. The investigators show that increasing intake temperatures advance combustion, therefore increasing peak temperatures and reducing CO and uHC emissions. Furthermore, this work compliments the work discussed above in confirming that the increased in-cylinder temperatures increase the NOx production as well.

Additional experimental work has shown that CO emissions gradually decrease with an increasing equivalence ratio and when increasing the cetane number of the fuel [18]. These findings also demonstrate that CO emission from a high cetane number fuel is significantly lower than that of a high octane number fuel. Also, the uHC trend seems to follow that of the CO production.

Apart from the key species mentioned, it is expected that the incomplete combustion present in the partial burn regime produces many additional trace species that are relatively unimportant. Also, as with any lean combustion, CO_2, N_2, and O_2 should be large products of partial combustion. However, these are seen to only be dilatants and modifiers of the charge air/fuel ratio, as opposed to chemically active species. So, the question at this point is whether the species likely to be present are capable of impacting SOC and RHR when in an initial HCCI charge mixture and, more specifically, how they might impact the combustion.

2.2. SPECIES' IMPACTS ON HCCI

Of the species produced during incomplete combustion events, those that possess the ability to impact next cycle combustion kinetics can be labeled as critical species and are the focus of this investigation. Not only is an investigation into the impact of these species pertinent to cyclic dynamics, but it is also beneficial to understand these effects as a potential method of intentionally introducing individual species to help control the combustion event. One such method involves generation of chemically active gas species through "on-board" partial reforming of primary hydrocarbon fuels. Several fuel reforming techniques exist through which this synthesis gas (syn-gas) can be produced with varying $CO/H_2/N_2$ compositions, along with additional trace species, that are dependent on both the hydrocarbon fuel being reformed and the technique used [21-23]. The addition of these reformate gases to engine combustion has been shown to impact engine performance and have the potential for use in influencing and stabilizing combustion. As a result, several investigators have looked into the impact that the species of CO and H_2, the two primary species in syn-gas, have on HCCI combustion.

There is supporting evidence that several chemically active species, which are typical byproducts of combustion, can potentially have a kinetic impact on the combustion of a hydrocarbon fuel. One such species, H_2O, a primary component resulting from combustion, has been shown by some to be able to chemically affect ignition delay in HCCI [24]. In this study, the authors discussed the effects of adding small amounts of H_2O and CO_2 on the auto-ignition delay in a rapid compression

machine fueled with iso-octane. They noticed that the presence of water tended to systematically decrease the ignition delay by a small amount, but CO_2 was not found to have any effect. In the study, they went so far as to separate the physical effect of the species, having large heat capacity, from the chemical effects before drawing conclusions. The same trend of ignition delay decreasing with increasing amount of added H_2O was also observed by Curran et al. [25].

Another less prevalent product that displays a possible ability to impact next cycle combustion lies in nitrous oxide (NO). Work performed by Dubreuil et al. [26,27] involved the addition of NO upstream of the inlet to an HCCI engine and was backed by the simulations of a zero-dimensional variable volume, single zone reactor model with a detailed chemical kinetic scheme for n-heptane/toluene blends. During the experimental investigation, they saw an impact of decreasing ignition delays as NO amounts increased up to 100 ppm. It should be noted that, while NO has been shown to impact SOC, it is not a likely candidate for species that significantly alters next cycle combustion during partial burn due to the unlikelihood of its presence in significant amounts after an incomplete combustion event. Specifically, under typical HCCI operation, NOx levels tend to be less than 10 ppm over a large operating range, although they do increase to slightly higher levels as equivalence ratios, and therefore peak temperatures, increase [18].

Some research has been conducted investigating the effect of CO addition on the HCCI combustion event in quantities similar to what is present in steady operating condition EGR with several primary fuel blends [26]. However, since they are

investigating from an EGR standpoint, the quantities introduced are only a fraction of what might be expected from a reformed gas, or even in EGR from engines operating in the partial burn regime, with a maximum amount introduced of 2000 ppm [26]. These low concentrations of CO showed little to no effect on the combustion characteristics examined, but the investigators do note the accelerating potential of CO.

Several numerical and experimental investigations have been performed on the effect of the addition of CO and various mixtures of it with H_2 that correspond to producible syn-gas mixture concentrations in HCCI combustion. Replacing a portion of the total intake fuel energy during HCCI with an equal amount of reformed gas energy has been shown to impact diesel-type fuel combustion. In this manner, enrichment with pure H_2 tends to have a stronger retarding effect on combustion than CO enrichment during syn-gas addition of a CO/H_2 mixture [4,5]. However, as calculated by the detailed simulations of Subramanian et al. [6,7], CO has potential to retard combustion at low initial temperatures (600K) and advance combustion at higher initial temperatures (1000K). These simulations were performed at a constant pressure basis with multiple detailed kinetic mechanisms for n-heptane/air mixtures. This potential of CO to have a nonlinear effect on SOC causes it to be a species of key interest as both a syn-gas component and a residual product.

One group of investigators observed that the impact of the reformed gas on combustion phasing depends on the primary fuel's octane number and that the addition of syn-gas mixtures tends to retard SOC when running low octane fuels, but that the impact on high octane fuel is rather dependent on inlet charge temperature [4,5,8]. The

same investigators demonstrated both experimentally and through numerical simulation that the two extreme cases of syn-gas compositions effectively retard SOC over a wide range of conditions, implying that any currently known method of producing on-board syn-gas would result in a H_2/CO ratio that would have a similar impact on combustion. The inhibiting effect of syn-gas addition on low octane fuels, at low temperatures, is believed to be the result of initial consumption of active OH radicals in the presence of syn-gas being replaced by less active HO_2 radicals [6,7,9]. At high temperatures, it is thought that the addition of CO increases the net production of OH radicals, accelerating the reactivity of the mixture [6].

Eng et al. have experimentally investigated the effects of the addition of syn-gas from a partial oxidation reformer (POx) to primary fuels of n-heptane and isooctane both with and without EGR [10]. The results show that POx addition to n-heptane retards peak pressure location and impacts RHR. The initial low temperature energy release that is characteristic of n-heptane and other two-stage fuels is inhibited by POx addition, while the peak RHR of the larger, high temperature release is enhanced by the addition. This agrees with the work performed by Hosseini et al. [5]. Conversely, when added to isooctane, it appeared that the peak pressure location and the peak in RHR were advanced due to the POx gas in the presence of large amounts of EGR. However, the large quantities of EGR present during combustion introduces a thermal effect into this investigation that may dominate the mixture, resulting in the conflict between this and the results described by other researchers [4,5]. Therefore, it is difficult to draw

detailed conclusions about the kinetic impact that the syn-gas species themselves contribute.

It is important to note, syn-gas addition to date seems to be on a cycle averaged basis, with reformate introduced upstream from the intake valve. Researchers have acknowledged the potential use of syn-gas addition as a cyclic control mechanism, but have not truly investigated the effect that the gas addition has on the effects driving the engine dynamics. While the work to date leads to a broader understanding of the syn-gas impact on HCCI operation, it does not provide the cycle-resolved details of the stochastic-deterministic effects that are necessary to understand the correlation of multiple engine cycles and eventually lead to the successfully implementation of cycle-to-cycle control methodologies.

It should be noted that some investigators have also delved into other engine modes that resemble HCCI with syn-gas injection. One such alternative mode is Reactivity Controlled Combustion Ignition (RCCI). RCCI is characterized by the injection of two separate fuels with substantially different ignition characteristics to achieve desired combustion characteristics on a cycle-to-cycle basis. This is similar to the proposed syn-gas influenced HCCI in that they are both LTC modes that rely on the physics of the charge in a compression initiated combustion event and both utilize the differences of combustion properties of two chemically active ‘fuels’. This differs from a syn-gas influenced HCCI engine in that the necessary reactants for syn-gas are still capable of being generated from a single hydrocarbon fuel, which is much more realistic

when considering a real-world application of only having to fill a single tank with one fuel at the pump.

To summarize, while a significant amount of research has been conducted in regard to utilizing generic EGR mixtures to impact combustion over many, often hundreds, of engine cycles, little has been done to investigate the specific chemical composition of the residuals under incomplete combustion and their impact on combustion on an individual cycle basis. Work to date lacks a thorough investigation of the cycle-to-cycle impact of chemical kinetics imparted by the feed-forward critical residual species in the partial burn regime of HCCI operation. Prior work has shown that, apart from the typical products seen in complete combustion, NO, uHC, and CO are species that can be regularly produced during HCCI incomplete combustion. Taking this a step further, several of these display potential to kinetically impact HCCI combustion. On top of this, syn-gas, composed primarily of CO, H_2, and N_2, is one potential method for HCCI control, that is, if the true impact of the CO/H_2 mixture on an HCCI combustion event can be determined. With little investigation into the effects that these species have during HCCI partial burn operation though, it is difficult to make conclusions as to their true impact up to this point. Therefore, this work will address the production, cycle carryover, and next cycle impact of critical species in and around the partial burn regime.

3. EXPERIMENTAL SETUP

An experimental investigation was performed for insight into the actual impact of species carryover on next cycle SOC and heat release during HCCI operation. The experimental data was collected in the Engine and Spray Dynamics Laboratory at Missouri S&T. Here, engine performance and combustion analysis was performed on the experimental HCCI engine setup described. A brief description of the equipment utilized and its capabilities is discussed below.

3.1. EXPERIMENTAL HCCI ENGINE SYSTEM SETUP

3.1.1. Engine Setup and Control. The experimental setup was based around a small, single cylinder, air cooled engine. Specifically, the engine was a Hatz 1D50Z diesel engine modified to operate in HCCI mode with a compression ratio of 14.5. The original engine setup was modeled after that used by Oak Ridge National Laboratory (ORNL). Engine specifications are depicted in Table 3.1.

Table 3.1. Modified Hatz engine specifications.

Number of Cylinders	1
Number of Strokes	4
Bore (mm)	97
Stroke (mm)	70
Compression Ratio	14.5
Displacement Volume (L)	0.517
Clearance Volume (L)	0.038
Intake Valve Opening* (ATDC)	345
Intake Valve Close* (BTDC)	133
Exhaust Valve Open* (ATDC)	116
Exhaust Valve Close* (BTDC)	342
Intake/Exhaust Valve Overlap (CAD)	33

**Valve events referenced in CAD at TDC of the power stroke and defined at the point of 0.15 mm lift*

The simplicity of a single cylinder engine was advantageous in the investigation of such cyclically resolved experiments because it eliminates the impact of additional variables present in multi-cylinder engines. The overall engine setup may be seen in Figure 3.1.

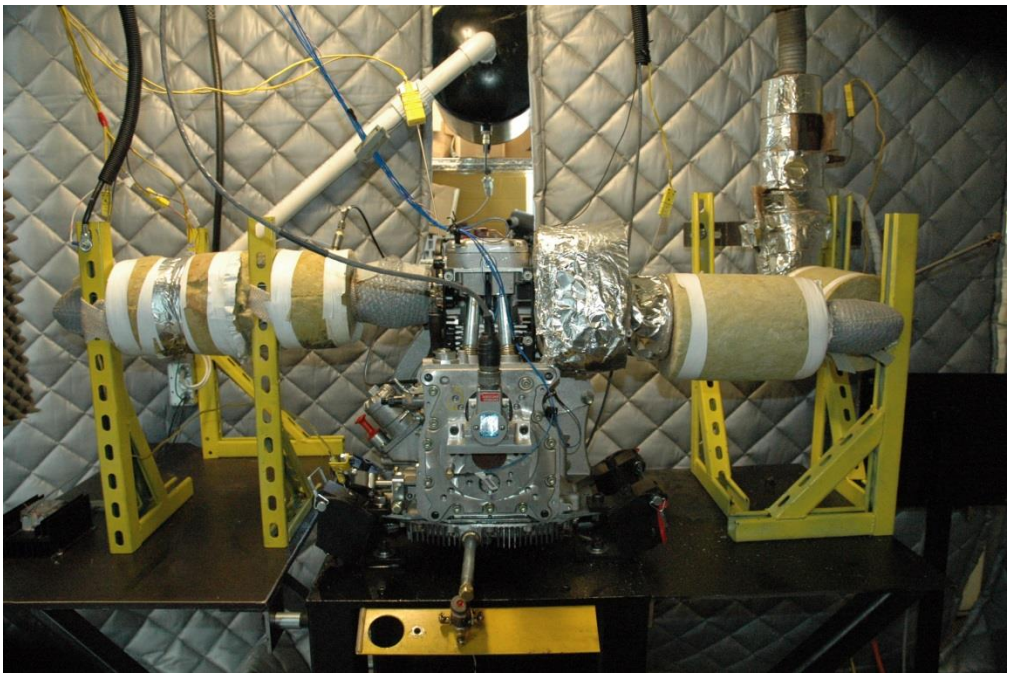

Figure 3.1. Modified Hatz 1D50Z HCCI experimental setup.

The output shaft of the engine is connected to a 30 HP Baldor absorbing/motoring electric dynamometer. This setup allows the dynamometer to either motor the engine or to act as a load on the engine, all while maintaining a constant, specified speed. Crank output feedback is monitored by a BEI Optical Shaft

Encoder with 0.2 degree crank angle resolution and a Lebow 1604 series torque transducer.

Since HCCI operation inherently lacks a precise control mechanism, such as a spark plug or fuel injector in traditional engine setups, the initial and boundary conditions become the crucial elements that dictate combustion phasing and overall engine behavior. Primary control variables for attaining various operating points are, therefore, the intake air temperature, engine speed, and fuel flow rate. As such, inlet air temperature plays a large role in the combustion phasing, and for control of this parameter, a 6 kW process air heater controlled by a process controller was utilized on the Hatz experimental setup.

The preheated air is mixed with vaporized fuel upstream from the cylinder in order to attain a homogeneous fuel/air mixture. The fuel delivery system sets the load point during engine operation through fueling rate and is composed of an in-house constructed fuel atomizer. This system consists of a low flow FMI metering pump that is used to precisely control the fuel fed into the atomizer and onto a cartridge heater. The heating element is powered by a variable transformer that allows a constant low-level voltage to be applied to the cartridge heater as a means to eliminate fluctuations in the heater temperature. The cartridge heater is set to a temperature above the boiling point but below the auto-ignition temperature of the fuel. In this manner the constant fuel flow that enters the atomizer drips onto the cartridge heater and is vaporized, but not ignited. The vaporized fuel is then fed into the intake air stream by a small air flow of approximately 5.5 liter per minute that pushes through the atomizer. Fuel flow rate

is calibrated on an individual fuel basis and verified with a rotameter during engine operation. Additional description of the experimental engine setup may be found in [15].

3.1.2. Measurement Instrumentation and Data Acquisition. In-cylinder pressure measurements were monitored using a Kistler 6045A pressure transducer that requires the use of a charge amplifier. A Kistler Dual Mode Amp Type 5010 amplifier set to 10 MU(bar)/Volt was recruited for such purpose. This pressure transducer was mounted flush with the inner surface of the engine cylinder head in order to not intrude on the cylinder volume or create hot spots along the chamber boundary.

Intake air flow was measured using the Merriam laminar flow element coupled to GE Druck and Omega pressure transducers. Experimental fuel to air ratio (F/A) can then be calculated using the measured intake air flow along with the known fuel flow rate. Apart from these parameters, the engine is outfitted with additional thermocouples and pressure transducers as a means to monitor supplementary engine parameters during operation.

Data acquisition was executed using a multiple rate/resolution data acquisition (DAQ) system that is capable of simultaneously capturing crank angle resolved and temporally resolved data with DAQ rates up to 200 kHz. LabVIEW was chosen as the interface to monitor and acquire engine data. A combustion diagnostic code has been developed in LabVIEW to provide real-time monitoring of combustion behavior for assessing data integrity during engine operation.

3.1.3. Residual Gas Injector. A Residual Gas Injector (RGI) was developed as an instrument for investigating the isolated impact of various gaseous species through the use of cyclically resolved, in-cylinder injection events during the engine intake stroke. The current work investigates the use of this device to inject carefully calculated mass amounts, based on CHEMKIN simulation results, of product species during partial burn engine behavior.

The RGI device consists of a single-coil solenoid valve, manufactured by Lee Company, attached to an injector body constructed of high grade steel. The geometry of the injector body was based closely on the dimensions of the original fuel injector for the Hatz 1D50Z. Therefore, since the fuel injector is not being utilized during HCCI operation, the RGI is capable of being added to the engine setup without modifying engine cylinder geometry but instead by simply replacing the fuel injector with the RGI. The constructed Residual Gas Injector may be seen in Figure 3.2.

Figure 3.2. Residual gas injector used for in-cylinder species addition.

This gas injection setup was calibrated according to the procedure described in [15]. Under normal use, combustion residue tends to build up in the small passages of the RGI, requiring cleaning with isopropyl alcohol and post-cleaning lubrication with WD-40. As a result, recalibration of the device is occasionally necessary in order to verify gas flow after cleaning the device. The most recent calibration data for the device may be found in Appendix A.

The Residual Gas Injector is operated on a separate system from the rest of the engine instrumentation. It is operated in a manner similar to that of a fuel injector using a Drivven Port Fuel Injector (PFI) Driver Module Kit. A LabVIEW FPGA VI was developed to control each driver channel on the PFI support card. Each channel is individually controlled for timing and duration and can be operated in real time.

The system was set up with an NI-cRIO 9022 Real Time Controller as the base chassis for communicating with the LabVIEW operating program. Equipping the cRIO chassis with NI-9411 and ESTTL cards allowed for engine position tracking. The engine pressure was monitored as an analog input using a NI-9215 card. This RGI operating system is outlined in Figure 3.3.

The RGI system described was run in parallel with the Hatz data collection system in order to allow for perturbations of critical gas species to be quickly added directly into the engine cylinder prior to intake valve close (IVC).

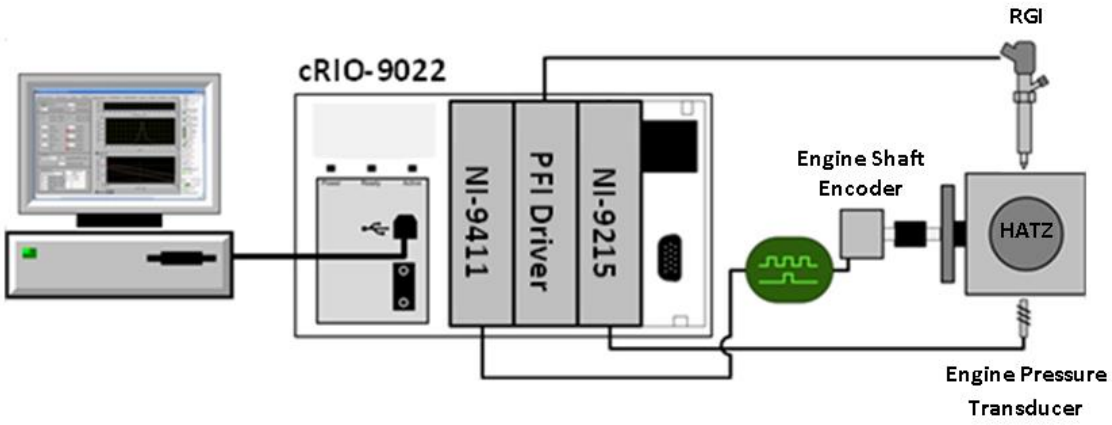

Figure 3.3. RGI operating system diagram.

3.2. ENGINE PERFORMANCE PARAMETERS AND ANALYSIS

The Hatz experimental engine data is characterized by a multitude of performance parameters resulting from the data collected during tests. These parameters are calculated in order to quantify engine behavior for impartial comparisons. Multiple key engine analysis techniques rely on the use of a zero-dimensional, single zone heat release analysis computed from the measured cylinder pressure data, cylinder volume, and their derivatives. This section will address the variables that make up the heat release calculation, along with other engine performance metrics. Additional details surrounding the process of the heat release computation are discussed in Section 4.1.3.

3.2.1. Cylinder Volume. Instantaneous cylinder volume, $\mathbf{V_\theta}$, is essential for the combustion heat release calculation. Using knowledge of the crank angle degree, along with Heywood's position equations [28], the engine volume at any instantaneous crank position is defined as Equation 1:

$$V_\theta = V_c + \frac{\pi B^2}{4}(l + a - s) \tag{1}$$

where V_c represents the clearance volume in cylinder, B is the engine bore, l is the connecting rod length, a is the crankshaft radius, and s is the distance between the crankshaft axis and piston pin axis. The s value in Equation 1 continuously changes based on the instantaneous crank angle θ at any moment during engine operation, and is described by the geometric relationship of Equation 2.

$$s = a\cos\theta + \sqrt{(l^2 - a^2\sin^2\theta)} \tag{2}$$

The cylinder volume derivative with respect to crank angle, $\frac{dV_\theta}{d\theta}$, is found by differentiating Equation 2 with respect to crank angle to produce Equation 3.

$$\frac{dV_\theta}{d\theta} = \frac{\mathrm{d}}{d\theta}\left[V_c + \frac{\pi B^2}{4}(l + a - s)\right] \tag{3}$$

Considering the fact that $V_c, B, l,$ and a remain constant based on engine geometry, the cylinder volume derivative equation reduces to Equation 4.

$$\frac{dV_\theta}{d\theta} = -\frac{\pi B^2}{4}\frac{\mathrm{ds}}{d\theta} \tag{4}$$

Then, taking the derivative of s with respect to θ yields Equation 5.

$$\frac{ds}{d\theta} = -\mathrm{asin}\,\theta\left[1 + \frac{a\cos\theta}{\sqrt{l^2 - a^2\sin^2\theta}}\right] \tag{5}$$

Finally, by substituting Equation 5 into Equation 4, results in the equation for instantaneous cylinder volume derivative based on crank angle, Equation 6.

$$\frac{dV_\theta}{d\theta} = \frac{\pi B^2}{4} a \sin\theta \left[1 + \frac{a\cos\theta}{\sqrt{l^2 - a^2\sin^2\theta}}\right] \tag{6}$$

3.2.2. Cylinder Pressure Smoothing. It is advantageous to smooth the collected cylinder pressure data before its use in heat release computations in order to eliminate any high frequency pressure waves resulting from cavity resonances that could skew the heat release analysis. A cosine low-pass filter was chosen to filter the raw pressure data collected on the Hatz 1D50Z. The general methodology for this data filtration includes performing a Fourier transform on the raw pressure data, multiplying the cylinder pressure spectrum by the cosine filter, and then, using an inverse Fourier transform to convert the filtered pressure back into the time domain.

3.2.3. Cylinder Pressure Rise Rate. As previously mentioned, the pressure rise rate must be monitored during engine operation in order to maintain operation within the healthy bounds of NVH. Therefore, the instantaneous cylinder pressure derivative with respect to $\boldsymbol{\theta}$ is calculated from IVC to EVO with Equation 7.

$$PRR = \frac{dP_\theta}{d\theta} = \frac{P_{\theta+h} - P_{\theta-h}}{2h} \tag{7}$$

In Equation 7 the h term represents the crank angle resolution of the shaft encoder. In this instance, utilizing the BEI Optical Shaft Encoder, the h value was 0.2.

3.2.4. Cylinder Temperature. The instantaneous cylinder temperature is used for computation of γ, the ratio of gas' specific heats, in the heat release calculation described in Section 4.1.3 to calculate this value, the fuel/air mixture is assumed to behave as an ideal gas with the thermodynamic properties of air. The calculation of this temperature is performed only during periods of a closed thermodynamic system, specifically, from Intake Valve Open (IVO) to Exhaust Valve Open (EVO). Combining conservation of mass with the ideal gas equation produces Equation 8:

$$T_\theta = \frac{T_{IVC} P_\theta V_\theta}{P_{IVC} V_{IVC}} \tag{8}$$

such that T, P, and V represent the temperature, pressure and volume, respectively, at either IVC, as designated by subscript 'IVC', or at the current crank angle, as designated by subscript 'θ'.

3.2.5. Heat Release. Once deriving all of its contributing variables, Heat Release Rate (HRR) can then be calculated utilizing Equation 9:

$$\frac{dQ_{ch}}{d\theta} = HRR = \frac{\gamma}{\gamma - 1} P_\theta \frac{dV_\theta}{d\theta} + \frac{1}{\gamma - 1} V_\theta \frac{dP_\theta}{d\theta} \tag{9}$$

where Q_{ch} represents heat release. In order to determine heat release (HR), Equation 9 is numerically integrated using the composite trapezoidal rule. This calculation then provides the basis for determination of additional engine performance parameters discussed below.

3.2.6. Engine Performance Measures. One measure of an engine's capacity to do work is the net indicated mean effective pressure (IMEPn). Simply put, this term is defined as the net work per engine cycle divided by the cylinder displacement volume. It is represented mathematically by Equation 10.

$$IMEPn = \frac{1}{V_d}\int_{V_0}^{V_{720}} P_\theta dV \tag{10}$$

The integration limits of V_0 and V_{720} in Equation 10 represent the initial and final cylinder volumes at the crank angle degree values of 0 and 720 respectively. On the four stroke Hatz engine, this 720 degree analysis indicates that integration, and therefore IMEPn, is taken over the entire engine cycle. By applying the composite trapezoidal rule, IMEPn can be determined from the smoothed engine pressure data using Equation 11:

$$IMEPn = \frac{1}{2V_d}\sum_{k=1}^{720/h}\left[P_{\theta_k+h} + P_{\theta_k}\right]\left[V_{\theta_k+h} - V_{\theta_k}\right] \tag{11}$$

where, again h represents the crank angle resolution of the shaft encoder and θ_k is the crank angle at the index k.

Another useful parameter is to identify the "efficiency" of the engine, as determined by the fuel conversion efficiency, η_f, and given by Equation 12:

$$\eta_f = \frac{P}{\dot{m}_f Q_{LHV}} \tag{12}$$

where $\dot{m}_f$ is mass flow rate of fuel inducted per cycle, $Q_{LHV}$is the lower heating value of the fuel, and P is engine power.

Additional critical measurements for HCCI experimental analysis are the CA10, CA50, and CA90. These values represent the crank angle at which the specified percent of the maximum cycle heat released occurs. For example, CA10 is the crank angle location at which 10 percent of the total heat release occurs during a given engine cycle. CA50 and CA90 are similar but represent the points of 50 and 90 percent heat release, respectively. All of these locations are determined by first performing heat release analysis on the pressure data, as will be discussed in Section 4, then determining the fractional heat release desired, and finally using this fractional value as a marker to determine the relative location in CAD for that cycle. Since HCCI lacks a clear ignition point, CA10 is generally recognized as SOC for HCCI engines. In line with general practice, SOC for this study is assumed to be CA10. Figure 3.4 depicts a typical HCCI single cycle heat release plot, with the CA10, CA50, CA90, and burn durations noted.

Furthermore, Burn Duration is a parameter representing the duration of the combustion event and is characterized by Equation 13.

$$Burn\ Duration = CA90 - CA10 \tag{13}$$

Any additional engine metrics will be discussed as they become pertinent to the discussion at hand.

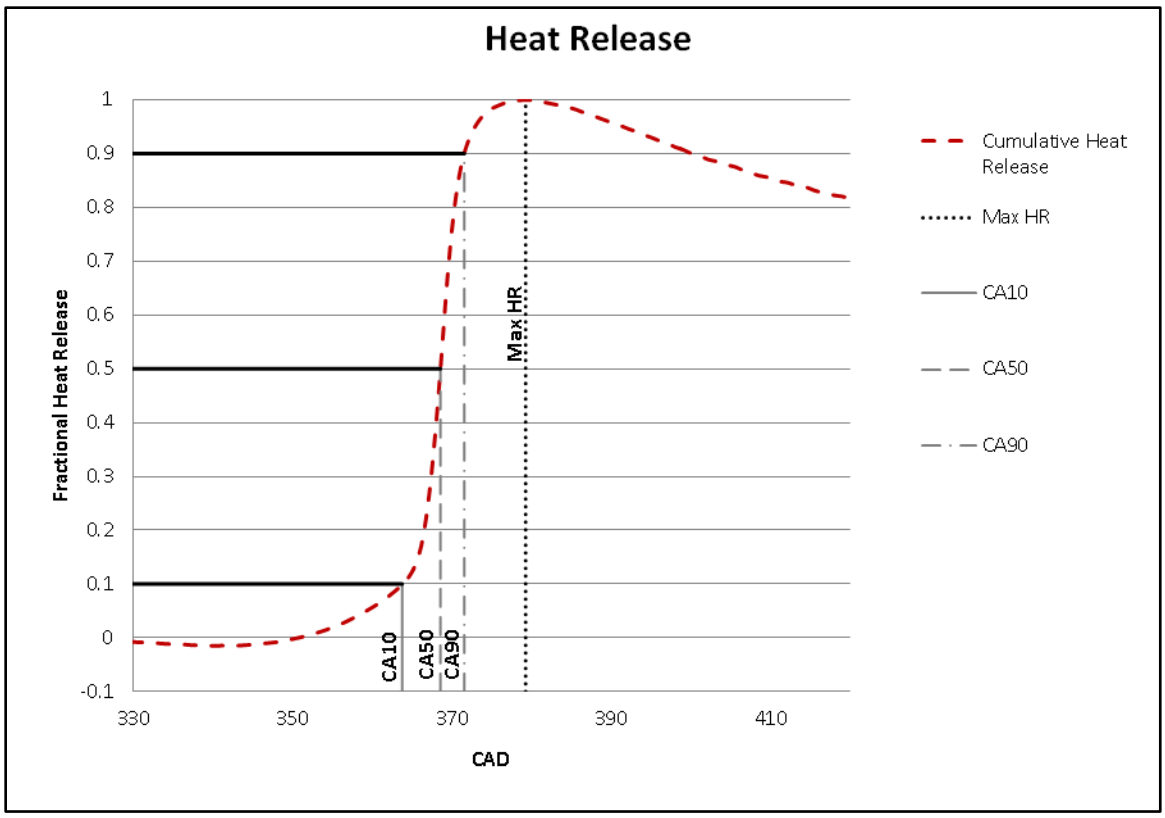

Figure 3.4. Cumulative heat release and corresponding CA10, CA50, and CA90.

3.3. OPERATING FUEL

The nature of the current investigation requires the use of an operating fuel of precisely known composition. Traditionally, the Missouri S&T Hatz experimental engine has operated on a blended 96 Octane Number (ON) research grade fuel, Indolene or Unleaded Test Gasoline 96 (UTG96). While this research grade fuel is sufficient for some aspects of HCCI research, the complex nature of this fuel prevents available chemical mechanisms from accurately describing its combustion reactions with confidence. Therefore, a disconnect previously existed between the simulated chemical kinetics and the experimental engine operation. As a result, a new fuel of known composition was

chosen as a means of directly relating chemical kinetics simulations to engine experiments.

When choosing a new fuel, it must first be considered what fuel the Hatz experimental engine is physically capable of operating on, and then what fuel would provide similar performance to the Indolene fuel blend that has been previously used. A fuel with comparable performance to Indolene would provide an easy comparison to previously run engine set points. Additionally, another key element revolves around the availability of a chemical kinetic mechanism that is capable of accurately predicting the combustion evolution and individual species concentrations of the chosen fuel. And finally, for both simplicity in the CHEMKIN simulations and the fact previous HCCI control model efforts at Missouri S&T were designed to simulate operation on a single stage fuel, it would be ideal to utilize a fuel with a single stage, gasoline-type, combustion event [29].

In general, there are two primary categories of fuel auto-ignition behavior. Since HCCI is so reliant on the auto-ignition of fuel, it is essential to understand the desirable qualities of these two separate instances. The two fuel auto-ignition behaviors are commonly referred to as single stage, experienced in gasoline-type fuels, and two-stage ignition, characteristic of diesel fuels. A two-stage fuel is characterized by a smaller initial 'cool flame' energy release that subsides and is followed by the primary high temperature energy release event, hence the two-stages. This behavior is expected of fuels with lower octane ratings. Conversely, single stage fuels tend to only have one energy release event and possess higher octane ratings, typically with an ON of 80+ [28].

A graphical comparison of the two different heat release events is shown in Figure 3.5 [30]. This figure compares the single stage ignition behavior of isooctane with the noticeable two-stage ignition behavior of an 80 ON primary reference fuel blend.

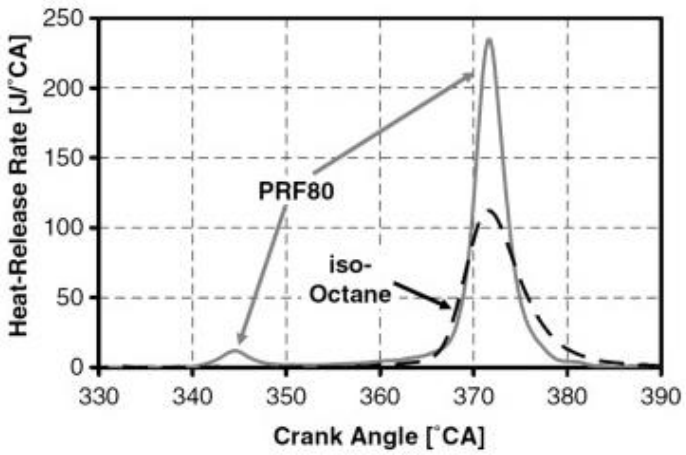

Figure 3.5. HCCI heat release for a single stage iso-octane and two-stage PRF80 blend [30].

The octane number of a fuel is traditionally used as one measure of a fuel's resistance to engine knock in spark ignited engines. In some ways, the nature of HCCI auto-ignition can be thought of as being similar to engine knock in spark engines, where the higher ON represents more of a resistance to knock. Therefore, the octane number was one of the first features considered when searching for a new Hatz operating fuel. For this study, a higher octane number would result in a single stage fuel, as desired for compliance with previous modeling efforts and would closely resemble behaviors of the fuel, Indolene, which has been readily used on the Hatz engine at Missouri S&T.

Additionally, full implementation of HCCI technology would likely require coupling this combustion mode with another mode such as SI. Therefore, the ability to operate in an SI mode, on a high octane gasoline-style fuel becomes a desirable parameter. Therefore, a higher octane fuel (90+ ON) was desired.

In choosing the new operating fuel, a comparison was made to the fuels that have been run on both the Missouri S&T and the ORNL Hatz experimental engines. Reviewing the ORNL literature and available data, it appeared that the majority of their operating points involved diesel-type fuels, with low octane numbers [31, 16]. Additionally, of the high octane fuels that they have used, many are gasoline surrogate fuels with complex composition or 4 and 5 component blends. These surrogate blends would be extremely difficult to accurately model chemically and even more difficult to justify that the model predictions resemble the experimental performance. However, ORNL has used an Isooctane/n-Heptane/ethanol blend with a Research Octane Number (RON) of 105 and Hydrogen/Carbon ratio of 2.313. While such fuel would be difficult to model, this shows that operation on a fuel with a very high RON is within reason. It should be noted the oxygenated nature of the ethanol blend affects the ignition in a different manner than a purely hydrocarbon blend. Another of the fuels resembling gasoline that researchers at ORNL have used was a 91 ON Primary Reference Fuel (PRF) blend of 2,2,4-trimethylpentane, more commonly known as Isooctane, and n-Heptane (91% Isooctane, 9% n-Heptane) [32]. This data gives testament to the idea of utilizing a high octane PRF blend. The CA10 of these fuels have been plotted in Figure 3.6 in comparison to Indolene at various inlet temperatures.

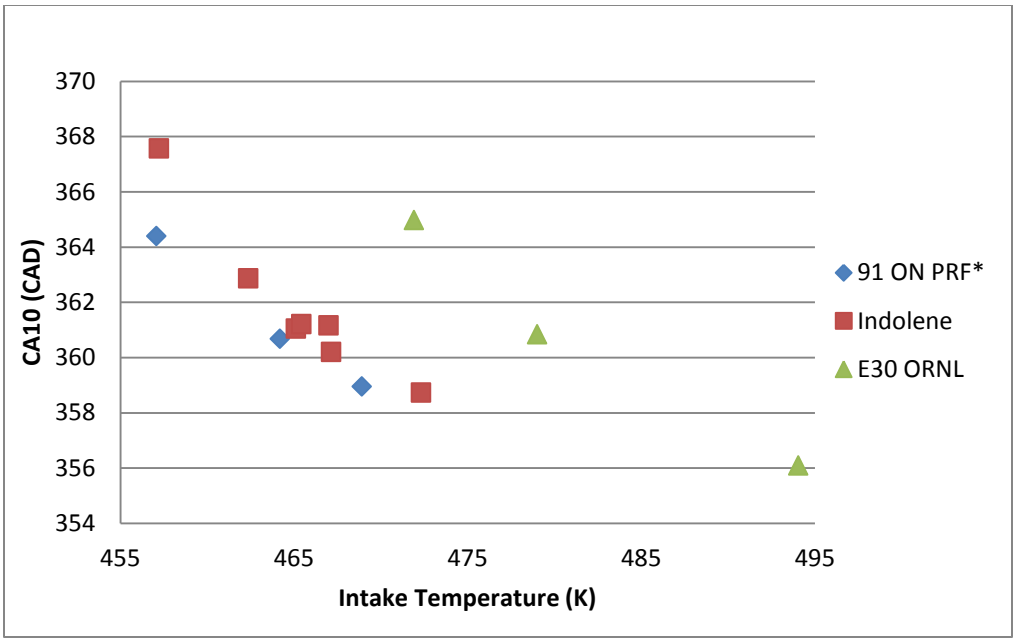

Figure 3.6. CA10 of high octane fuels run on Hatz HCCI engine.

From Figure 3.6 it may be noticed that all three of these high octane fuels display similar trends in their CA10 behavior and may therefore behave similarly during auto-ignition. This plot supports the use of a high ON PRF fuel. Such a fuel has been shown effective by ORNL, and would be a simple enough mixture to use available PRF chemical mechanisms for CHEMKIN simulations.

Possibly a better indication of the auto-ignition characteristics of a fuel lies in its Octane Index (OI) rather than its RON. Similar to the RON, the octane index is characterized by higher values representing more of a "resistance" to auto-ignition. The calculation of this fuel characteristic is outlined in Equation 14.

$$OI = \mathrm{RON} - \mathrm{KS} \tag{14}$$

In this equation, S is known as the fuel sensitivity and is determined by the difference between the RON and Motored Octane Number (MON). Primary reference fuels have the same octane numbers for both the research and motor methods, meaning that the fuel sensitivity value for a PRF fuel is essentially zero, and therefore its OI value is equal to its RON [28]. The value of K in Equation 14 is dependent on the normalized air/fuel ratio, λ, as well as T_{comp15}, which is defined as the in-cylinder temperature when the pressure reaches 15 bar during the compression stroke. This T_{comp15} value is an arbitrarily chosen term in order to represent the pressure/temperature history of the mixture [33]. The K value is dependent on these terms through the expression of Equation 15.

$$K = 0.00497T_{comp15} - 0.135\lambda - 3.67 \tag{15}$$

Considering that, under the present HCCI operation, the intake temperature is used as a combustion phasing control, this K value will vary with engine set-point due to the dependence of T_{comp15} on the charge temperature at the start of compression. Therefore, the OI also tends to vary with engine set-point. With this in mind, data from [29] was used to calculate the OI of a Toluene Reference Fuel (TRF) with a RON of 104, Indolene (UTG 96), and a prediction for the OI of a 96 PRF. These OI values are displayed Figure 3.7. Looking at Figure 3.7 it again appears that a high octane PRF blend, in this case a 96 octane PRF, would fit into the auto-ignition range of other fuels that have been used on the Hatz experimental engine. This provides additional

evidence that the Hatz engine would not have any issues operating on a PRF fuel such as this.

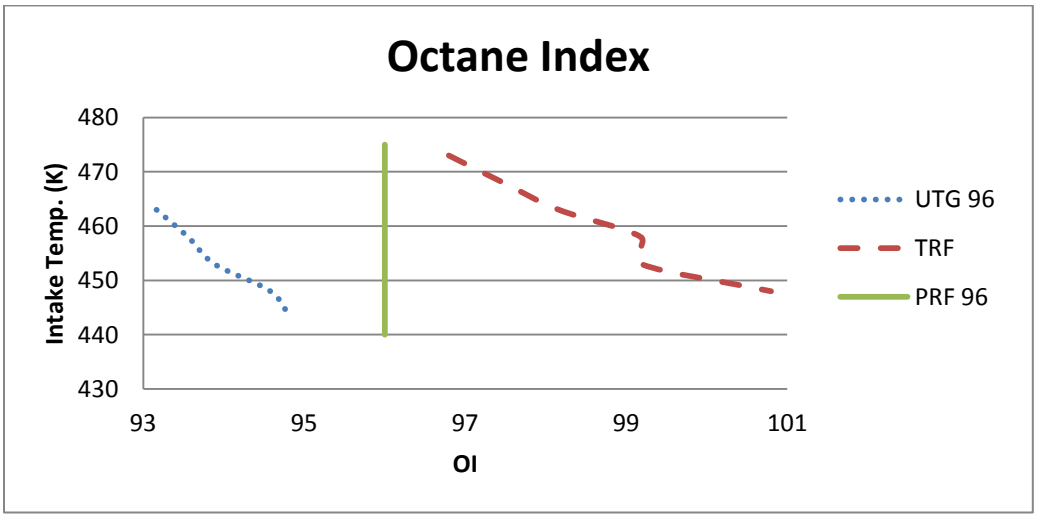

Figure 3.7. OI of high octane fuels run on Hatz HCCI engine.

Therefore, the fuel that was chosen as the base fuel for testing was a simple 96 ON PRF blend of 2,2,4-trimethylpentane, C_8H_{18}, and n-Heptane, C_7H_{16} (96% isooctane, 4% n-heptane by volume). This fuel possesses the single stage ignition characteristics desired, has the same octane number and was expected to possess auto-ignition timing similar to Indolene, and there are several PRF chemical mechanisms available for accurate prediction of the combustion behavior of the PRF mixture. Also, the 5-state thermodynamic model will be adaptable to the C/H ratio of the 96 PRF for future studies. This has been shown in Bettis' initial investigation of the model's adaptability to

Isooctane's C/H ratio and the fuel flexibility by adjusting the Arrhenius rate parameters to fit the fuel [29].

3.4. DYNAMICAL DATA TOOLS

Apart from general engine performance metrics, there are also additional methods of data characterization that are beneficial, especially when exploring operation in the partial burn regime. These tools provide routes of more definitively identifying the presence of relationships and trends in output data behavior while limiting the risk of noise tainting the interpretation.

3.4.1. Return Maps. One valuable tool in analyzing the dynamics of the partial burn regime is a return map. Return maps become a useful tool in their ability to identify correlations between consecutive engine cycles without resorting to the cycle averaging of parameters. Essentially, the plot of a return map consists of the parameter value of one cycle, cycle 'i', plotted vs. the value of the subsequent cycle, cycle 'i+1'. When plotting data in this way, groupings of circular, unstructured data patterns that emerge represent a lack of influence from one cycle to-the-next. This type of seemingly unstructured data is indicative of the strong presence of a random Gaussian distribution, referred to in this work as stochastic behavior. Conversely, if a structured pattern emerges in the plot, often as structured 'arms' that emerge off of a stochastic base grouping, then this indicates that a stronger relationship between the two consecutive cycle parameters exists. That is, this represents the dominance of deterministic behavior.

3.4.2. Symbol Sequence Analysis. Symbol sequencing analysis is another useful tool utilized in order to provide a deeper, more quantitative look into the dynamical tendencies of the HCCI experimental engine. Symbol sequencing is a fairly simple method of analyzing system dynamics while minimizing the effects of noise and measurement errors in the data. With this method, partitions are defined amongst the data in order to separate similar data points into bins of the same characteristic 'symbols'. These partitions are generated in an equiprobable manner, such that an equal number of data points fall into each bin. The 'symbols' that define the bins are merely sequential numbers, and in this work, only two bins were utilized, correlating to a binary categorization of the data where values falling above the partition are represented by a '1', and those falling below the partition are represented by a '0'. While the use of additional partitions technically increases the resolution of the analysis, one must be careful because at the same time you lose the distinction of sequences as well. What this means is that at the extreme case, a large enough number of bins for categorization of the data provides no more insight than raw, un-partitioned data. This leaves an inherent benefit in maintaining a small enough number of partitions in order to generate distinguishable sequences. Figure 3.8 displays a set of partial burn sample data, along with a calculated partition, that has been categorized according to a binary symbol sequencing. In this figure, all data points falling above the line were categorized as '1' and any data below the line was categorized '0'.

After the grouping of data has occurred, the symbolic categories are then organized into sequential patterns within the data. The length of these data sequences

is a user-defined variable of the analysis, and, ideally, should be chosen based on the pattern length that is capable of capturing the most deterministic tendencies buried in the data. It should be noted that too long of sequences would limit the number of possible occurrences of these patterns within a dataset. Or, in order to capture a statistically significant number of data points to effectively capture long sequences would require impractically, or even impossibly, long data sets depending on the specific application and the data acquisition system limitations.

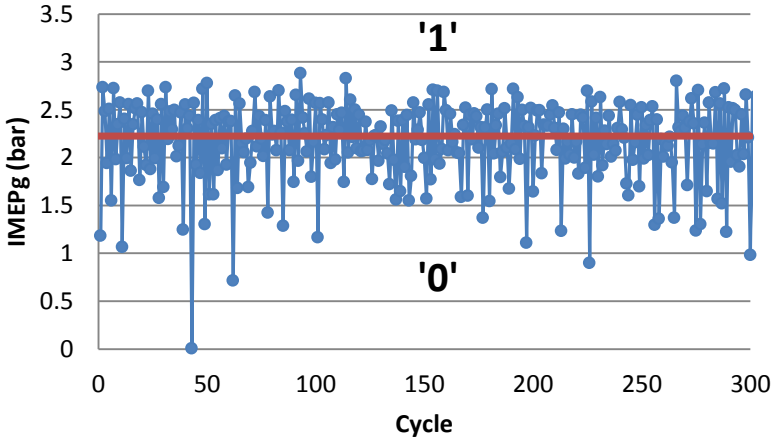

Figure 3.8. Sample symbol sequencing data separated by line for binary partition.

After identifying the sequences present in the data, the number of occurrences of each pattern is then tallied for display in a histogram. When looking at the histogram data, the dominant sequences will appear as peaks rising above the other data. Histograms with large dominating peaks are justification to classify the data as deterministic, with obvious sequences trending more frequently within the data. On the

contrary, if all sequences have comparable occurrence frequencies, then the bars will fall along similar values, representing random, stochastic data. Perfectly random data would be represented by all sequences occurring with precisely the same data and would fall on the baseline frequency, Equation 16:

$$F_b = \left(\frac{1}{n_{part}}\right)^{l_{seq}} \tag{16}$$

where n_{part} represents the number of partitions used, and l_{seq} represents the sequence length. Comparing frequency values back to the baseline frequency is a quick way to gauge how stoichiometric the data is. The resulting symbol sequencing histogram with binary symbols and a sequence length of 5 for the sample data above is portrayed in Figure 3.9.

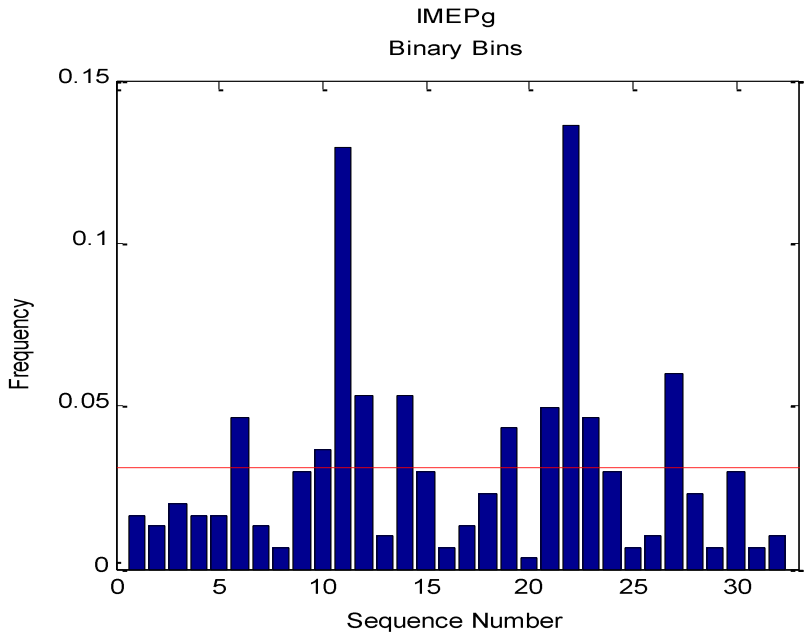

Figure 3.9. Sample histogram of symbol sequence analysis results.

From this sample data, a deterministic tendency is observable by the dominance of sequences 10 and 21 which represent binary sequences of '01010' and '10101'. If all sequences fell near the baseline frequency noted by the red line at 0.0313, this data would be classified as stochastic.

Identifying the most effective sequence length in order to capture deterministic patterns for given sets of data is attainable through the calculation of a modified Shannon entropy. Determination of modified Shannon entropy is done through the use of Equation 17:

$$H_s = \frac{1}{\log n_{seq}} \sum_k p_k \log p_k \tag{17}$$

where p_k is the probability of observing sequence k and n_{seq} is the number of different sequences observed in the time series. More conventional modes of Shannon entropy vary from this definition in that they use the number of possible sequences as opposed the number of observed sequences. In utilizing modified Shannon entropy for identifying optimized sequence length, it should be known that a Shannon entropy value of one indicates completely random data. However, values of less than one indicate the presence of cycle-to-cycle correlations, where lower values represent stronger correlations in the data. Therefore, in determining the ideal sequence length, Shannon entropy can be utilized in order to identify the number of cycles to incorporate, sequence length, over which the most significant correlations would occur by identifying which instance produces the lowest entropy values.

3.5. EXPERIMENTAL PROTOCOL

For the simulation set-point definition, a handful of experimental engine set-points were chosen as the baseline conditions for averaging parameters that would define simulation runs. These engine operating points were chosen for their ability to encompass a range of equivalence ratios and load points, as determined by fueling rate, that resemble a variety of typical engine operating conditions. The actual experimental investigation took a deep dive into two slightly different engine set-points that are addressed in detail in Section 6. The set-points considered for firing tests on the HCCI setup were at a constant engine speed of 1800 rpm and are displayed in Table 3.2. The fuel used was the PRF 96 octane blend of 96% 2,2,4-trimethylpentane and 4% n-Heptane by volume, as discussed in Section 3.3.

Table 3.2. Experimental base set-points for simulation.

Operating Regime	Intake Temp (K)	Fuel Rate (g/min)	Average Equivalence Ratio	Average CA10 (CAD)	Average CA50 (CAD)	IMEPn (bar)
Steady State	235	6.0	0.30	359.6	362.6	3.22
Partial Burn	203	6.0	0.29	359.2	375.8	2.15
Steady State	226	7.5	0.37	360.6	363.0	3.80
Partial Burn	197	7.5	0.36	360.5	379.4	2.77
Steady State	208	9.0	0.45	361.0	362.7	4.30
Partial Burn	192	9.0	0.43	362.6	383.7	3.34

In order to achieving each set-point, the inlet temperature was incrementally varied at a specified fueling rate and allowed to stabilize at each point. Initial mapping

with the PRF fuel operating regime was conservatively based on the previous operating capabilities of its similar counterpart, Indolene. For the stable points, the temperature was incrementally increased until either the engine was limited by PRR at its upper load limit, or the CA50 value was at or very near TDC. These points were referred to as steady state conditions and were based on the discretion of the operator. Additional steady state points were achieved by incremental decreases in the inlet temperature. At each designated inlet temperature, the engine was allowed to run for several minutes until exhaust temperatures, pressure rise rates, and heat release values stabilized before any data collection occurred. The partial burn conditions were achieved by additional decreases in inlet temperature until charge combustion was phased late in the engine cycles and continued engine operation was difficult to sustain. These partial burn regimes are where incomplete combustion and erratic engine performance tend to be more prevalent. These therefore, were the areas of primary interest during this study.

The upper load limit for the Hatz experimental engine was characterized by excessive PRR of roughly 10 bar/CAD. Near this limit, noise, vibration and harshness (NHV) begin to elevate to a point of concern. Excessive NHV can eventually lead to the damage and degradation of engine components. Therefore, operation above this limit is avoided in order to preserve the integrity of the Hatz experimental engine.

The equivalence ratio, φ, is a parameter that quantifies the relationship between the actual fuel/air ratio and the stoichiometric fuel/air ratio. This value is calculated from Equation 18. The fuel-specific stoichiometric fuel/air ratio for the 96 ON PRF used in

this study was calculated to be 0.06607 through the use of thermochemistry. When $\varphi = 1$, the fuel/air mixture is at precisely stoichiometric conditions. In situations of $\varphi < 1$, the mixture is considered lean, and when $\varphi > 1$ the mixture is fuel rich. HCCI operation falls well into the lean mixture conditions.

$$\varphi = \frac{(F/A)_{actual}}{(F/A)_{stoich}} \tag{18}$$

The Hatz experimental engine was run at sustainable-partial-burn conditions during the majority of the experimental investigation of Section 6. The set-points were chosen such that, if the inlet temperature was lowered another 1-2 degrees, combustion would enter deep into the partial burn regime and begin to destabilize to an unsustainable operating point. While entering deeper into partial burn operation would experience further amplified cyclic-to-cycle dynamics and likely amplified response to species mass injections, it would also allow combustion to drift until completely lost, at a rate that would prevent long datasets from being collected. The chosen approach allowed for the preservation of operating conditions that characterize the partial burn limit, but where sustained operation was still achievable for lengthy data collection sequences. Additionally, isolated cases were intentionally run within the stable regime as comparative references. Such instances are noted when discussed. Overall, the experimental conditions correlate closely with the intake temperatures that defined initial conditions of the predictive simulations run, as discussed in Section 5, but do not align precisely due to general assumptions and uncaptured system losses of the model.

Regarding injection parameters, species mass injection for most experimental cases was chosen to occur during the intake stroke of the engine. It was desirable for the injection to take place at the earliest period of the intake stroke and over a short window of time so that the specie mass has the maximum time possible to mix with the inlet charge and create a more homogeneous mixture. More specifically, the injection initiated at approximately 30 CAD ATDC, immediately after EVC, and most injections concluded by 45 CAD ATDC, before IVC. In this manner, it is believed that the injected CO mass was able to sufficiently mix with the air/fuel charge being inducted into the cylinder, without losing any of the injected mass out of the exhaust port. The injection pressure chosen was 1000 psi. This was held constant for all test cases. The chosen line pressure ensured that the injection mass resolution was fine enough to accommodate all injection set-points and still ensured that accidental backflow into the valve would not occur, considering that the gas line pressure exceeded all anticipated cylinder pressures.

Large datasets of 1000 cycles and 1500 cycles were collected as a means of capturing the full extent of engine dynamics. These datasets were analyzed through the use of time series comparisons, symbol sequencing techniques, and return maps. Sensitivity investigations involving sinusoidal mass injection patterns were run and were evaluated by examining the FFT power content of the responding engine performance metrics when the injected specie mass was introduced in a periodic manner. Additional specifics of the data collected during this investigation are discussed in Section 6.

4. CHEMICAL KINETICS SIMULATIONS

In order to closely investigate the impact of residual product species on next cycle combustion, it is first essential to understand the potential species and their respective concentrations that can take part in the feed-forward process. To address this, chemical kinetic simulations were embraced as a means of emulating the complex combustion process occurring during HCCI operation. These simulations predict the product species concentrations, temperatures, and pressures resulting from any combination of desired inlet and boundary conditions. The details of these chemical kinetic simulations follow.

4.1. HCCI COMBUSTION SIMULATIONS

A chemical kinetics simulation has been developed as a means of predicting the combustion products in an HCCI engine during partial burn operation. This simulation was used to determine the specific mass concentrations of critical species that present themselves under various degrees of incomplete combustion and may be carried, through internally trapped residuals, to future engine cycles. A constant volume CHEMKIN structure was chosen as the construct of the simulation in order to resemble the near constant volume that is often exhibited in HCCI operation. This system will better depict the combustion that occurs in HCCI engine operation than the constant pressure simulations that are often used by other researchers.

4.1.1. CHEMKIN Chemical Kinetics Simulations. The program chosen for use in the chemical kinetic simulations was CHEMKIN. CHEMKIN is a Fortran-based program originally developed by Sandia National Laboratory for the analysis of gas-phase chemical and plasma kinetics [34]. During this work, all simulations were run on Intel's Visual Fortran XE 2011 compiler. The general construct of the CHEMKIN program used for the simulations follows the layout depicted in Figure 4.1.

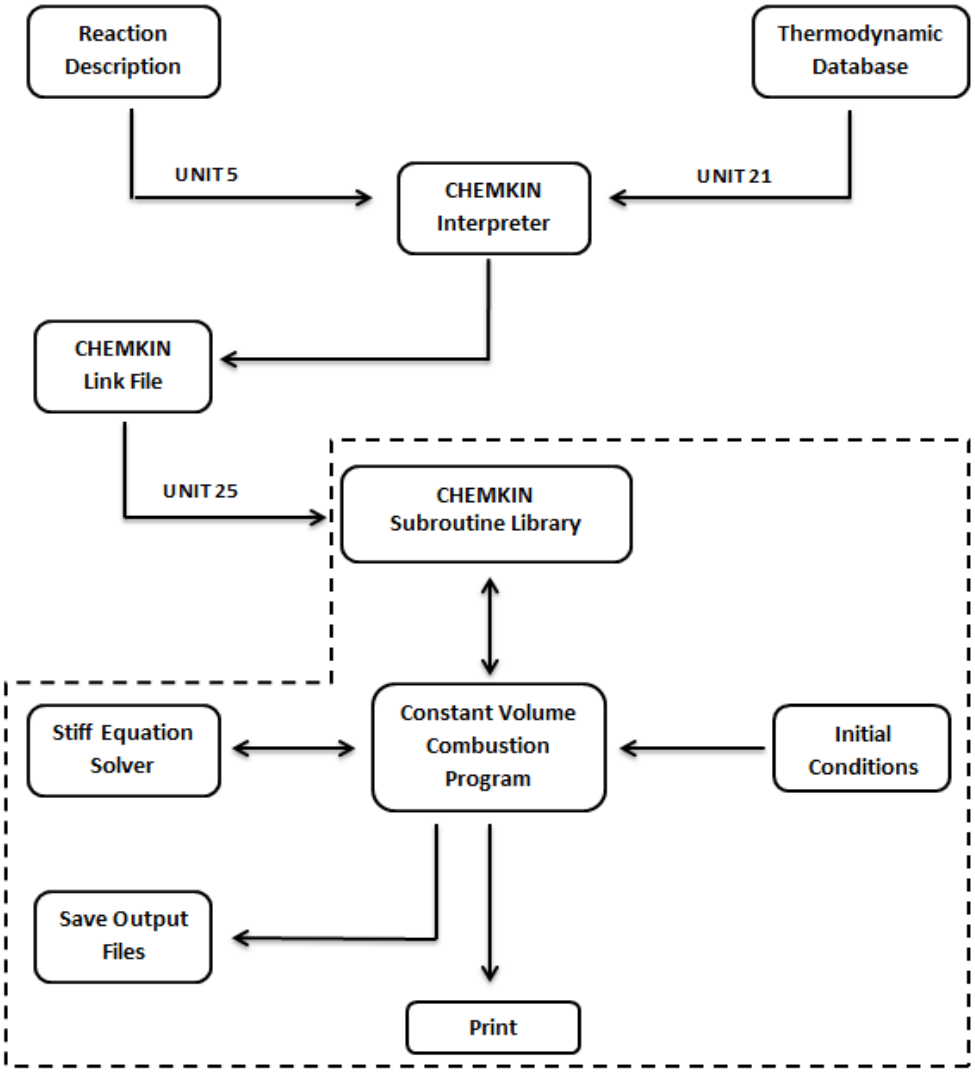

Figure 4.1. Diagram of CHEMKIN program structure.

It can be seen from Figure 4.1 that the process begins with the description of a set of chemical elements, species, and reactions through the Reaction Description file. This user-specified file is a compilation of extensive knowledge of chemical reactions and their individual rate constants. Many researchers have invested significant efforts into developing both highly complex, detailed chemical mechanisms and simpler, reduced or skeletal chemical mechanisms to describe the behavior of reactions by isolating crucial species, reactions, and rate constants associated with them. For each chemical reaction specified within a mechanism there exists a symbolic reaction description, followed by three Arrhenius coefficients (pre-exponential factor, temperature exponent, and activation energy). The general forward reaction form that CHEMKIN assumes is an Arrhenius temperature dependence adhering to the form of Equation 19:

$$k_{f_i} = A_i T^{\beta_i} exp\left[-\frac{E_i}{RT}\right] \tag{19}$$

where k_{f_i} is the forward reaction rate being calculated, A_i is the pre-exponential factor, T is the temperature, β_i is the temperature exponent, E_i represents the reaction's activation energy, and R is the universal gas constant. Additionally, enhanced third body efficiencies for selected species can be specified following reactions which contain arbitrary third body species to more fully describe certain reactions.

The development of chemical kinetic mechanisms requires extensive knowledge of the fuel-specific chemical reactions occurring and is beyond the scope of this investigation. Therefore, well validated mechanisms were chosen from the literature

for use with these constant volume simulations. Specifically, the mechanism developed by Tsurushima for the combustion of Primary Reference Fuel (PRF) blends composed of Isooctane, C_8H_{18}, and n-Heptane, C_7H_{16}, was chosen as the mechanism for use in this research [35]. This mechanism has been well validated by Tsurushima against experimental shock tube ignition delay data and intermediate profiles from gas-sampling experiments in an HCCI engine and has been shown to provide an accurate representation of the progression of temperature and species evolutions under HCCI combustion conditions [35]. This mechanism is based off of a reduced PRF kinetic model by Tanaka *et al.* with main modifications involving the additional consideration of intermediates, olefins and aldehydes, and consideration of beta-scission of alkyl radicals in parallel to the low-temperature reactions.

It should be noted that there exist both highly detailed and skeletal, reduced mechanisms that are capable of describing combustion to a variety of degrees of accuracy. While highly detailed mechanisms are a more thorough representation and often provide a more accurate depiction of the progression of combustion reactions, they are more computationally expensive. As a result, skeletal and reduced mechanisms are often employed for their computational speed in use with complex CFD simulations with highly refined grids. The mechanism by Tsurushima that was chosen for this work contains 33 species and 38 reactions and is considered a skeletal mechanism [35]. Considering that computational time was not of great concern under the present study, a more detailed mechanism would have been ideal for use in this simulation for its accuracy. However, a mechanism size constraint resulting from the

32-bit addressing of the CHEMKIN version in use prevented the utilization of extensively complex chemical reaction mechanisms, which often contain descriptions of hundreds of species and thousands of reactions and, in return, require 64-bit addressing. Another constraint of this version of CHEMKIN is that it lacks the additional capabilities for describing other reaction dependencies, such as complex pressure dependencies, that are contained in the newest versions of CHEMKIN. Many new reaction mechanisms utilize these capabilities in order to describe chemical reactions that do not fit the Arrhenius form. Therefore, these reaction mechanisms are incompatible in the version of CHEMKIN used in the current study.

Along with the chemical reaction descriptions, it is necessary to provide a table of thermodynamic properties describing each species used in the reaction mechanism. This is depicted in Figure 4.1 as the Thermodynamic Database. The thermodynamic data follows a format similar to the NASA standard and declares the atomic weight of each species, polynomial fit parameters for standard-state enthalpy, entropy and specific heat relations, and the temperature range over which polynomial fits to the thermodynamic data are valid. Overall, for every chemical species in question, the thermodynamic table consists of seven coefficients for each of two temperature ranges.

These two user-supplied inputs, the Reaction Description and the Thermodynamic Database, are read by the CHEMKIN Interpreter, and all pertinent information on the elements, species, and reactions is written to a binary LINK file that provides these details to the CHEMKIN library. The CHEMKIN library, and in turn the

LINK file data, can then be called by the constant volume simulation on an as-need basis.

The constant volume combustion program, as described in Section 4.1.2, provides the main structure outlining the operating conditions of the combustion simulation. This program reads a series of user-defined input parameters from an input .DAT file and then calls on the CHEMKIN subroutine library as needed during simulation operation to obtain species information, thermodynamic properties, and reaction rate parameters. The constant volume structure utilizes a stiff differential equation solver to numerically integrate the system's defining equations and calculate the temperature and species progression as the code steps forward in time.

As the program runs, some of the output is printed directly to the screen, and, upon completion, the pressure, temperature, heat-release, and species evolution during the combustion process are saved to output files for data analysis to follow. A full description of the CHEMKIN program and all of its gas-phase subroutines is available in [34].

4.1.2. Constant Volume Combustion Structure. A constant volume, zero-dimensional, adiabatic system was chosen as the basic conditions for the chemical kinetics simulations within CHEMKIN. This structure is one simple method of mimicking the near constant-volume combustion that typically occurs in HCCI while eliminating complexities that are added as more variables are introduced to a simulation. It was believed that the choice of this configuration would better resemble the combustion during HCCI operation than the constant pressure structure that is often employed by

other researchers. The simulated charge is assumed to be a perfectly premixed, homogeneous fuel/air mixture. The basic structure of this type of problem considers the reactants at each point within the volume to react at the same rate. Therefore, no temperature or compositional gradients are present within the mixture. This means that a single bulk-gas temperature and set of species concentrations is sufficient in describing the evolution of the system. The general principle behind the development of the modeled fixed-mass reactor is to develop a system of first-order ordinary differential equations (ODE's) whose solution describes the temperature and species evolution within the mixture. Figure 4.2 provides a summary of the assumed constant-volume system characteristics.

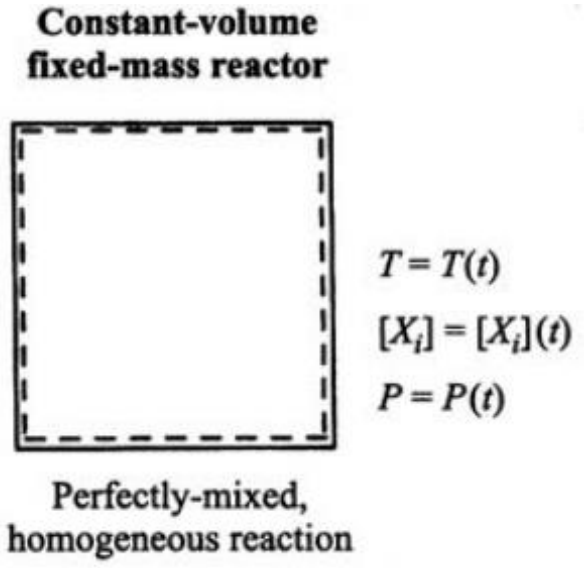

Figure 4.2. Assumed system structure.

The starting point for development of the ODE's is the rate form of the conservation of energy for a fixed mass system. Specifically, Equation 20 is considered:

$$\dot{Q} - \dot{W} = m\frac{du}{dt} \tag{20}$$

where $\dot{Q}$ is the heat transfer rate to the system, $\dot{W}$ is the work production term, m is the mass within the system boundaries, and $\frac{du}{dt}$ is the time rate of change of the specific internal energy. Since the system is held at a constant volume, there is no work being produced, meaning that $\dot{W} = 0$. The specific internal energy of the system may be expressed in terms of chemical composition as:

$$u = \frac{U}{m} = \frac{\sum_{i=1}^{N} N_i \bar{u}_i}{m} \tag{21}$$

where N_i and $\bar{u}_i$ are the number of moles and molar internal energy of species i, respectively. Differentiating Equation 21 yields Equation 22.

$$\frac{du}{dt} = \frac{1}{m}\left[\sum_i \left(\bar{u}_i \frac{dN_i}{dt}\right) + \sum_i \left(N_i \frac{d\bar{u}_i}{dt}\right)\right] \tag{22}$$

Then, assuming ideal-gas, Equation 22 becomes:

$$\frac{d\bar{u}_i}{dt} = \frac{\partial \bar{u}_i}{\partial T}\frac{dT}{dt} = \bar{c_v}\frac{dT}{dt} \tag{23}$$

where $\bar{c_v}$ is the molar constant-volume specific heat of species i, and $\frac{dT}{dt}$ represents the time rate of change of the bulk gas temperature. Equation 23 provides the desired link

to the system temperature. The connection to the system's chemical composition, N_i, and chemical dynamics, $\frac{dN_i}{dt}$, are based in the definition of molar concentration, $[X_i]$, and the production rate expression, $\frac{d[X_i]}{dt}$ or $\dot{\omega}_i$, respectively.

$$N_i = V[X_i] \tag{24}$$

$$\frac{dN_i}{dt} = V\dot{\omega}_i \tag{25}$$

The volume of the system is represented by V, and the $\dot{\omega}_i$ values are calculated by the CHEMKIN library from the information provided by the chemical mechanism input. Equations 23 – 25 can then be substituted into the Equation 22, and this result substituted into the reduced first law equation. Final simplification is made by recognizing the relationship between the molar internal energy of species i, $\bar{u}_i$, to the molar enthalpy of species i, $\bar{h}_i$, and the universal gas constant, R_u, as Equation 26.

$$\bar{u}_i = \bar{h}_i - R_u T \tag{26}$$

Upon noting this, the completed differential equation describing the temperature change of the system becomes Equation 27.

$$\frac{dT}{dt} = \frac{\frac{\dot{Q}}{V} + R_u T \sum \dot{\omega}_i - \sum \bar{h}_i \dot{\omega}_i}{\sum([X_i]\bar{c}_{v,i})} \tag{27}$$

Therefore, the set of partial differential equations that constitutes the system description is Equation 27 combined with the chemical production rate equations for

each species considered, which are calculated from the CHEMKIN code based on the specified reaction properties. These equations, with specified initial conditions of temperature and species concentration, are solved by a stiff differential solver in order to determine the evolution of temperature and composition during combustion.

Other parameters of interest during combustion are the system pressure, P, and pressure rise rate (PRR). In order to determine these, it is convenient to differentiate the ideal-gas law under the constraint of a constant volume system and apply the definition of $[X_i]$, Equation 24. This results in Equation 28.

$$P = \sum_i [X_i] R_u T \tag{28}$$

The expression for the pressure derivative is attained by differentiating the ideal-gas law, subject to the constant volume constraint, and applying the definitions of $[X_i]$ and $\dot{\omega}_i$ from Equation 24 and Equation 25. This results in the expression for the pressure derivative, $\frac{dP}{dt}$, Equation 29.

$$\frac{dP}{dt} = R_u T \sum_i \dot{\omega}_i + R_u \sum_i [X_i] \frac{dT}{dt} \tag{29}$$

Equation 29 completes the analysis of the homogeneous, adiabatic, constant-volume combustion process.

In order to begin a simulation, initial conditions to the constant volume combustion, including equivalence ratio, temperature, and pressure at IVC are specified in the input file by the user. Additionally, the presence of other species may be

specified in mass amounts within the premixed initial charge. This feature makes it possible to investigate the effects of species present at IVC due to either internally trapped EGR species or the mass addition of species directly in-cylinder by the RGI. Adiabatic compression is assumed to occur to compress the initial charge to TDC through use of the specified compression ratio. It is also possible to simply specify the initial conditions as they are after compression and bypass the adiabatic compression assumption of the code. The simulation then holds the volume constant and begins the iterative process of solving the set of partial differential equations describing combustion at these conditions.

Figure 4.3 represents a more detailed look into the variables calculated and passed between the various subroutines that constitute the constant volume structure. The details of Figure 4.3 fit carefully into the CHEMKIN structure within the outlined portion of Figure 4.1. The complete constant volume program code may be found in Appendix B.

4.1.3. Partial Burn. The primary region of concern in this study was the operating regime of partial burn, where incomplete combustion is prevalent. Therefore, during chemical kinetic simulations, it was essential to look at cases of incomplete charge burn. In the current model of an adiabatic, isochoric system, the need for an incomplete burn simulation became an area of concern, since, under the conditions that the simulation was designed, no energy was being removed from the system. This effectively prevented combustion from displaying partial burn behavior. As a result, incomplete combustion in the simulation is not possible unless the combustion process

is forced to end before the entire heat-release process takes place. Therefore, the simulated 'partial burn' is forced on the system by stopping the progression of the simulation at points based on the fractional amount of the maximum possible heat-released. This maximum possible heat-release value is determined by the total initial fuel energy present in the system.

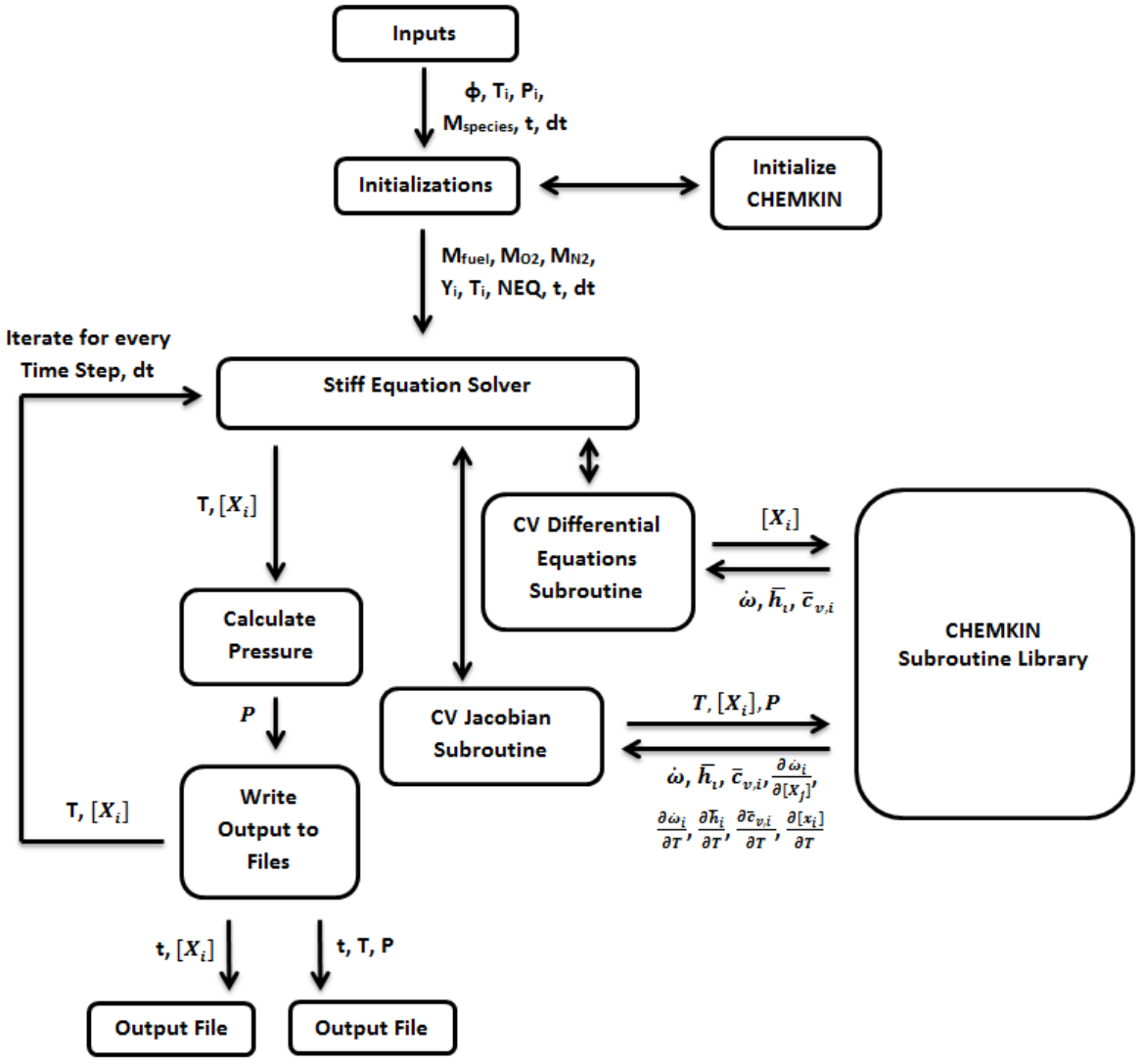

Figure 4.3. Constant volume operating structure.

Another essential piece of the puzzle is not only forcing the combustion at specified heat-release fractions, but also relating these incomplete combustion levels to experimental partial burn cases in order to predict realistically attainable incomplete burn conditions. Therefore, previously collected experimental heat-release data was used as the basis for determining the simulation partial burn set-points.

The Hatz experimental engine at Missouri S&T is complete with data post-processing programs capable of analyzing heat-release in a manner described by Heywood [28]. This heat-release calculation takes advantage of the collected cylinder pressure data to quantify the net chemical energy released based on the first law of thermodynamics. This analysis relates measurable in-cylinder pressure fluctuations directly to the amount of fuel chemical energy released during the evolution of the combustion process. A basic first law analysis is utilized, beginning with Equation 30.

$$\delta Q_{CH} = dU_s + \delta Q_{HT} + \delta W + \sum h_i dm_i \tag{30}$$

In Equation 30, δQ_{CH} is the chemical energy of the system, dU_s is the sensible energy, δQ_{HT} signifies the energy lost to heat transfer, δW is a term for the piston work, and the mass flux term, $\sum h_i dm_i$, represents the sum of the mass energy transfer across the boundary through the crevices. The experimental data processing neglects the energy losses to heat transfer or crevice effects. Therefore, it only accounts for the chemical energy converted to usable piston work, equal to pdV, and the change in sensible energy, where U_s is assumed to be given by $mc_v(T)$, with m as the mass in the

system and T as the mean charge temperature. With this, Equation 30 becomes Equation 31.

$$\delta Q_{CH} = mc_v dT + pdV \tag{31}$$

Then, incorporating the ideal gas law, while neglecting changes in the gas constant R, results in an expression of the form of Equation 32.

$$\delta Q_{CH} = \frac{c_v}{R} V dP + \left(\frac{c_v}{R} + 1\right) pdV \tag{32}$$

The final step in developing the experimental heat-release analysis involves Equation 32 requiring a value for ${c_v}/{R}$. Here, the ratio of specific heats, γ, for both the burned and unburned gases is used with the expression in Equation 33, but is held constant during combustion. This method has been shown by [28] to provide adequate results.

$$\frac{c_v}{R} = \frac{1}{\gamma - 1} \tag{33}$$

Applying Equation 33 to Equation 32, the net heat-release rate is thus given by Equation 34.

$$\frac{dQ_{CH}}{d\vartheta} = \frac{\gamma}{\gamma - 1} P_\vartheta \frac{dV_\vartheta}{d\vartheta} + \frac{\gamma}{\gamma - 1} V_\vartheta \frac{dP_\vartheta}{d\vartheta} \tag{34}$$

From this, the net heat-release was calculated with the Hatz data processing code in Matlab through the numerical integration of Equation 34 using the composite

trapezoidal rule. This method also formed the basis for calculating all CA10, CA50, and CA90 experimental values.

While the output from the experimental data processing code produces a net heat-release value, the simplicity of the simulation leads it to predict a gross heat-release value by not quantifying the energy lost through boundary-wall heat transfer and crevice leakage. Therefore, an approximate gross value for the experimental heat-release is required for comparison between the two. In order to address this, Equation 34 is revisited. The processing code from the Hatz pressure data produces a net heat-release value, and, since there are no experimental measurements of the boundary temperatures (in this instance the cylinder wall temperatures), accurate set-point specific heat transfer approximations become difficult to implement as a means of calculating gross heat-release. To address this issue, Equation 34 was integrated across a crank angle window that produces an assumed net heat-release value. First, Equation 34 was used to calculate HRR values throughout the entire engine cycle. Then, the HRR data was evaluated to determine the CAD when the HRR dropped to zero during the engine cycle. This corresponding CAD was then used as a bound for integration. More precisely, Equation 34 was integrated over a window from IVC to the point when HRR decreased to zero after the main energy release event. This produced values of cumulative HR that were assumed to be approximately equal to the gross heat-release. Figure 4.4 depicts the manner in which the HR was calculated. This result applied to experimental engine runs provided the necessary information needed to quantify the experimental gross heat-release and relate it to a simulated heat-release amount.

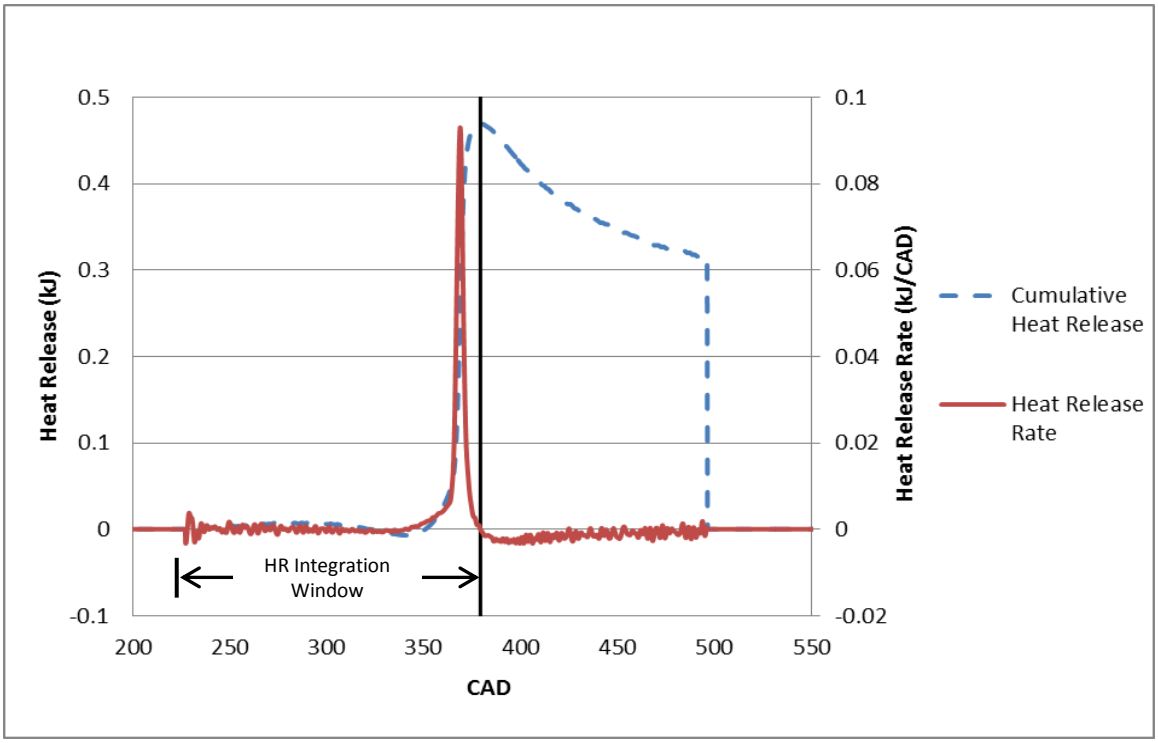

Figure 4.4. Heat-release calculation window based on HRR.

The simulated gross heat-release was calculated in a similar manner as the experimental, beginning with the first law analysis as described in Equation 30. However, the simulation has slightly different capabilities than the experimental calculations, and therefore progresses differently. In the current simulation, no losses through heat transfer across the system boundary, or any mass flux to the crevice are accounted for due to the adiabatic, fixed-volume assumptions. Furthermore, since the simulation was designed as a constant-volume system, there is no work expended through piston motion, causing the work term to fall out as well. The remaining terms simplify the energy balance to Equation 35.

$$\delta Q_{CH} = dU_s = mc_v dT \tag{35}$$

This term can then be differentiated with respect to time in order to determine RHR as Equation 36.

$$\frac{dQ_{CH}}{dt} = mc_v \frac{dT}{dt} \tag{36}$$

Similar to the experimental case, Equation 36 was numerically integrated as the simulation progressed to determine the heat-release at each time step. In this manner, the combustion simulation process could be halted at the first time step that achieves the desired fractional heat-release as determined from the experiments.

When comparing the simulated vs. experimental partial burn, a fractional heat-release amount was used. To calculate this percent heat-release for both circumstances, the heat-release was simply normalized against the initial fuel energy present in the cylinder, as shown below by Equation 38:

$$\%\, Heat\ Release = \left(\frac{\int \frac{dQ_{CH}}{dt}}{m_f * Q_{LHV}} \right) * 100 \tag{38}$$

where m_f is the initial mass of the fuel that is in the cylinder at IVC and Q_{LHV} is the lower heating value of the fuel.

A potential modification to this method would be to add either a heat transfer model to the simulation, or to make it a variable volume simulation based on the time rate of change of a cylinder volume. These would both act as energy dissipating methods that could remove energy from the system to inhibit complete combustion.

4.2. COMBUSTION SIMULATION VALIDATION

In order to validate the accuracy of the constant volume CHEMKIN structure that was developed, it was necessary to compare the output from the new model to a known solution under the same conditions. This comparison provides confidence that the simulation is behaving as expected and, therefore, producing output that is an accurate representation of the combustion process.

For the validation of the newly developed constant volume CHEMKIN simulation, assistance was sought from outside sources to provide the necessary data. Through correspondence with Dr. Charlie Westbrook, a senior member of the LLNL staff and combustion expert, data was provided for several test cases that were run on the most recent version of ChemkinPro under the adiabatic, constant volume conditions that replicate the environment of the newly created CV program described in Section 4.1.2 [36]. Test cases on ChemkinPro were run using not only the Tsurushima mechanism that is utilized for this study, but also the detailed PRF mechanism developed at LLNL [37]. Due to the detailed nature of the LLNL mechanism, consisting of 1034 Species and 4238 reactions, along with its wide use and acceptance among the combustion research community, it is anticipated that it is very accurate in its predictive capabilities, and, therefore, a worthy benchmark for comparison of the reduced mechanism in use for this study. The data attained from the ChemkinPro simulation runs was compared to the output produced on the constant volume CHEMKIN program for validation. The validation set-points were based on two typical conditions for HCCI operation and are displayed in Table 4.1.

Table 4.1. Simulation validation set-points.

$T_{initial}$ (K)	$P_{initial}$ (atm)	Equivalence Ratio	PRF Octane Number
950	28	0.28	96
950	28	0.40	96

4.2.1. Temperature Profile Validation. One parameter worth validating was the predicted bulk gas temperature. For this, the temperature profile predicted by the reduced mechanism operating on ChemkinPro was related back to the CHEMKIN solution. These results are displayed in Figures 4.5 and 4.6.

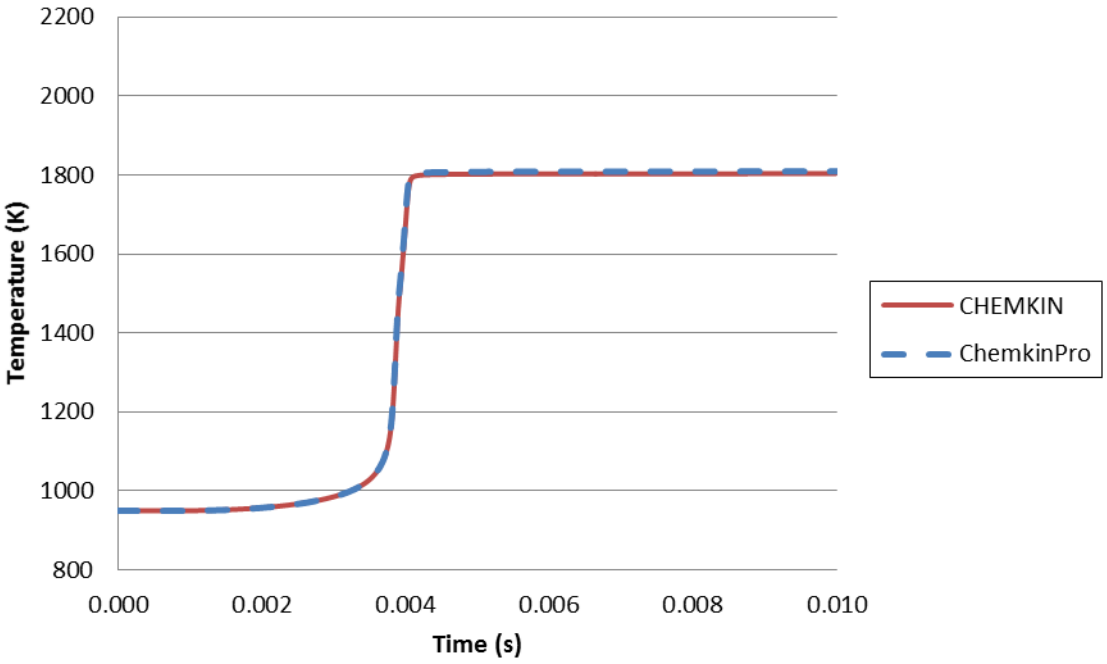

Figure 4.5. Temperature validation for $\varphi = 0.28, T_o = 950\ K, P_o = 28\ atm$.

Looking at Figure 4.5, it appeared that both final temperature predictions for the 0.28 equivalence ratio fall very close to one another. Specifically, the ChemkinPro output for the reduced mechanism predicted a final temperature of 1808 K, and the CHEMKIN constant volume code predicted a final temperature of 1803 K with the same mechanism.

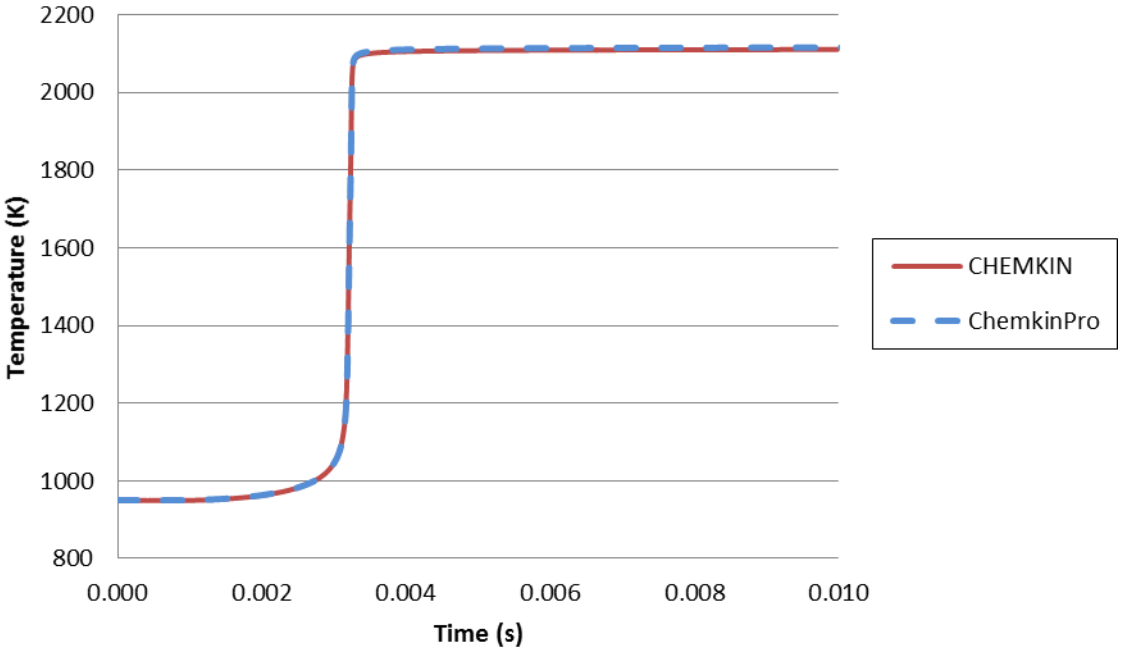

Figure 4.6. Temperature validation for $\varphi = 0.40, T_o = 950\ K, P_o = 28\ atm.$

Figure 4.6, displays the temperature predictions for the 0.40 equivalence ratio and indicates that the final gas temperatures fall close to one another. The ChemkinPro output for the reduced mechanism predicted a final temperature of 2118 K, and the CHEMKIN constant volume code foresaw a final temperature of 2110 K with the same

reduced mechanism. The minute differences in the maximum temperatures, along with the general agreement in the overall temperature profiles of Figures 4.5 and 4.6 support the validity of the new constant volume CHEMKIN structure.

4.2.2. Pressure Profile Validation. Similarly, the predictive accuracy of the constant volume CHEMKIN structure was verified for its pressure predictions. Under the same conditions specified in Table 4.1, the pressure estimates were calculated with ChemkinPro and compared to the constant volume CHEMKIN structure results, displayed in Figures 4.7 and 4.8.

From Figure 4.7 it can be seen both predictions for the 0.28 equivalence ratio fall very close to one another. Specifically, the ChemkinPro prediction with the reduced mechanism forecasted a final pressure of 54.17 atm, and the CHEMKIN constant volume code predicted a final pressure 53.14 atm with the same mechanism.

In Figure 4.8 it can be seen that the pressure predictions for the 0.40 equivalence ratio also lay near one another. More precisely, the ChemkinPro calculation with the reduced mechanism predicted a final pressure of 63.91 atm, and the CHEMKIN constant volume code predicted a slightly lower final pressure of 62.20 atm with the same mechanism.

Both validation cases resulted in slightly lower anticipated pressures from the CHEMKIN reduced mechanism in comparison to the ChemkinPro reduced mechanism output, with a maximum discrepancy of 2.7% in the case of the 0.40 equivalence ratio. However, considering that pressures are not the primary output desired from the simulations, these very slight differences were considered to be well within an

acceptable margin of error for this study. Also, these two reduced mechanism outputs occur at almost precisely the same instant in time, further validating the output of the new constant volume code.

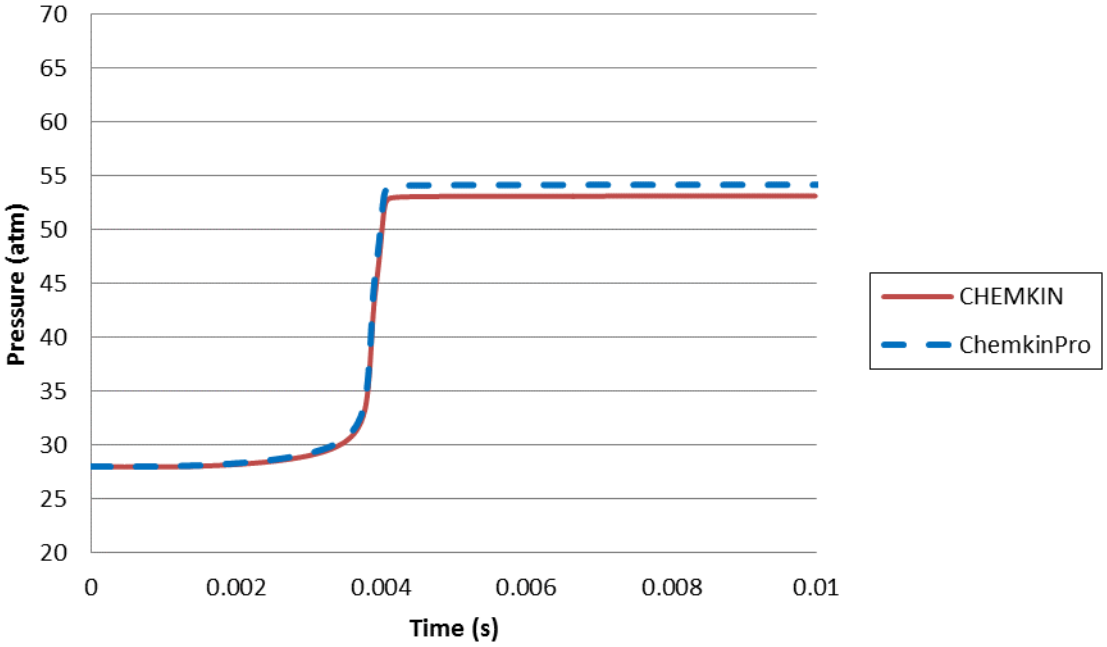

Figure 4.7. Pressure validation for $\varphi = 0.28, T_o = 950\ K, P_o = 28\ atm.$

4.2.3. Species Evolution Validation. Since the key result of the simulation was to predict species production amounts for engine cycle carryover, the validation of species data was, therefore, a critical element to the validity of the simulation. For this, several species mole fraction amounts were compared between the CHEMKIN and ChemkinPro output with the use of the reduced Tsurushima mechanism. The species compared for validation were O_2, CO_2, CO, H_2O, C_7H_{16}, and C_8H_{18} for combustion under

conditions of both validation set-points. The results from these simulations are displayed in Figures 4.9 and 4.10

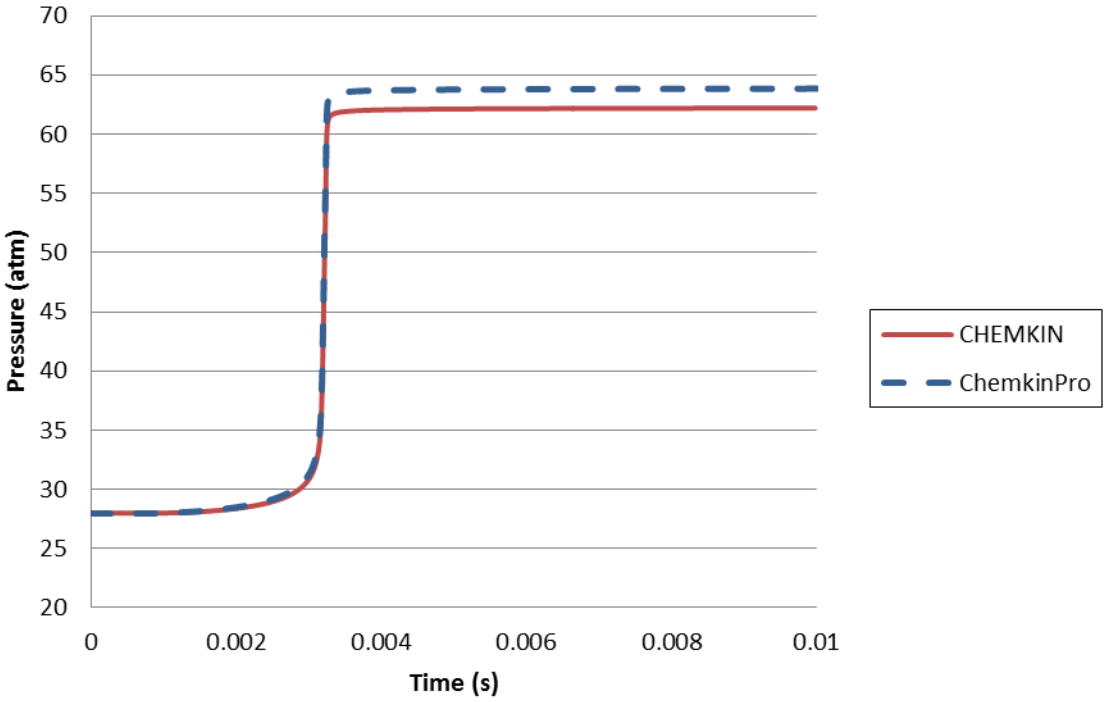

Figure 4.8. Pressure validation for $\varphi = 0.40$, $T_o = 950\ K$, $P_o = 28\ atm$.

The plotted output data from Figures 4.9 and 4.10 show very good agreement between the two programs for the mole fractions of the specified species at the test cases. This agreement between CHEMKIN and ChemkinPro is seen in both the magnitudes and time evolution of the species in question. The consistency of all parameters thus far implies good agreement between any parameters that were not addressed during the validation process.

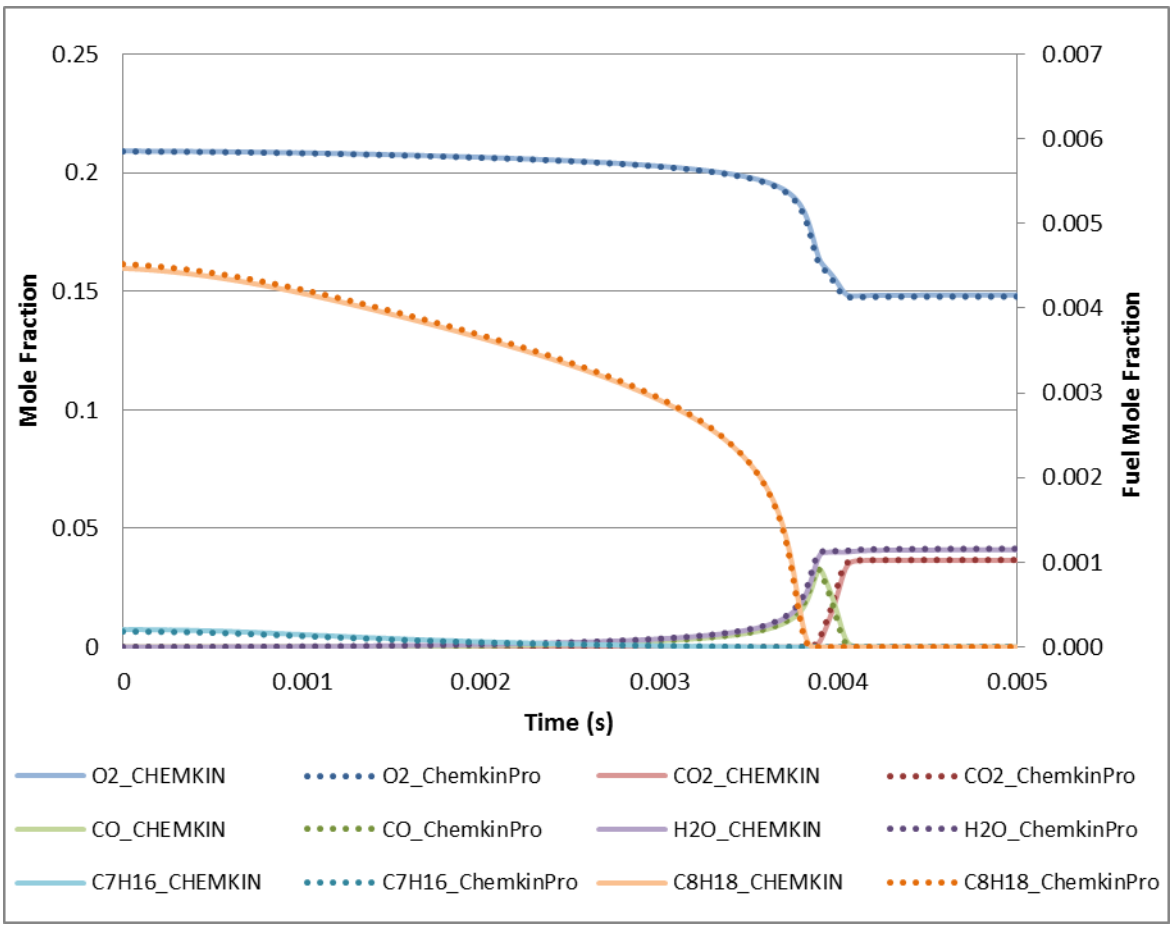

Figure 4.9. Species validation for $\varphi = 0.28$, $T_o = 950\ K$, $P_o = 28\ atm$.

Additionally, although the mechanism has been validated by its author, it was still worthwhile to compare the CHEMKIN output from the reduced mechanism to the available ChemkinPro output from the detailed LLNL mechanism in order to delve deeper into the overall accuracy of the reduced mechanism under the conditions of this investigation [35]. This is seen in Figures 4.11 and 4.12.

When comparing back to the detailed mechanism, it is noticeable that the reduced constant volume CHEMKIN results are shifted in time.

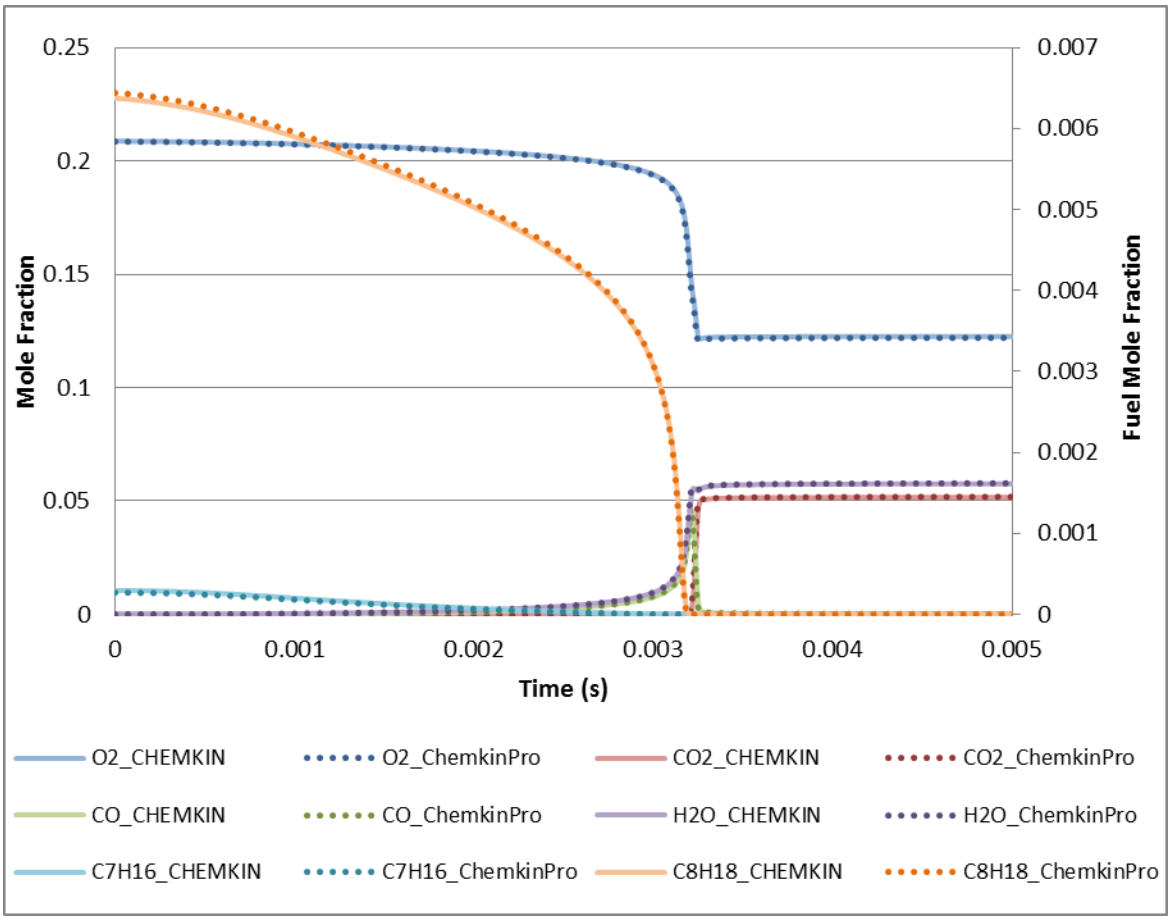

Figure 4.10. Species validation for $\varphi = 0.40, T_o = 950\ K, P_o = 28\ atm.$

The two solutions showed comparable trends in regards to species progression, and both captured the effects of varying equivalence ratio from 0.28 to 0.40, as in Figure 4.11 and Figure 4.12. However, in both figures, the reduced mechanism predicted an earlier oxidation process. This was consistent with early prediction seen in the temperature and pressure comparisons as well. So, it can be noted that, although the two reduced mechanism outputs strongly agree with one another, they do vary in time from the output of the detailed LLNL mechanism.

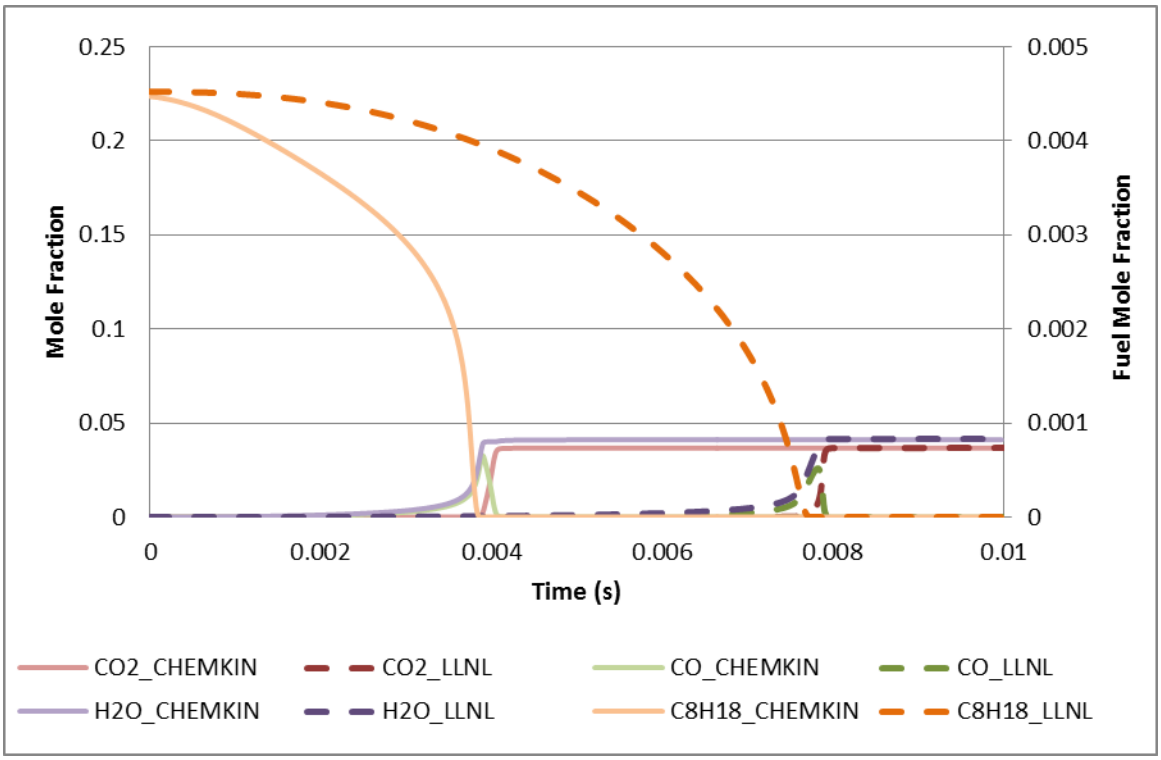

Figure 4.11. Species validation for $\varphi = 0.28, T_o = 950\ K, P_o = 28\ atm$.

When considering the context of this investigation, the time accuracy of the reduced mechanism becomes significantly less important. The purpose of these simulations was primarily to predict the species concentrations resulting from incomplete combustion. The level of incomplete combustion was measured and dictated by the percentage of total fuel energy released during combustion, as described in Section 4.1.3, not on a time basis. So, in general, the time accuracy of the solution is not a necessary luxury for this investigation since the simulations are specified on an energy release basis. Furthermore, when looking at the relative behavior, that is the impact of equivalence ratio, it appears that the trends are properly captured by the mechanisms. The scaled differences between the ignition delays at

both equivalence ratios are comparable, showing that the reduced mechanism is capturing the impact of equivalence ratio. Overall, it is noticeable that the relative behavior is properly reproduced by both mechanisms but a slight, acceptable difference between ignition delays consistently presents itself.

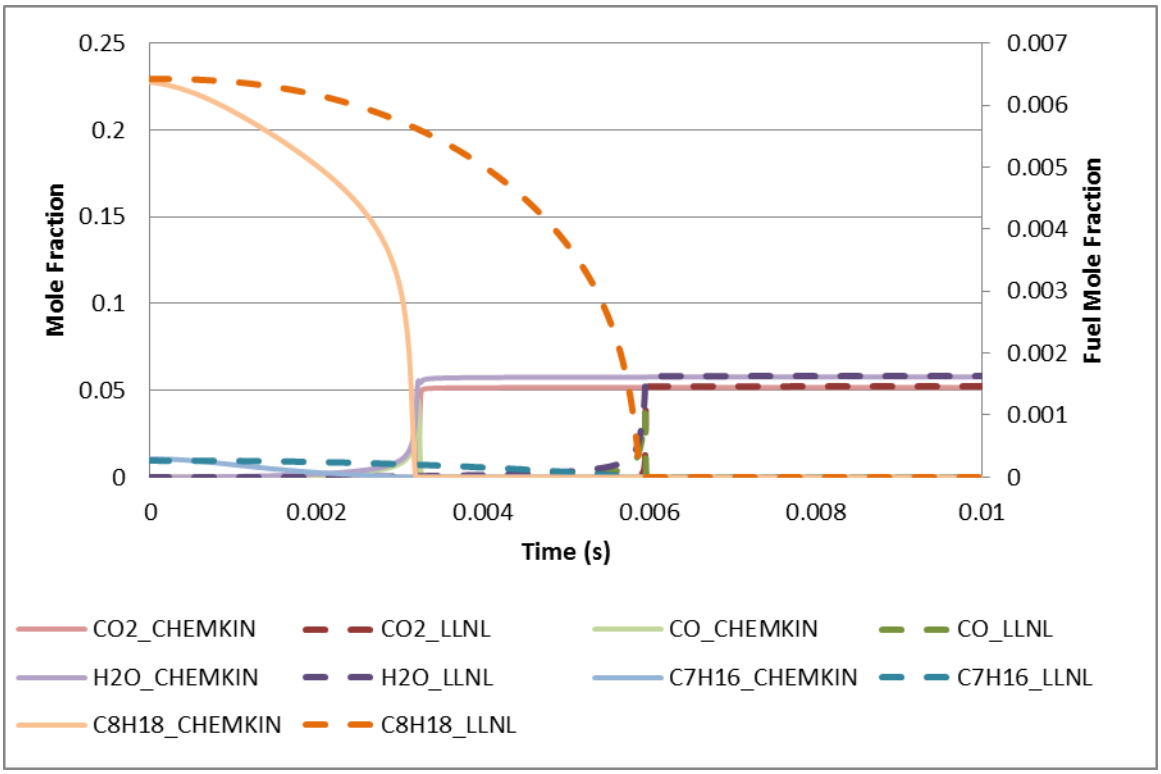

Figure 4.12. Species validation for $\varphi = 0.40, T_o = 950\ K, P_o = 28\ atm.$

The comparisons in Figures 4.11 – 4.12 between the ChemkinPro solutions provided by Dr. Charlie Westbrook to the CHEMKIN solution from the newly developed constant volume program provide solid support that the newly developed constant volume structure is behaving as desired. The results from both programs when using

the reduced Tsurushima mechanism show impressive agreement in the predicted temperature, pressure, and species behavior during HCCI conditions, and the differences that do exist are most likely a result of the countless improvements that have been made over the years in the Chemkin program to develop ChemkinPro. As a result, the new code can be used with confidence, knowing that it is correctly applying the governing constraints of an adiabatic, isochoric system to the chemical kinetic simulations.

5. SIMULATED SPECIES PRODUCTION

The newly validated constant volume, adiabatic chemical kinetics simulation was shown to sufficiently predict the product species evolution of the inlet charge during combustion under the desired conditions, based on experimental set-points. Combustion in the partial burn regime tends to stop premature of complete charge burn. As a result, the progression and species evolution of such combustion can be simulated through the application of incomplete chemical kinetic simulations. This Section addresses the simulated partial combustion using constant volume CHEMKIN simulations and the specific predicted species concentrations associated. Additionally, calculated feed-forward amounts of the predicted residual species are addressed from one cycle to the next. These feed-forward mass amounts become the foundation for controlled mass injections in the experimental investigation.

5.1. CRITICAL SPECIES PRODUCTION

The first step in prediction of feed forward CO amounts is the simulation of CO production under conditions representative of a partial burn set-point. In order for the constant volume combustion simulations to accurately capture the realistic engine conditions, the simulation input parameters must accurately represent the experimentally achievable HCCI operating conditions. In basing the simulations off of previous experimental conditions, predictive CO production quantities were determined for use in the analysis of next-cycle feed forward mass amounts.

5.1.1. Simulation Set-points. In order to accurately predict the combustion evolution during HCCI partial burn, it was essential to replicate the true engine operating conditions that pertain to experimentally achievable partial burn conditions. As such, the test matrix for the chemical kinetics simulation points was defined based off of previously obtained experimental engine data. This was used as a method of ensuring that the simulations were emulating actual engine set-points, for maximum confidence in relating them back to the engine experiments. With this method, it was likely that the engine may physically achieve the set-points and CO production levels represented by these simulated runs. Therefore, efforts were made to accurately quantify experimental operating parameters and utilize the equivalence ratios, inlet temperatures, and completion of combustion based on achievable heat release. However, it should be noted that, if supplying initial intake temperatures to the simulation, the intake temperatures for the simulation would be lower than those seen experimentally as a result of the model assuming an adiabatic compression process. The experimental charge mass loses a portion of its thermal energy during compression. In order to most accurately account for these losses, it was decided to specify initial simulation temperatures based on approximate experimental SOC temperatures near TDC, therefore bypassing the simulation's compression assumptions altogether. These were the temperatures of the cylinder charge when the engine first experiences a positive heat release rate during the compression stroke on experimental, partial burn test cases. Similarly, the initial simulation pressures are based on the pressure at TDC after the compression stroke of a hot motored experimental engine. This point of

maximum compression was the source of the chosen pressure due to the late-phased nature of partial burn combustion assuming to initiate near the TDC position, where pressures and temperatures are highest before energy release from the charge begins. With these values, the conditions that define the set-points for the chemical kinetic simulations were determined and directly related to the experimental engine operating points. These set-points are displayed in Table 5.1 below. Note that the simulation pressures are all initially at the same value. This is the case because, while experimental inlet temperatures vary with set-point, the pressures at TDC for these points vary only a slight amount, from approximately 27.5 atm to 27.8 atm. Such small variations in the initial pressures were neglected, and all simulation set-points were assumed to experience an initial pressure of 27.5 atm.

Table 5.1. Set-points for chemical kinetic simulations based off of experimental data.

Combustion Regime	*Fueling rate (gpm)*	*Engine Speed (rpm)*	*Equivalence ratio (φ)*	*Initial Temperature (K)*	*Initial Pressure (atm)*	*Charge Mass (g)*
Steady State	6	1800	0.28	1210	27.5	0.36688
Partial Burn	6	1800	0.28	1105	27.5	0.36688
Steady State	7.5	1800	0.35	1140	27.5	0.36854
Partial Burn	7.5	1800	0.35	1075	27.5	0.36854
Steady State	9	1800	0.42	1115	27.5	0.37021
Partial Burn	9	1800	0.42	1050	27.5	0.37021

To properly correlate the simulations to the experimental test cases, it is also essential to understand what percent heat release quantities are attainable during

partial burn operation. That is, identify what varying degrees of incomplete charge combustion are typically experienced. Therefore, an effort was made to quantify the achievable burn completeness by looking at previous experimental cases run at partial burn and averaging the percent heat released across each set-point. The heat release data from experimental engine runs were calculated in a manner consistent with the description in Section 4.1.3. Of these, the heat release data from the partial burn cases were averaged over the collected engine cycles for each collected set-point, providing the average percent energy released values used for dictating simulation points. As a result it was confirmed that the Hatz experimental engine has achieved set-points with average percent heat released values ranging from 52% total heat released to as high as 99% heat released. When looking at the CO production predictions, these bounds of combustion 'completeness' encompass the full range of CO production amounts that are predicted in the simulations of Section 5.1.2, validating that the masses predicted are achievable in an experimental environment.

5.1.2. Simulation Results. The CHEMKIN simulation was run for each partial burn set-point relating to the fueling rates of 6.0, 7.5, and 9.0 gpm and the conditions of Table 5.1 discussed above. The constant volume CHEMKIN simulation was designed in such a way that it outputs both mole fraction and mass fraction species evolution during combustion. However, since the feed forward amounts for experimental exploration are on a mass basis, the mass fraction output was the primary area of interest. So, the mass fraction species production results for select species of the 6.0, 7.5, and 9.0 gpm partial burn parameters are depicted in Figures 5.1, 5.2, and 5.3, respectively.

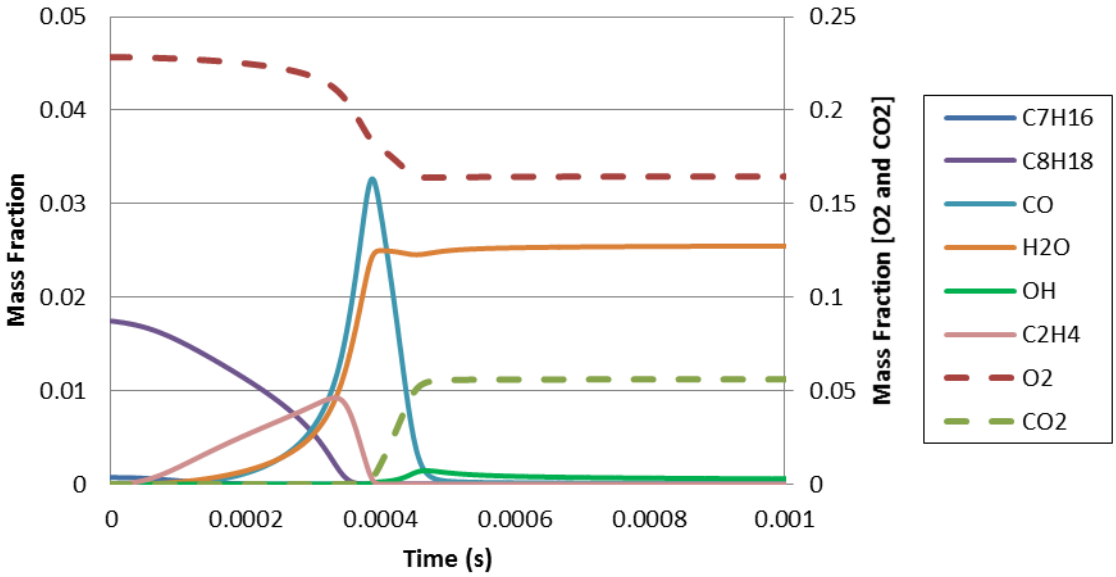

Figure 5.1. Predicted species mass fraction during combustion at 6.0 gpm partial burn set-point.

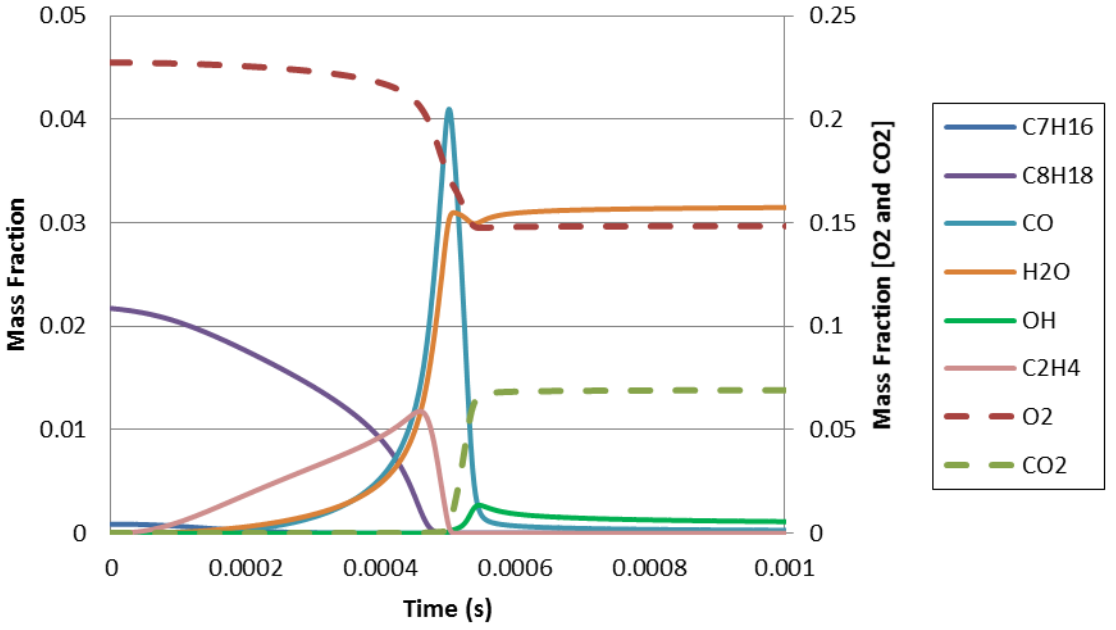

Figure 5.2. Predicted species mass fraction during combustion at 7.5 gpm partial burn set-point.

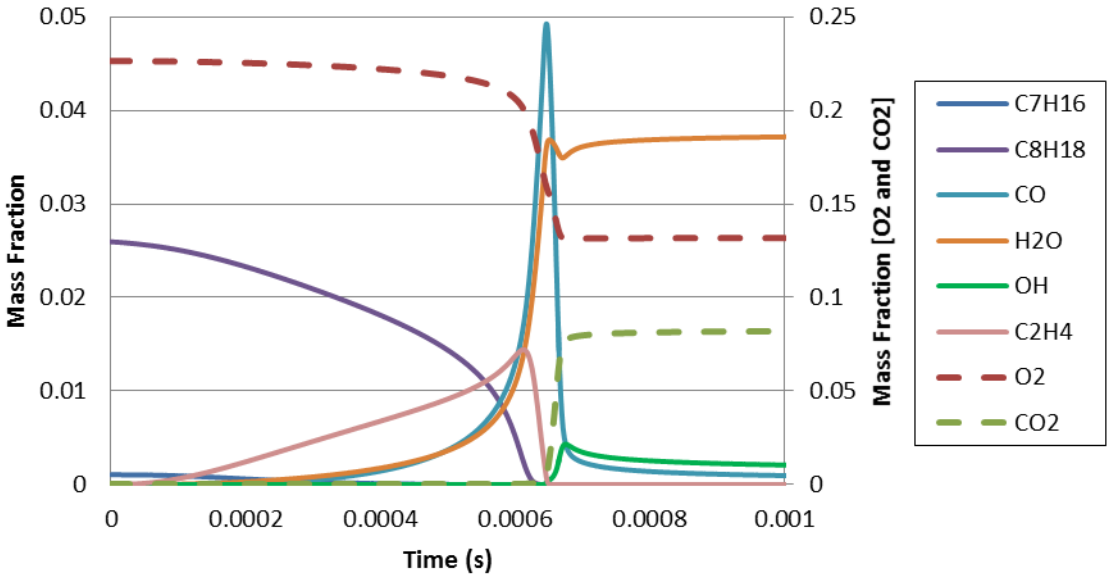

Figure 5.3. Predicted species mass fraction during combustion at 9.0 gpm partial burn set-point.

These figures demonstrate that as expected, when under a situation of complete charge burn, combustion would result in extremely low CO content in the final products. However, there is a notable spike in CO as an intermediate species of combustion and, under partial burn circumstances, these intermediate charge compositions become the end products of incomplete charge consumption. This means that CO as a combustion product would significantly increase under partial burn circumstances to the point that, under some set-point circumstances, nearly 5% of the resultant products are CO.

Since severity of simulated partial burn is based on a percent heat release, it is helpful to observe the percent heat release progression alongside the CO evolution. CO mass fraction produced and heat release are plotted in Figure 5.4 for the 7.5 gpm load case.

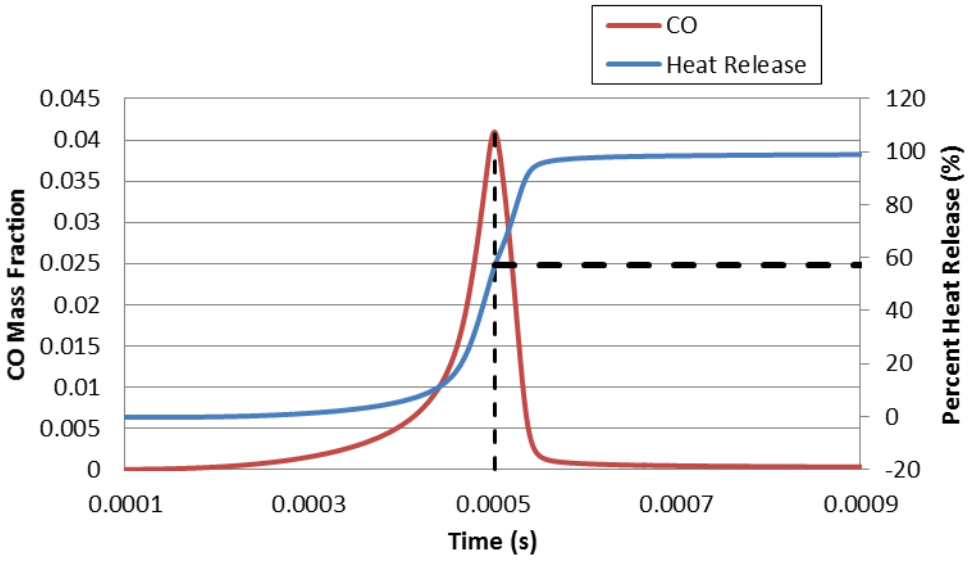

Figure 5.4. CO production and percent heat release for 7.5 gpm partial burn.

From Figure 5.4 it can be seen that the maximum predicted CO production would occur at a combustion event stopping after roughly the 56% energy release point. Such a quantity is quite attainable within the partial burn regime, as it falls within the range of previously run experimental heat release conditions.

It is curious to compare the CO progression with respect to heat release between set-points to identify commonalities in the CO progression. At the same time, it is also possible to convert the mass fraction of CO to an actual mass amount produced by taking into account the known charge mass of each set-point, displayed above in Table 5.1. Figure 5.5 plots these CO mass values against heat release.

When looking at CO production for all three fueling rate set-points against heat release, it becomes clear that the peak in production is around the 56-57% heat release

point under all three instances. In all of these partial burn simulation conditions, the CO production follows a very similar progression in relation to the heat released.

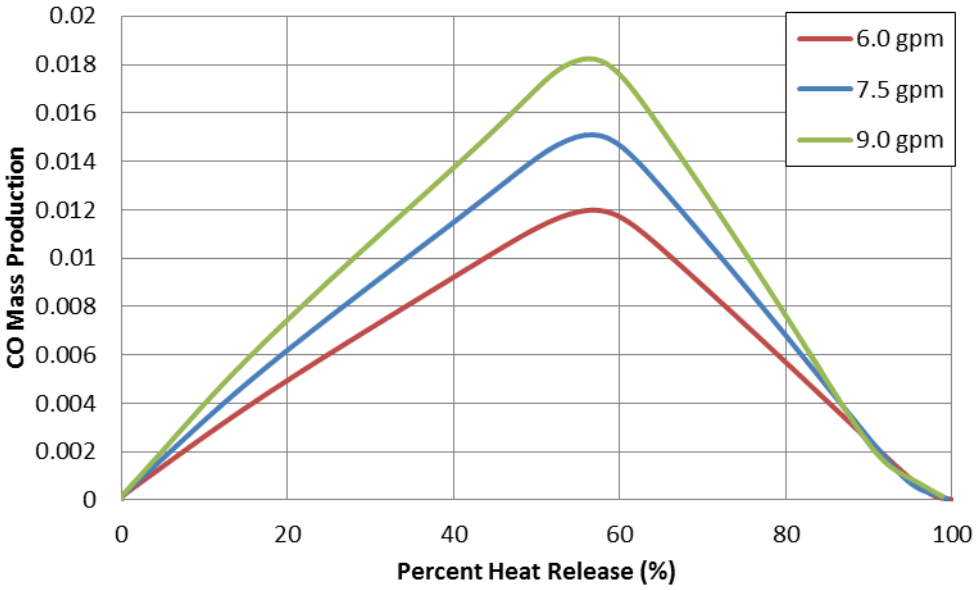

Figure 5.5. CO mass production vs. heat release at 6.0, 7.5, and 9.0 gpm partial burn cases.

5.2. NEXT-CYLCE RESIDUAL CARRYOVER

Regardless of whether external EGR is utilized, internal combustion engines inherently allow a portion of exhaust gas products to become trapped internally in the cylinder from one cycle to the next as a result of engine geometry and valve timings. This inherent feed-forward mechanism is the basis for the nature next-cycle carryover of CO. This internally trapped EGR has been studied by others and can be approximated based on previous researchers' empirical models. Utilizing such models, cycle-to-cycle

feed forward amounts of the simulated product mixture were calculated based on the specific geometry and engine parameters of the experimental Hatz engine for use during experimental gas injection investigations.

5.2.1. Residual Gas Fraction Calculation. While the simulations shed light on the various species produced under partial burn conditions, this does not quantify the mass amounts of the individual residual species that are fed forward to future engine cycles as internally trapped residuals. Therefore, a quantitative look into the feed forward mass amounts of the predicted exhaust species must be performed. To calculate the amount of inherently trapped EGR, that is, the residual gas fraction, a predictive model from [38] was employed, which accounts for both the gas trapped in the cylinder at exhaust valve close (EVC) and the gas present due to backflow from the exhaust to the cylinder during intake/exhaust valve overlap. The first contributor to the forward-fed EGR, the gas trapped in-cylinder at EVC, is relatively simple to determine, and can be found using basic knowledge of the compression ratio and set-point pressure and temperature averages. However, the flow behavior during valve overlap is far more complex, increasing the difficulty in modeling such backflow amounts. This backflow into the cylinder is a significant contributor to the internally trapped residuals.

The first necessary calculation for the predictive model is that of the engine specific Overlap Factor (OF). This factor characterizes the flow passage during the backflow period for a specific engine's geometry. The empirical expression for overlap factor, in degrees/meter, is shown in Equation 39 [38]:

$$OF = \frac{1.45}{B}\left(107 + 7.8\Delta\theta_{ov} + {\Delta\theta_{ov}}^2\right)\frac{L_{v,max}D_v}{B^2} \tag{39}$$

where B represents the engine bore in mm, $\Delta\theta_{ov}$ is the crank angle degrees of valve overlap, $L_{v,max}$ is the maximum valve lift in mm, and D_v is the maximum valve seat diameter, also in mm. The latter two quantities, $L_{v,max}$ and D_v, are the averaged maximum values of the intake and exhaust valves. The expression of Equation 39 provides a good estimate of the OF value for engines with typical cam profile designs. Utilizing this expression, and the variable values corresponding to the engine in Table 5.2, the Hatz experimental engine at Missouri S&T was calculated to have an OF of 0.6585.

Table 5.2. Hatz engine overlap factor parameter values.

Overlap Factor	*B (mm)*	*Valve Overlap (CAD)*	*Max Valve Lift * (mm)*	*Valve Inner Seat Diameter * (mm)*
0.6585	97	33	8.912	32

** Average of maximums between intake and exhaust valves*

After determining the OF for the engine, an expression for the residual gas fraction could be evaluated. Together with Equation 39, the actual residual fraction carryover amount, α_r, can be calculated with Equation 40:

$$\alpha_r = 0.401\frac{OF}{N}\left[1 - e^{\left(-4.78\left(1-\frac{P_i}{P_e}\right)^{0.7} - 153.8\left(1-\frac{P_i}{P_e}\right)^{4.5}\right)}\right]\frac{P_e}{P_i}\frac{T_i}{T_e} + \frac{1}{r_c}\frac{P_e}{P_i}\frac{T_i}{T_e} \tag{40}$$

where N is engine speed, P_i is inlet manifold pressure, P_e is exhaust manifold pressure, T_i is inlet charge temperature, T_e is exhaust gas temperature, and r_c is the compression ratio of the engine. Since the inlet and exhaust pressures and temperatures tends to vary from one engine operating set-point to the next, this residual fraction fluctuates as well and needs to be calculated for each individual operating set-point.

5.2.2. Feed Forward Residual Amounts. Through the use of the residual gas fraction analysis described in Section 5.2.1, the residual gas fraction was capable of being determined for the individual engine set-points under consideration. For calculation of the feed forward percentages, as defined by Equation 40, the necessary state definition values were taken directly from previously collected Hatz experimental engine data at each of the baseline engine set-points with the PRF96 fuel. Among these required parameters for the feed forward amount calculations were the inlet pressures and temperatures, and exhaust pressures and temperatures at each engine set-point. The intake temperatures and pressures used were the average values from 1000 consecutive engine cycles, measured across the entire engine cycle during the representative baseline set-points. Intake pressures for each set-point were taken from upstream pressure measurements in the intake manifold, while exhaust pressure values were taken as the average pressure between EVO and EVC from a pressure transducer placed close to the exhaust port of the engine. Exhaust temperatures were approximated based on averaging the exhaust manifold temperatures between EVO and EVC that were recorded by an exhaust port mounted thermocouple. Table 5.3 depicts

the feed forward set-point parameters and their resulting internally trapped residual gas fractions.

Table 5.3. Residual gas fraction set-points.

Fuel Rate (gpm)	*Intake Temperature (K)*	*Exhaust Pressure (bar)*	*Intake Pressure (bar)*	*Exhaust Temperature (K)*	*Residual Gas Fraction*
6.0	475	0.991	0.965	553	0.0608
7.5	470	0.988	0.968	599	0.0552
9.0	466	1.004	0.965	692	0.0483

Logic dictates that the feed forward mass of CO not only depends on the residual gas fraction, but also the amount of CO produced during an engine cycle, which is directly related to the percent heat released in that cycle. Constant volume simulations predicted CO production maximums near a 56% heat release point. As mentioned previously, the experimental Hatz engine has been run under conditions of as low as 52% average heat release. While this is not assumed to be a minimum obtainable value, it acts as a validation that the Hatz engine possesses the potential to achieve the predicted peak CO production amount near a 56% heat release point, along with any other value of predicted CO production curve.

By assuming a homogeneous product mixture after partial burn, utilizing the simulated production masses, and accounting for the residual gas fractions, the CO feed forward amounts were determined for the range of partial burn conditions. Feed forward mass amounts are plotted in Figure 5.6.

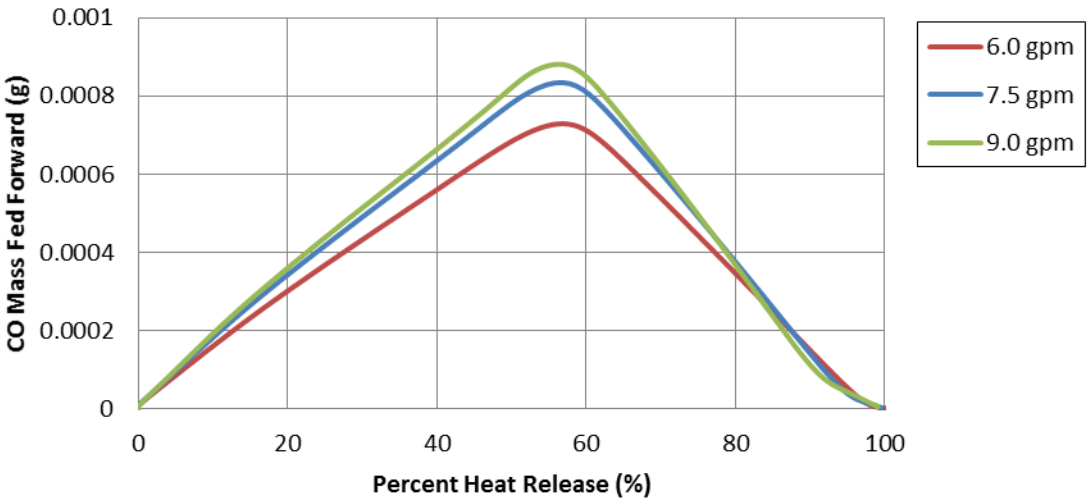

Figure 5.6. Next-cycle feed-forward mass of CO at 6.0, 7.5, and 9.0 gpm partial burn cases.

While it was seen that there is potential for a rather significant amount of CO to be produced during these partial burn instances, it is clear that the amount of this CO carried to the next cycle as internally trapped residuals is only a small fraction of the total generated. It is observable from these feed-forward values that the actual feed forward amounts of CO at the three engine load cases do not vary as significantly as the mass amounts produced at the three cases, as shown in Figure 5.5. This is due to the fact that, while CO production experiences a marked increase as the fueling rate climbs from 6.0 gpm to 9.0 gpm, when taking into account the set-point dependent residual gas fraction that follows an opposite decreasing trend, the delta between the cases is significantly reduced. Since the current study is interested in the potential impact of CO on combustion, it is of interest to begin the experimental exploration of the CO impact

with the maximum potential CO amounts. As such, the resulting maximum feed-forward mass amounts of CO are available in Table 5.4.

Table 5.4. CO predicted mass production amounts.

Fuel Rate (gpm)	*Max CO Mass Fraction*	*Max CO Production (g)*	*Residual Gas Fraction*	*Max Feed-Forward CO (g)*
6.0	0.03267	0.01199	0.06082	0.0007290
7.5	0.04098	0.01510	0.05525	0.0008343
9.0	0.04923	0.01822	0.04831	0.0008803

These values are the mass amounts that were then taken and fed into the experimental Hatz HCCI engine in order to determine their impact on next-cycle combustion and the related cyclic dynamics. Additionally, although simulation investigation was performed across the fueling rates of 6.0, 7.5, and 9.0 gpm, the focus of the experimental exploration was limited to the mid-point fueling rate instance of 7.5 gpm. This was done in order to delve deeper into the fundamental variables of the CO injection as opposed to taking a broader look at the effect that equivalence plays in this effect. Therefore, the feed maximum forward mass of 0.0008343g of CO became the primary interest. It should be noted though, that any future work regarding specific control algorithm generation would need to investigate the specific impact at various equivalence ratios in more detail before robust control methods could be employed.

6. EXPERIMENTAL SPECIES INJECTION

The influence that CO possesses on next-cycle engine performance was investigated through the use of precisely controlled experimental in-cylinder injection tests. These were approached with an attempt to relate the CO injection back to the effects of the internally trapped CO during partial burn and to explore the underlying potential for manipulating HCCI engine dynamics through the use of direct in-cylinder CO injection.

CO became the primary species of interest in this investigation due to its likely presence during incomplete combustion and its potential for nonlinear impact on engine dynamics that was found in the literature, as discussed in Section 2. The predicted feed forward CO mass amounts under achievable HCCI incomplete burn conditions from Section 5 were the basis for all injection quantities during experimental CO injection tests.

It should be noted that, with the injection of an active species, there are still a variety of potential sources behind any combustion influence experienced. One of the intriguing aspects of CO is its potential for dynamically impacting the chemical kinetics of the combustion evolution. That is, the addition of CO may possess the ability to accelerate or decelerate the chemical reactions that lead to a simultaneous cylinder mass combustion event and impact the intermediate reactions that occur during combustion. Such kinetic impact could manifest itself as significant alterations of engine performance and cycle-to-cycle dynamics.

Alternatively, the addition of active species into the combustion chamber will also be a known addition of energy to the system. Even if lacking a chemical kinetic effect, an active species will still be altering the chemical energy in the system, effectively increasing the amount of fuel that the combustion event has available for utilization. The question then becomes whether the combustion event is able to utilize this newly available energy. Therefore, any impact seen requires teasing away to separate the likely energy effect from any kinetics effect.

A third possible effect is that of a thermal impression. HCCI dynamics are heavily governed by the initial charge temperature and the thermal boundary conditions, that is, the engine block temperatures. Increases in initial charge temperature allow critical ignition temperatures to be reached earlier during compression, and a heated engine block reduces charge energy losses though heat transfer. This relationship is directly eluded to by the control method utilized on the Hatz experimental engine, whose set-point stability is directly manipulated by altering intake charge temperature. So, the injection of an expanded gas specie may impact the thermal conditions defining the initial charge temperature or the block temperature over time.

Taking these aspects into consideration, the experiments were aimed at understanding the injected CO's influence on cycle-to-cycle dynamics, determining whether such an influence has potential for controlled driving of combustion dynamics, and isolating the sources of impact on combustion, whether they are chemical kinetics, energy addition, or thermal effects.

6.1. BASELINE HCCI DYNAMICS

Before diving into CO's impact on the cycle-to-cycle dynamics of an HCCI engine, it is first beneficial to understand general HCCI tendencies and define baseline conditions seen under typical engine operation. These baseline experiments provide a standard picture of the HCCI engine's behavior to act as a reference against future experimental set-points. It should be noted that the 7.5 gpm fueling rate became the sole focus of this work, at a constant engine speed of 1800 rpm. The two general baseline engine set-points for the primary case of 7.5 gpm were collected over 1000 engine cycles and are detailed in Table 6.1.

Table 6.1. Baseline set-point summary.

Operating Regime	*Intake Temperature (°C)*	*Fuel Rate (gpm)*	*Engine Speed (rpm)*	*Equivalence Ratio (φ)*	*Avg. CA10 (CAD)*	*Avg. CA50 (CAD)*	*IMEPg (bar)*	*COV of IMEPg (%)*
Partial Burn	196	7.5	1800	0.39	370.8	377.3	1.63	17.80
Steady State	203	7.5	1800	0.39	364.2	366.7	2.11	4.02

The case under the most scrutiny in this work was the partial burn instance identified in the table of baseline set-points. Table 6.1 highlights the difference in performance and general engine behavior between a stable operating point and that of the partial burn regime. In general, partial burn is characterized by lowered IMEP values, retarded CA10 and CA50 heat release points, and increased COV.

It should be noted that, because the Hatz experimental setup is an air cooled engine, and given the nature of HCCI being reliant on the governing physics of the intake charge, its operating set-points tend to be heavily governed by the initial charge intake and boundary conditions. As a result of this, the natural day-to-day variance in the engine's ambient conditions impacts engine performance significantly. Therefore, it is often necessary to adapt to the conditions of the day in order to achieve the same operating behavior, which has caused some of the partial burn set-points within this investigation to have intake temperatures that vary by a degree or two from this baseline. Such cases are noted.

It can also be noted that the 203°C stable operating point used in this study is by no means the 'most stable' point achievable by the engine. It merely represents a more stable condition chosen for use here as a stable reference and goes to show that an intake temperature difference of only 4 degrees can have a substantial impact on stability and performance. Intake temperatures could continue to be increased in order to drive operating parameters toward a stronger set-point still.

Looking at the cycle resolved performance data such as IMEPg, the difference in the baseline set-points' stability is captured by the change in magnitude and the variance within a set-point, depicted in Figure 6.1 below.

As expected, the stable point with a 203°C intake temperature maintains a fairly tight band of IMEP values, with little stray from the mean value of 2.11 bar. On the contrary, the partial burn baseline shows characteristics that can be expected in an unstable operating region, such as a lower mean IMEP value of 1.63 bar, along with the

increased COV, depicted by the wide spread in data points. Similar characteristics can be seen in SOC, represented by CA10, and combustion phasing, represented by CA50, of the two baseline points in Figure 6.2.

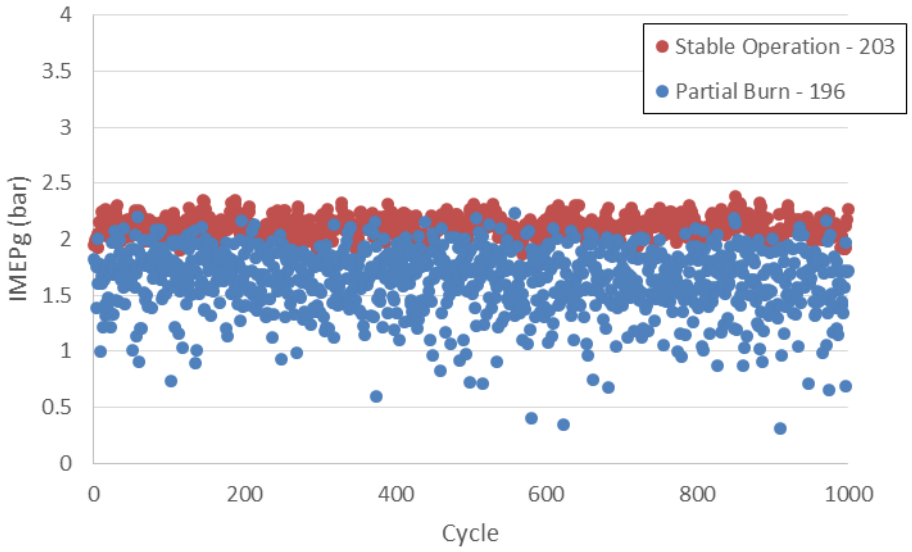

Figure 6.1. Cycle-to-cycle IMEPg for baseline set-points.

Figure 6.2 demonstrates the wide distribution band of heat release and performance data that identifies with partial burn's instability compared to the steady state case. The retarded heat release of partial burn in CA10 and CA50 is likewise easily observed here. Generally speaking, as intake temperatures are reduced at a given fueling rate, CA10 and CA50 will progressively phase later in the engine cycle until combustion becomes unsustainable. Most other engine characteristics have a tendency

to follow similar trends of a mean value shift and increase in variance when entering partial burn operation.

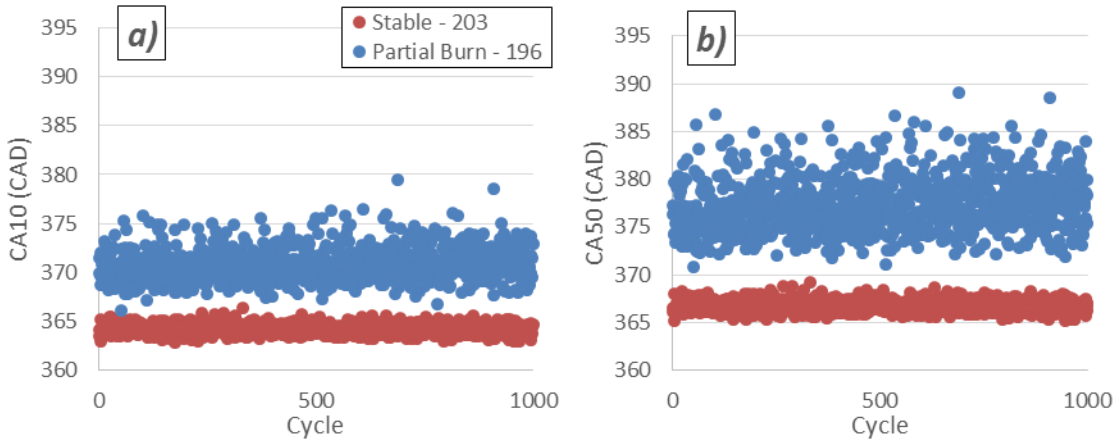

Figure 6.2. Cyclic baseline engine performance. *a*) CA10. *b*) CA50.

Apart from general characteristics and mean values of the collected data, a glance at the cycle-to-cycle dynamics is critical in understanding the characteristic engine behavior at these set-points, especially since recognizing the shift in these dynamics is essential in understating CO's impact on HCCI. Return maps provide one such look at these cycle-to-cycle interactions by pulling out correlations between a given cycle and its next successive cycle. Such representations of the baseline conditions are observable in Figures 6.3 and 6.4.

The steady state return maps in Figure 6.3 represent a common instance of stochastic engine behavior with a random Gaussian distribution and little structure. Return maps with relationships other than a stochastic grouping are present in the

partial burn instance of Figure 6.4, with structured, deterministic 'arms' of data points extending from the stochastic base gatherings. This structure is an indicator of increasingly prevalent deterministic relationships, determinism, in the partial burn data. This structure is observable on both the IMEPg and the CA10 return maps.

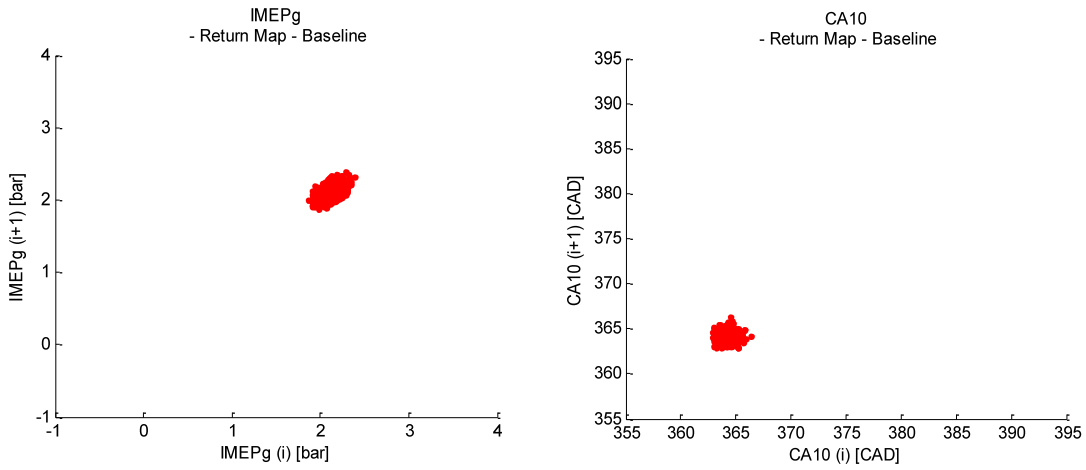

Figure 6.3. Baseline steady state return maps. *a*) IMEPg. *b*) CA10.

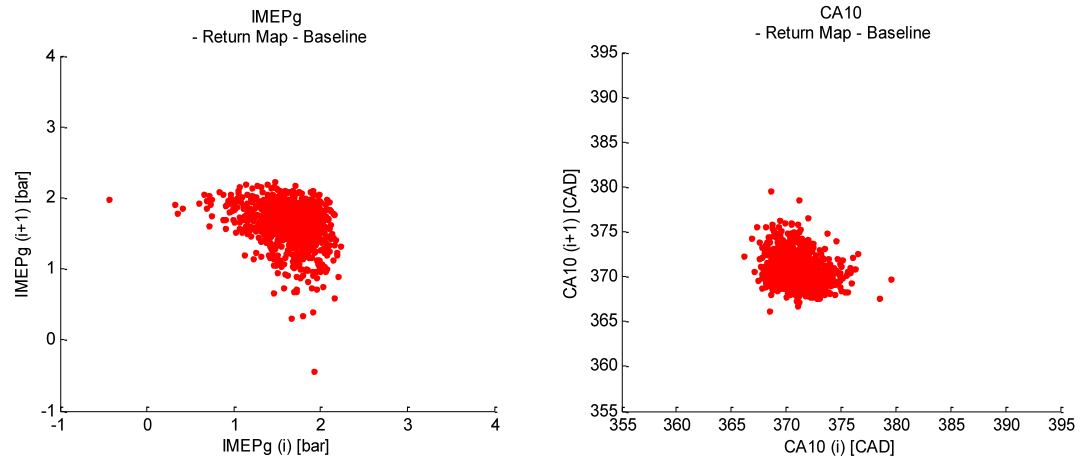

Figure 6.4. Baseline partial burn return maps. *a*) IMEPg. *b*) CA10.

Additionally, symbol sequencing was employed as means of a more quantitative classification of the dynamics present in the partial burn baseline set-point. For this, the techniques described in Section 3 were performed on the same 1000 cycle partial burn data from above. Consistent with the discussion in Section 3, a binary partition was used, and sequence length was determined through the use of Shannon entropy.

Shannon entropy was used in order to determine the optimal sequence length for isolating the presence of determinism in the data. Shannon entropy was calculated for the IMEPg data of the baseline partial burn set-point with a binary symbolic partition at increasing sequence lengths. The results are visible in Figure 6.5.

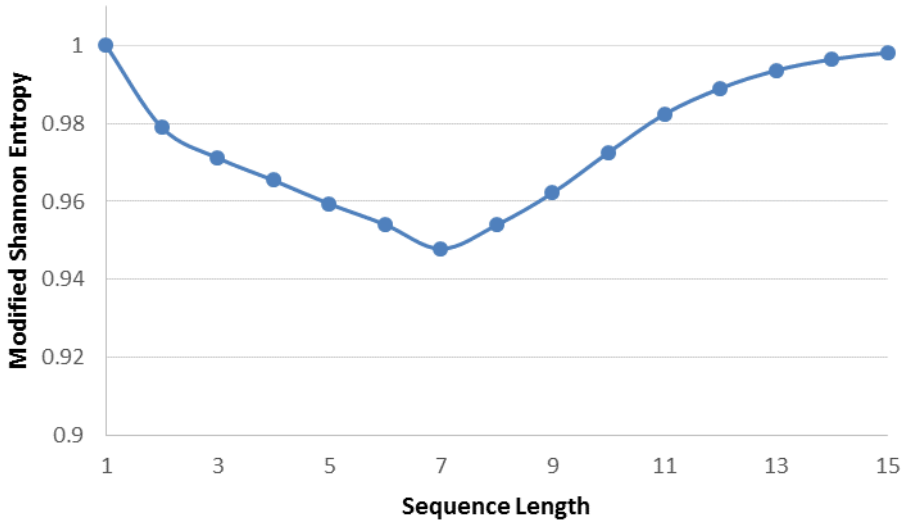

Figure 6.5. Modified Shannon entropy for IMEPg partial burn baseline data.

Shannon entropy values reach their minimum at a sequence length of 7 cycles. This indicates that the influence of previous engine cycles on IMEPg data can be traced

back to the past 7 cycles and therefore, that this is the sequence length capable of identifying the most deterministic behavior present in the data. While this may be the ideal sequence length to use, application of this sequence length was not feasible for many of the data-sets of this investigation. The analysis must be able to maintain a large enough ratio of data to possible sequences that it allows for statistically meaningful results. Symbol sequencing in this work is utilized in the analysis of as few as 450 engine cycle segments of data to characterize engine dynamics before and after species injection sequences. A sequence length of 7 would result in a ratio of data size to number of possible sequences of 450:128, which is not an appropriate ratio to produce reliable results. So, as a means of increasing this ratio, sequences of length 5 and 6 were considered without greatly impacting the analysis since their modified Shannon entropies only deviate from the minimum value by 0.011 and 0.006 respectively. When applying these sequence lengths to the baseline partial burn data, the symbol sequence histograms of Figure 6.6 results.

It was noticed that in reducing the sequenced length from 7 to 6, little was lost in comparing the two resultant histograms. In fact, value was likely added due to the increased ratio of data to possible sequences. By adhering to a sequence length of 6, this ratio was maintained within the bounds of sequencing analysis used by other researchers [39, 14]. Looking at analysis with sequence length 5, there was additional notable loss of determinism depicted.

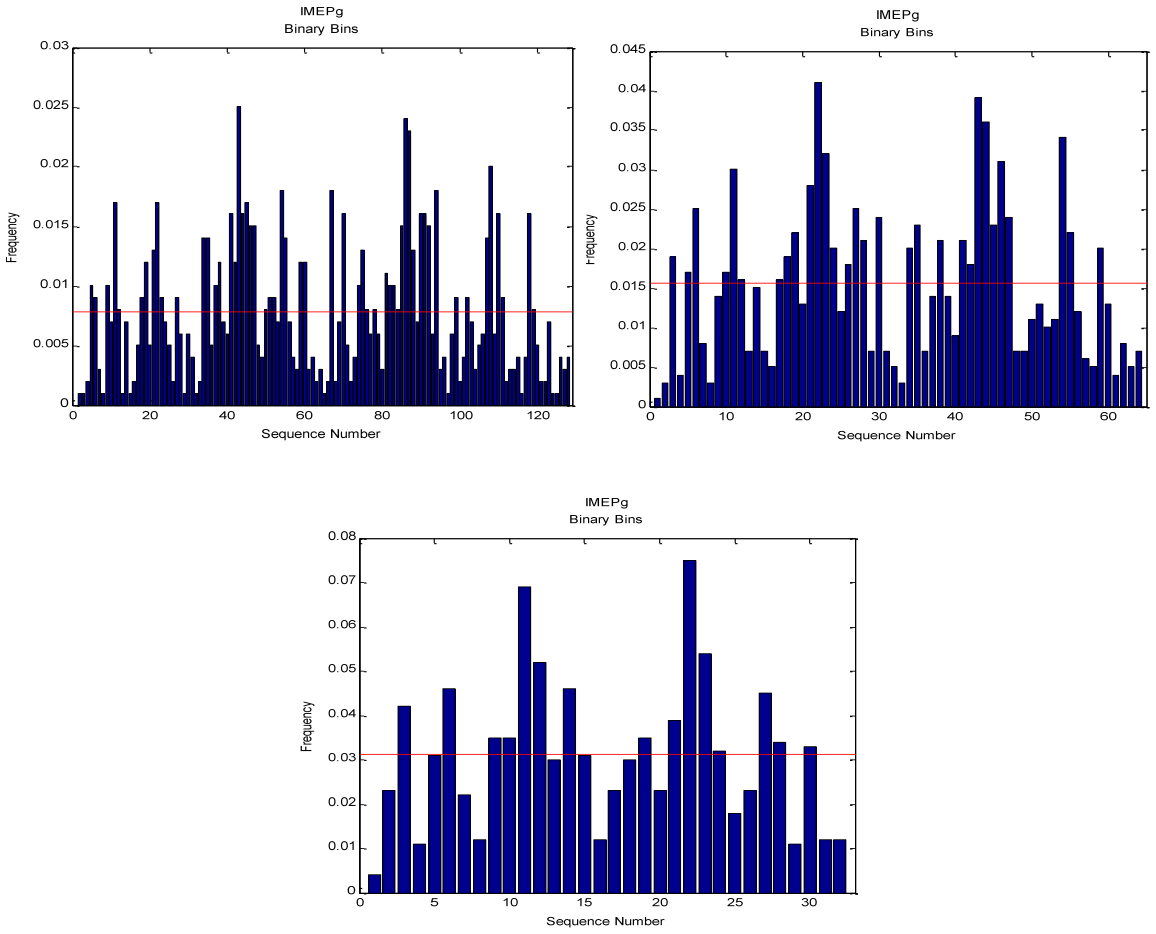

Figure 6.6. Binary bin symbol sequencing of baseline partial burn IMEPg data with varying sequence length. *a*) Length of 7. *b*) Length of 6. *c*) Length of 5.

For example, when looking at frequency occurrence in sequence length 6 data, there are additional peaks apart from the dominant sequences of 21 and 42 that occur at only slightly lower frequency. However, in sequence length 5 data, the two peak sequences of 10 and 21 occur notably more often than all other sequences. As a result, the sequence length of 6 was chosen to be used as the standard for all sequence length analysis going forward. This sequence maintained the repetitive '010' and '101'

patterns buried in the data, characteristic of switching back and forth between zone while allowing for a reasonable data sample size.

The defined symbol sequencing analysis parameters with sequence length of 6 was utilized for analysis of the baseline experimental data. The results of the partial burn baseline can be seen in Figure 6.7 below.

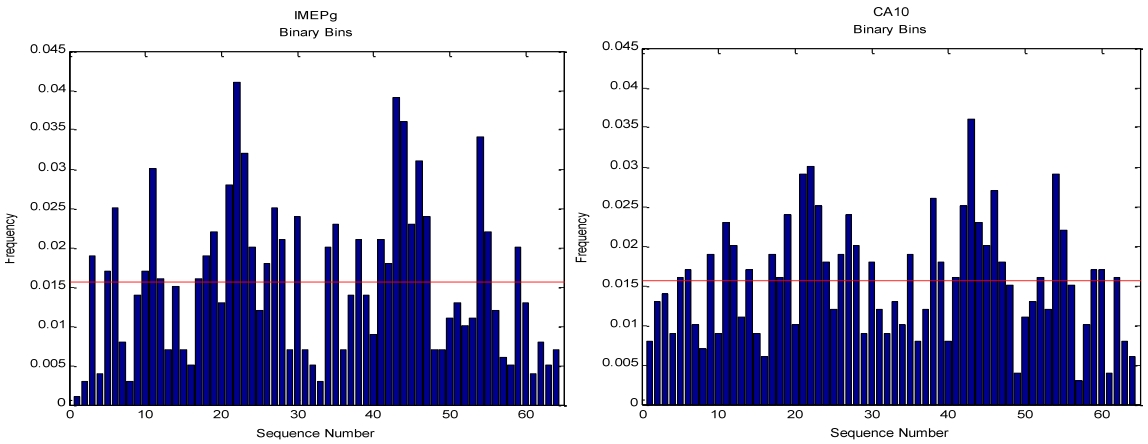

Figure 6.7. Symbol sequence distribution of partial burn baseline. *a*) IMEPg. *b*) CA10.

The key aspects to note from Figure 6.7 are the peaks in the occurrences of sequences 21 and 42 above. These sequences converted back to binary are '010101' and '101010', respectively. These cases of alternating engine cycles above and below the binary partition represent alternating cycles between early and late phased combustion events. Such patterns and general dominance by a few sequences are expected in the partial burn regime. Other prevalent sequences in both the IMEP and

CA10 data are 10, 22, 45, and 53, which are all sequences that are heavily composed of oscillations between the two symbolic zones.

Stable operation does not experience the same general distribution of sequence occurrences. Instead, a rather even distribution of cycle-to-cycle sequences is expected. This even distribution of sequences represents the dominance of a more random, stochastic engine behavior, which is characteristic of stable operation. Figure 6.8 represents the IMEPg and CA10 symbol sequence analysis for the 203°C steady state condition of 1000 consecutive engine cycles.

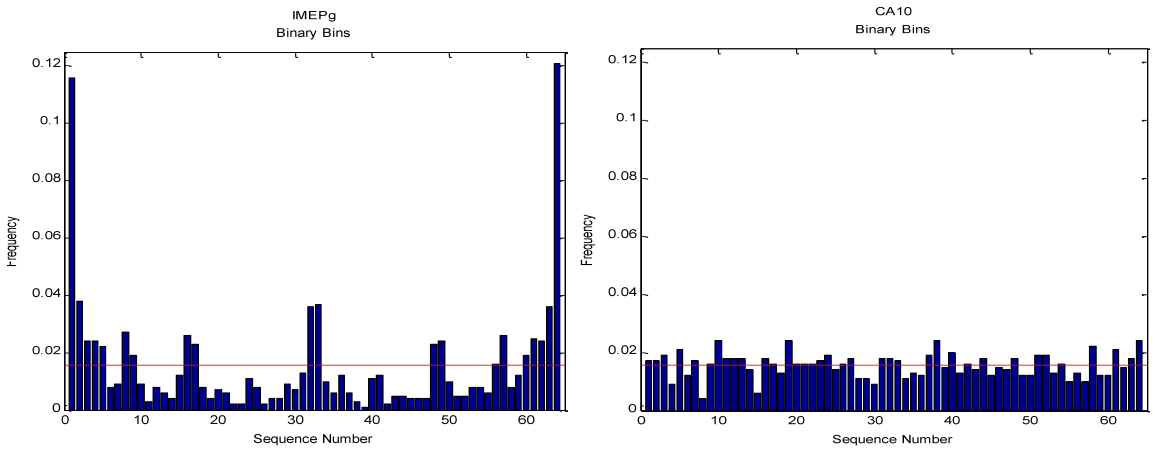

Figure 6.8. Symbol sequence distribution of steady state baseline. *a*) IMEPg. *b*) CA10.

It can be seen in Figure 6.8 that the distribution of sequences is fairly even in the case of CA10, with two primary peaks presenting themselves in the IMEPg analysis. The vastly dominant peaks that frame the IMEP data are that of '000000' and '111111'. In this steady state operating case, these peaks represent steady behavior in IMEPg

output, with 6 consecutive engine cycles resulting in similar output. This would not be a surprise in a true steady state instance. The other two sequences that catch attention are the centered sequences 31 and 32, which represent ‘011111’ and ‘100000’. These are also indicative of steady behavior, but simply preceded by a single cycle at the opposing state. The red line across the data is the baseline frequency, the frequency indicative of a random Gaussian distribution of data. Comparing the series data to the calculated baseline frequency of 0.0156, it is observable that the CA10 data sequences all fall quite close to the value, supporting the idea of stochastic dominance at steady state operation.

6.2. CONTROLLED CO INJECTION

Building off of the baseline HCCI set-point analysis and getting into the core investigation, long sequences of CO injections were performed on the engine while operating at the baseline set-points. The injected mass of CO was determined by the partial burn feed forward mass amounts that were predicted in Section 5. 1500 cycle data sets were taken in order to fully capture the cycle-to-cycle dynamics of the partial burn region before injection, the impact that injection has on those dynamics, and the resulting cyclic behavior resulting after injection is ceased. Additionally, efforts were made to isolate the source of any change in cycle-to-cycle dynamics, whether it is chemical kinetics, energy addition, or thermal effects.

6.2.1. CO Impact at Partial Burn. CO injections of mass amounts equal to predicted maximum feed forward values of 0.0008343g per cycle were injected in-cylinder for 600 consecutive cycles at a partial burn engine set-point with an intake

temp of 199°C. Additionally, approximately 450 engine cycles were collected on both sides of the injection window in order to monitor engine dynamics leading into and exiting the CO addition. When looking at the injection results, depicted in Figure 6.9 and Figure 6.10 it is immediately apparent that the CO injections had a significant impact on IMEPg and the combustion development captured by CA10 and CA50.

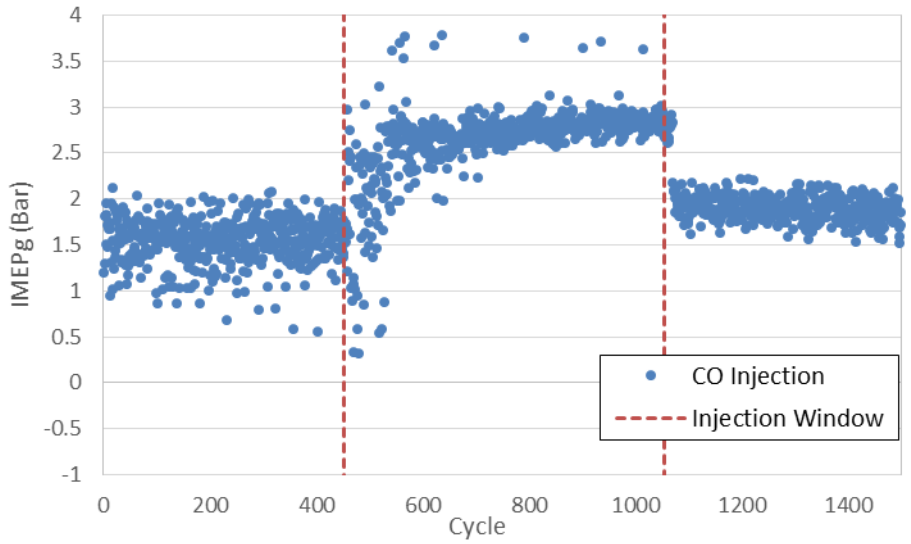

Figure 6.9. IMEPg of max predicted CO injected for 600 cycles at partial burn.

During CO injection, IMEPg is aggressively increased. Such advancement is likely tied to chemical effects to some degree, including any energy added to the system through the CO. During this IMEP advancement there is a noticeable change in the cyclic dynamics leading into the stronger resulting output. IMEPg experiences an initial increased cyclic dispersion that is then pushed to a point of stability. The CO injections drive combustion from an initially unstable operational point at the edge of the partial

burn regime before CO addition to a more stable point after injections subside. This is observable in Figure 6.9 by the wide distribution of data points leading into injection window, and a tighter band of data resulting after injections.

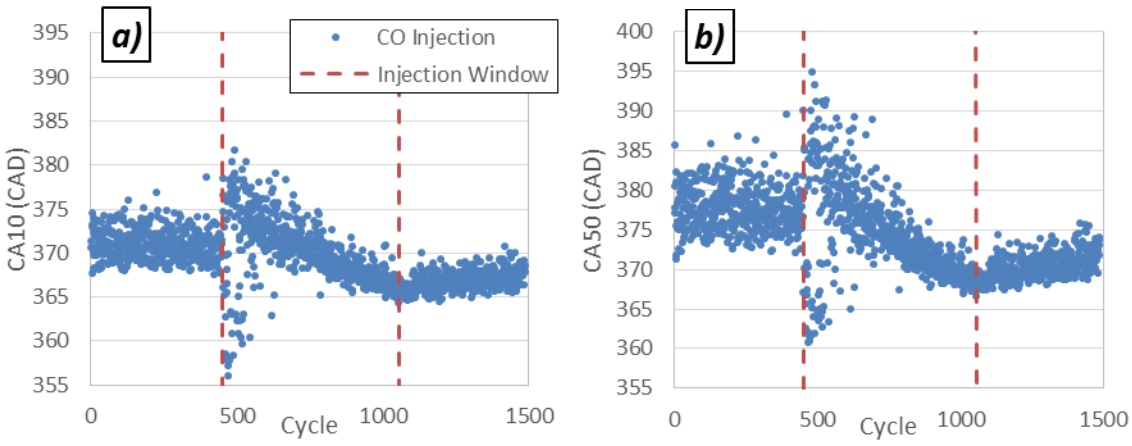

Figure 6.10. Effect of max predicted CO injected at partial burn for 600 cycles. *a*) CA10. *b*) CA50.

Along with this trend of driving IMEP toward a stronger, more stable point, the injections likewise drive the combustion parameters of CA10 and CA50 to more advanced and more stable points, as seen in Figure 6.10, again characterized by the narrower distribution band following injections. The average values leading into and out of injections are outlined in Table 6.2.

Not only are the mean values shifted toward stronger operating values, but the resulting increase in stability is validated further by looking at the variance in cycle averaged parameters in the regions immediately surrounding injection. There is a

decrease in COV of IMEP, CA10, CA50, and Burn Duration from pre to post injection operation. These COV values are calculated in Figure 6.11, where the decrease in variance can be visualized.

Table 6.2. Mean values of combustion before and after partial burn CO injections.

	IMEPg (bar)	***Peak Pressure Rise Rate (bar/deg)***	***Max Heat Release (kJ)***	***CA10 (CAD)***	***CA50 (CAD)***	***Burn Duration (degrees)***	***Max Cyclic Exhaust Temp (°C)***
Before Inject	1.55	0.21	0.129	371.03	377.43	23.21	421.83
After Inject	1.90	1.19	0.135	366.88	370.76	9.91	425.71

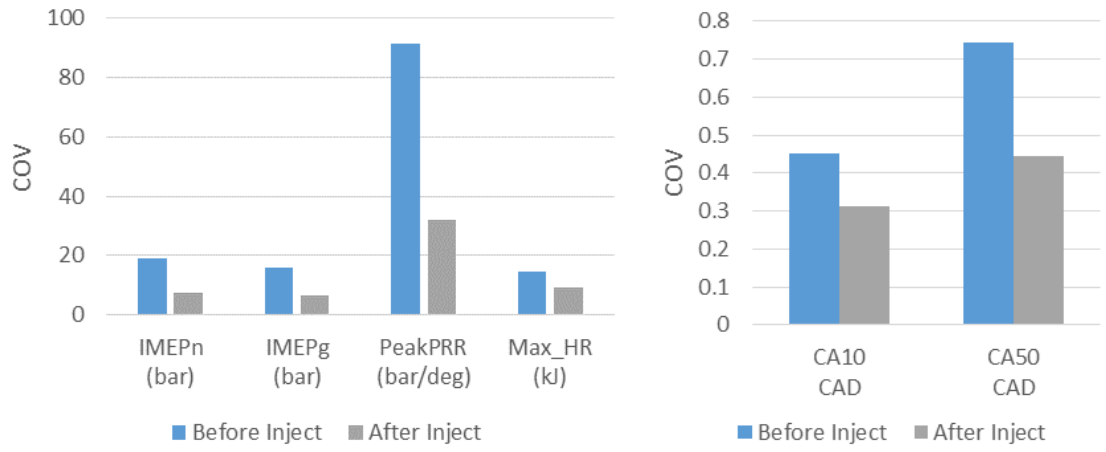

Figure 6.11. COV before and after 600 cycle CO injection sequence at partial burn.

While the final resulting CA10 and CA50 operating characteristics are advanced on a macroscopic scale across the data, the truly interesting aspect of the species addition is the occurrence of an immediate initial retardation of the CA10 and CA50

values. A more in depth look at the dynamics associated with this is addressed later, along with additional experiments run to help tease out the source of this jump.

After the jump at the start of injection, a progressive, steady advancement of CA10 and CA50 values in Figure 6.10 occurs, along with a steadily decreasing burn duration, across the injection sequence. This progressive shift is supportive of the idea that a small change in the thermal conditions may be occurring as heat builds over time. This is likely the result of the engine heating due to the stronger combustion events experienced over many successive cycles. As the boundaries of combustion heat up, the combustion phasing is advanced toward a more stable position closer to TDC.

When considering thermal effects, it is curious to take a look at exhaust temperatures. The maximum cyclic exhaust temperatures follow a trend similar to that of IMEP. Figure 6.12 displays these results.

The stronger combustion event initiated by the CO addition is reflected in the jump in maximum cyclic exhaust temperatures in Figure 6.12. However, as CA50 combustion phasing begins to advance and move away from EVO, the peak temperatures move forward and away from EVO as well. This reduces the temperatures measured at the exhaust port, causing the negative slope within the injection window data. Looking at post-injection max exhaust temperatures compared to those initially experienced, there is little change from the initial mean temperature of 421°C to 425°C. This small delta supports the idea that any thermal impact building over the injections is relatively small.

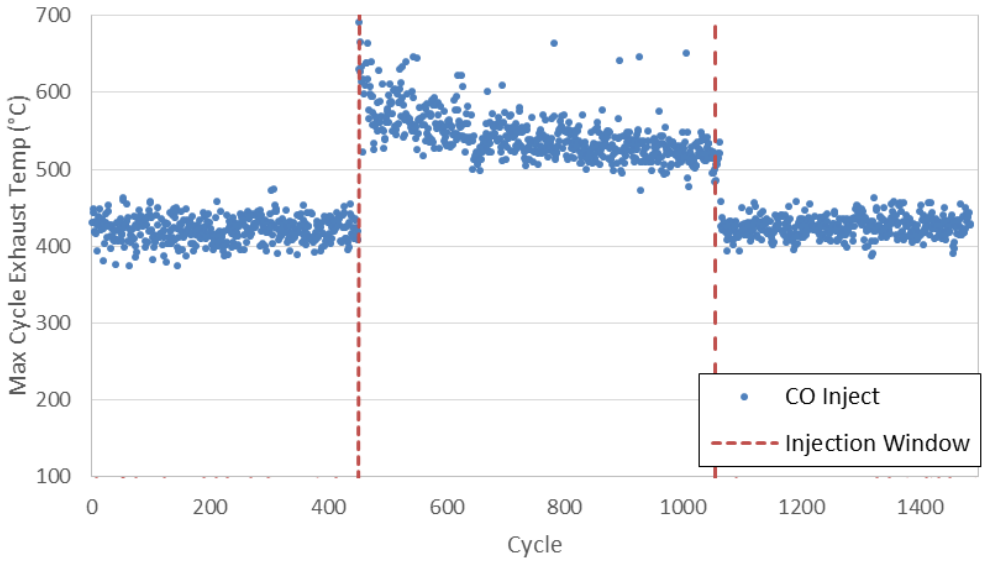

Figure 6.12. Maximum cycle exhaust temperatures during CO injection at partial burn.

When injecting in the partial burn regime, the most intriguing aspect of the IMEPg response is not necessarily in the increased IMEP value itself, but rather, in the shifting dynamics that begin with injection and result in the stable output later in the CO injection sequence. This shift in cycle-to-cycle dynamics could be the key in the utilization of CO as a combustion control mechanism and hold details relating to the behavior experienced in partial burn HCCI operation.

6.2.2. CO Impact at Stable Operation. It is also interesting to observe the same injection mass of CO introduced to a more stable engine set-point. In doing this, the same mass, approximately 0.0008343g, of CO were injected for 600 consecutive engine cycles at a stable operating point with an intake temperature of 203°C. The results, depicted in Figure 6.13 and Figure 6.14 demonstrate a similar general trend as that seen in the partial burn regime of driving up IMEP and overall pushing combustion to a more

stable point. However, injection in this more stable region lacks the initial inhibiting shift in SOC and combustion phasing that was seen at partial burn and likewise has an absence of the amplified transitional engine dynamics experienced with partial burn addition.

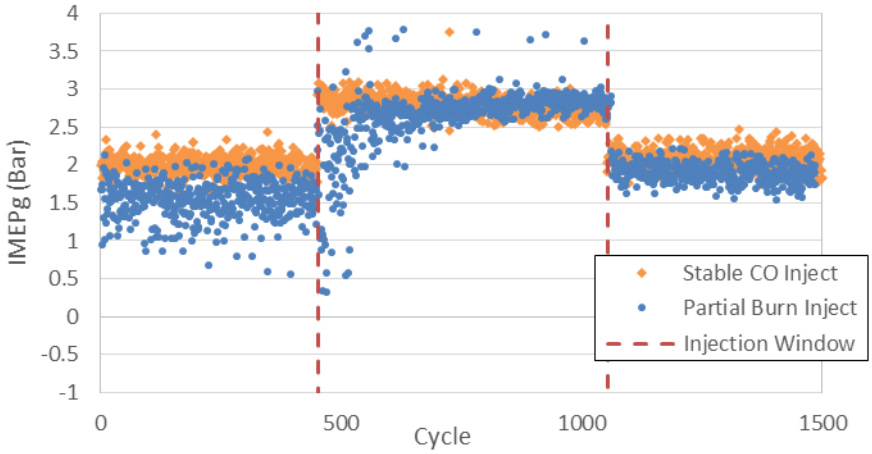

Figure 6.13. Compare CO impact on IMEPg at steady state and partial burn.

When comparing the partial burn and steady state injections, it is apparent that some of the effects of CO become amplified at partial burn operation. The introduction of CO at partial burn experiences an immediate shift, retarding most cycles' SOC and combustion phasing, that is not experienced at a stable set-point. Another aspect seen in partial burn that disappears at steady state injection is a magnification of cyclic dispersion. This is apparent in the heat release parameters and in the IMEPg data over the first several hundred injections.

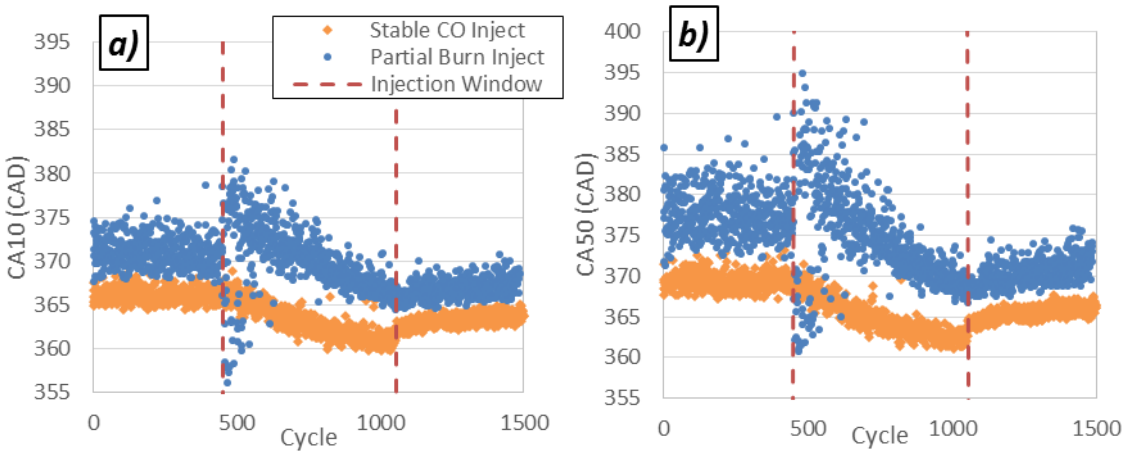

Figure 6.14. Compare injections of CO at steady state and partial burn. *a*) CA10. *b*) CA50.

Honing in on the CA10 and CA50 progression across the injection timeframe, the slow advancement of these heat release characteristics in the steady state injection again supports the thought that a thermal dependency of combustion may be pushing this steady shift forward in heat release characteristics. Also interesting is that the stable point resulting after injections cease does not seem to be sustainable. This can be seen somewhat in the data of both injection set-points above, with a slow drift of CA10 and CA50 values away from the newly established operating point in the last 450 engine cycles collected. When allowing the engine to run for an extended period of time after a similar partial burn CO injection sequence, the engine's behavior reverted back toward a more unstable operating point, similar to its initial state. Figure 6.15 demonstrates this reversion of IMEPg data by showing the initial injection data, along

with two additional datasets that were collected nearly 9 minutes after injections ceased and again at nearly 24minutes after injections stopped.

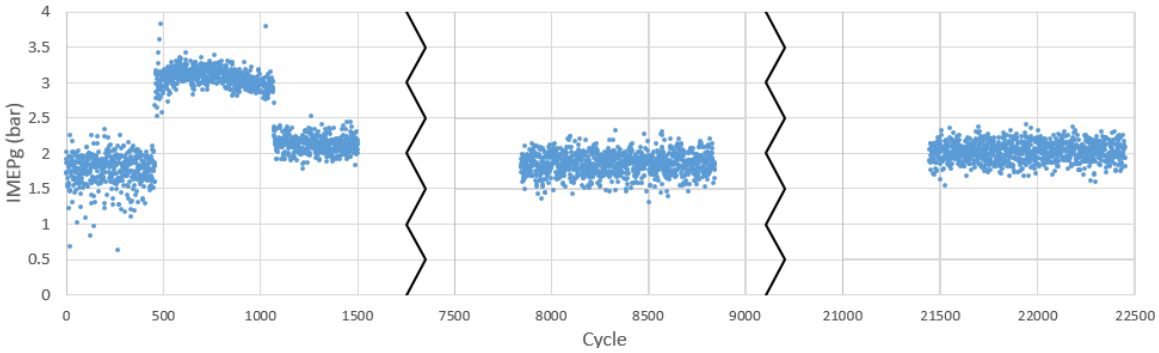

Figure 6.15. IMEPg data for extended engine run following 600 cycles of partial burn CO injections.

This slow reversion over an extended period of time is indicative of thermal losses that occur after removing the additional chemical promotion from CO but still operating at the lower partial burn intake temperature. This is a critical element to take into account if attempting to utilize these injections as a means of HCCI control. While they may be able to push combustion from a partial burn, unstable operating point to a more desirable realm of stability, this is only a temporary adjustment and not a fully sustainable stability point without additional system variables being modified. When considering application in a transition region between engine modes, this may provide enough temporary stability to guide the engine through a mode transition before the new, stabilized engine mode takes control of engine operation.

6.2.3. Calculated Thermal Impact of Expanded Gas. An additional thermal variable to consider is related to injecting of a compressed gas. Being that the gases injected into the cylinder are initially compressed gasses and are being expanded through the injector as they pass into the combustion chamber, there is a corresponding thermal effect of the expanded gas that needs to be considered. The introduction of the cooled expanded gas lowers the average charge mixture temperature. To determine the extent of the charge temperature reduction, an idealized isentropic expansion calculation, followed by a quick energy balance, was performed as a quick investigative exercise. Equation 41 was used with isentropic expansion assumptions:

$$T_2 = T_1(\frac{P_2}{P_1})^{\frac{\gamma-1}{\gamma}} \tag{41}$$

where T_1 and P_1 are the temperature and pressure before expansion through the valve, and T_2 and P_2 are temperature and pressure after expansion. Additionally, γ is the ratio of specific heats of CO, which for this instance was assumed a constant value of 1.4. Initial gas temperature is room temperature, assumed to be 25°C and initial pressure is the line pressure of 1000psi. Final pressure is the pressure within the cylinder during IVC which was assumed to be atmospheric, 1 atm or 14.7 psi. Applying these assumptions results in a calculated expanded gas temperature of -183°C. Carrying this value forward to an energy balance, along with the mass amount injected of 0.0008343g CO, provides us with the idealized bulk charge temperature. At a partial burn set-point the CO would be mixing with a charge mass of approximately 0.3268 g at a temperature of 199°C. With these values, the minimum resulting charge temperature after an

injection event is calculated to be 198.33°C, a difference of only 0.67°C. It should be noted that for simplicity's sake, the assumptions made for this calculation were based on unrealistic, irreversible flow. In reality, the impact on charge temperature would be even smaller, meaning a higher final mixture temperature.

While such a small impact on temperature appears seemingly negligible, there is some support from the data that this could be one of the underlying drivers for some of the initial impact on cycle dynamics during CO injection. That is, when operating in the partial burn regime, engine behavior is more sensitive to intake charge temperature effects than at stable operating points. This is seen in general engine operation where, if on the edge of the partial burn regime, adjusting the intake charge temperature by 1 or 2 degrees can drastically alter the operating set-point. So, one key question is whether such a minute difference in charge temperature, on the order of 0.5°C, will impact combustion in the partial burn regime to the extent experienced in the CO injections. If so, this would speak further to the highly sensitive nature of partial burn operation with respect to thermal conditions. However, this explanation may not capture all of the cycle-to-cycle dynamics experienced at early injections. That is, chemical kinetics of the CO addition may be a contributor to the retarding of CA10 and CA50, along with turbulence and charge mixing induced in the cylinder form the injection event.

6.3. CO INJECTION DYNAMICS

It is especially desirable to better understand CO's impact on the cycle-to-cycle dynamics immediately after injections begin. Looking closely at the transition from

partial burn set-point to the injection driven set-point, it can be deduced that the initial impact of the CO addition is one of amplification of the cycle-to-cycle dynamics.

6.3.1. CO Injection Dynamics - Return Maps. Further characterizing these initial dynamics during injection becomes a challenge due to the transience in the data as the mean values migrate across the injection window. An interesting way of following these dynamics involves the use of a progressive return map. In the progressive return maps below, the temporal shift in dynamics is captured through the use of progressively shading the data point coloration. This coloration varies from initial, darkly shaded data points, to the final, lightly shaded data points. Figure 6.16 displays return maps for the IMEPg data leading into and exiting the injection frame.

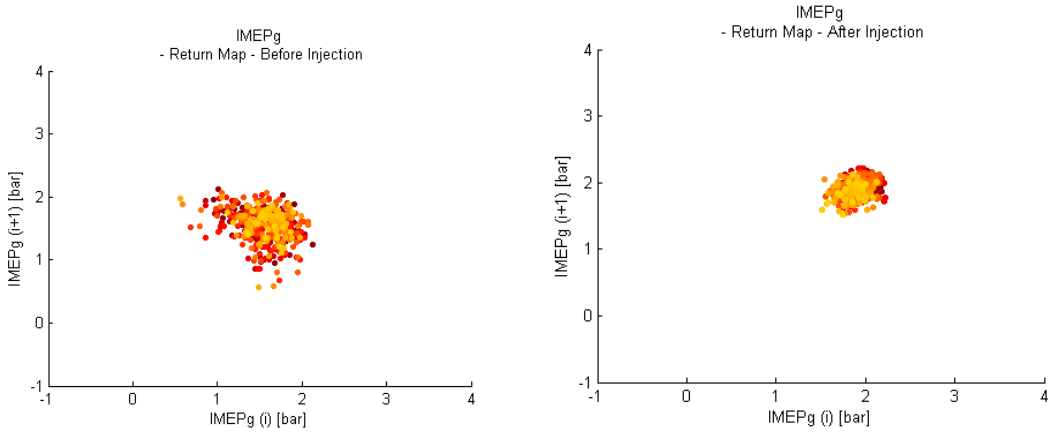

Figure 6.16. IMEPg return maps at partial burn. *a*) 450 cycles before CO injection. *b*) 450 cycles after CO injection.

When comparing the two plots in Figure 6.16, there is a clear change in the IMEPg cycle-to-cycle dynamics from the 450 engine cycles before the injections

occurred to the 450 cycles after they subside. The initial partial burn set-point exemplifies a rather unstable operating condition, as noted by the broad distribution of data. Additionally, this point demonstrates some deterministic structure beyond a purely random distribution. The structure is indicative of amplified deterministic behavior in the partial burn regime. The post injection data on the other hand has evolved to a stable operating point with tighter, more stochastically grouped data dominating the dynamics.

During injection, the progression of the engine dynamics is quite interesting at these points. Figure 6.17 depicts the return map for IMEPg during the 600 injection cycles.

When looking at the data point shading, the progressive stabilization can be seen in the tightening of data point distribution as the point coloration lightens with time. Except for a few outliers, the later injection points, noted by the orange and yellow coloration are group in a fairly tight, stochastic grouping at a higher magnitude than before injection. Additionally, there are two small deterministic groupings that show up at strong cycle IMEP output throughout the CO injection timeframe and become less frequent toward the end of the injection sequence.

Furthermore, Figure 6.18 is able to capture the stabilization progression of the CA10 and CA50 values during injection. It can be seen that the data in these images begins as widely dispersed points at the beginning of the injections and is driven toward a stable operating point.

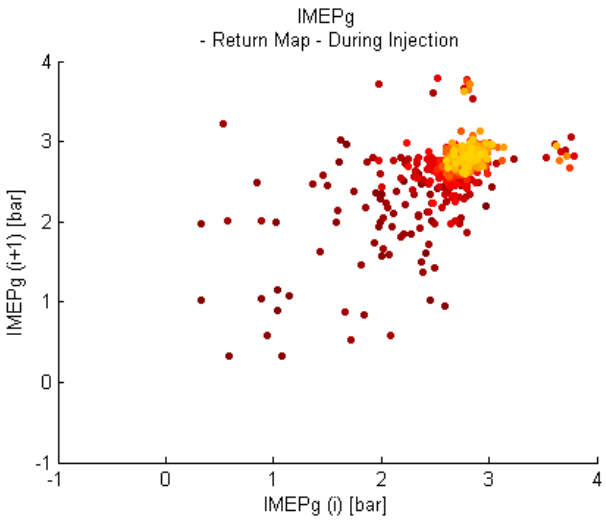

Figure 6.17. Progressive IMEPg return map during CO injection cycles at partial burn.

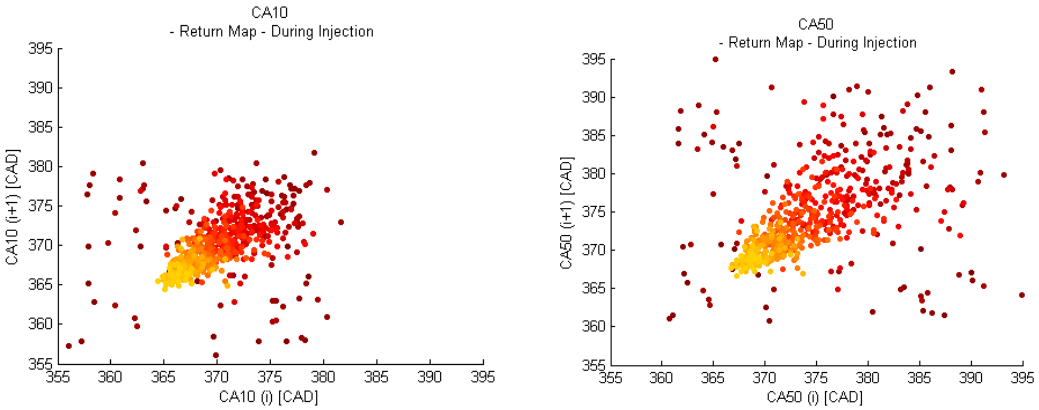

Figure 6.18. Progressive return maps during CO Injection at partial burn. *a*) CA10 evolution. *b*) CA50 evolution.

During injections, the IMEPg performance value and the heat release characteristics of CA10 and CA50 phasing are all driven from initially unstable set-points with some slightly structured dynamics, indicated by the wide dispersion of dark data points, toward more stable set-point, represented by the dense concentration of lightly

shaded data points. Similarly, CA10 and CA50 heat release values are pushed from an unstable, wide distribution of dark data points, to a grouped, higher concentration of data points in yellow. The initial wide distribution of points is interesting because it is an amplification of the dynamics in the data from before the injections began. So, the CO first increases the magnitude of the cycle-to-cycle dynamics and then decreases as time progresses.

Another curious occurrence that depicts amplified behavior when entering the CO injection cycle window is in the maximum cycle heat release. Looking at the cyclic heat release in Figure 6.19 there is an initial bifurcation that seems to occur at the start of injection at partial burn operation, with heat release events grouping at points of either strong heat release events or what is believed to be near complete cycle misfires.

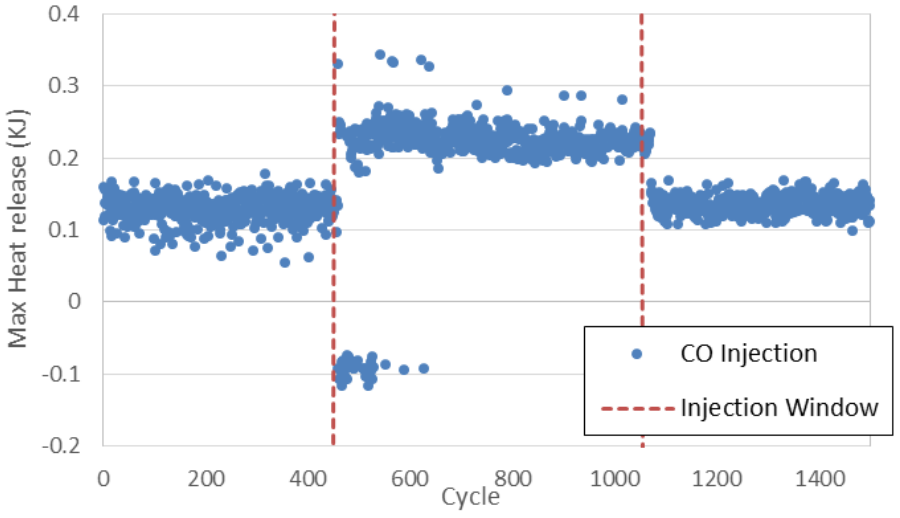

Figure 6.19. Max heat release when injecting CO for 600 cycles at partial burn.

The bifurcation trend is abandoned after injection of 100-150 cycles. At that point, the engine seems to reach a more stable set-point which overcomes any of the initial amplified effects due to the CO introduction and settles around a consistent heat release value. Looking at the return maps for the heat release in Figure 6.20, the progression from structured determinism in partial burn to the stochastically dominated stable operation is centered around a temporary extreme amplification of the deterministic tendencies that lead to cycle misfires during early CO injection cycles. As the injections continue, the heat release stabilizes toward a stochastically dominated set-point. Then, at least for the 450 cycle time period after injections stop, the engine maintains its stochastic tendencies but at a reduced magnitude.

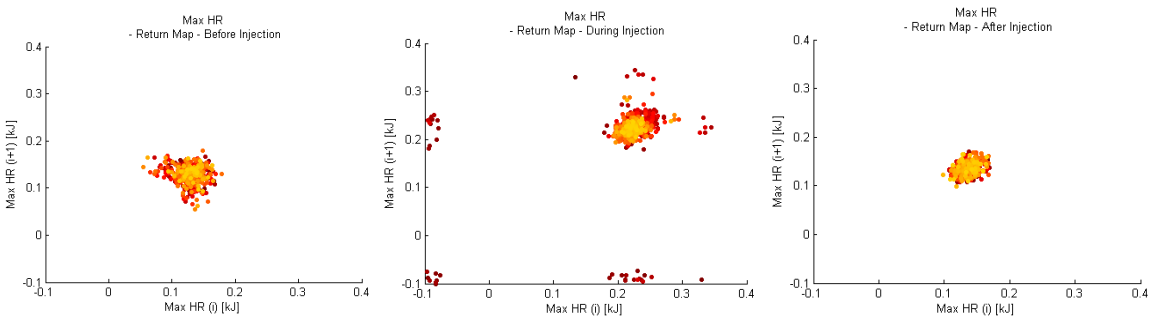

Figure 6.20. Heat release return maps during partial burn. *a*) Before CO injections. *b*) During CO injections. *c*) After CO injections.

6.3.2. Symbol Sequencing. Similar to the baseline case, it is worth looking at the additional characterization of the dynamics seen before and after CO injection performed through the use of symbol sequencing. While, ideally, it would be desirable

to perform symbol sequencing on the cyclically resolved engine data during injections, this results in unreliable data due to the transient nature of the mean values. Therefore, symbol sequencing was only beneficial in characterizing the dynamics before and after injection sequences. As such, Figure 6.21 represents the symbol sequencing for IMEPg data before and after 600 cycles of injections were performed.

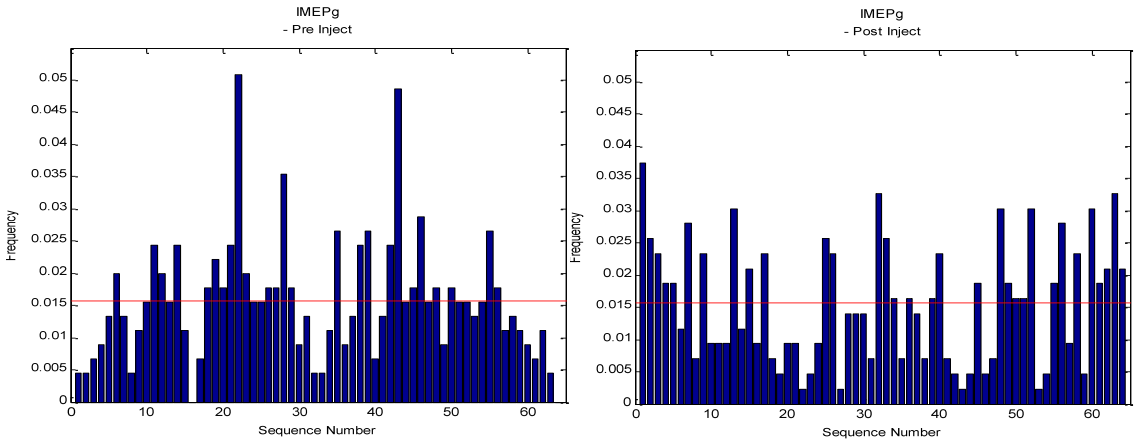

Figure 6.21. Symbol sequence of IMEPg data before and after CO injections at partial burn.

Figure 6.21 supports the observation that CO injection took the engine dynamics from a state of more deterministic behavior, changed the engine's dynamics, and pushed it to a more stable, stochastically dominated set-point. Before injection, the data was dominated by peaks in the frequencies of sequences 21 and 42, which are sequences of alternating high and low output and have been shown as characteristic of the baseline HCCI partial burn data with deterministic tendencies. On the other hand,

the post injection sequence occurrence frequency more closely resembles that of the stable baseline data, with sequence occurrences gravitating toward the baseline frequency, without the dominant peaks at sequences21 and 42. The structure post injection also show an increase in the sequences at the far ends of the spectrum. Granted, these changes are not as clean of a distribution as seen in previous steady state points, but it is still an indication of modified cycle-to-cycle dynamics toward more randomly distributed stable behavior.

While the effect of the CO on partial burn operation is noticeable in mean performance response and in a shift in engine dynamics, the initial injection exploration does not resolve whether the engine's response is primarily that of chemical kinetics, additional chemical energy, thermal impact, or even mixing effects. Realistically the true source is some combination of these three variables, but further isolating the primary contributing factor is desirable.

6.4. AIR INJECTIONS

The primary question around the impact that CO has on HCCI combustion dynamics is whether the injection of the critical species affects the chemical kinetics of the combustion events, whether it is merely a thermal effect, or even if it is promoting additional mixing, turbulence, or stratification of the cylinder charge. To address this concern, a set of air injection tests was performed.

6.4.1. Air Injection at Partial Burn. Air was injected into the cylinder at a partial burn set-point with intake temperature of 200°C. Mass amounts of these injections were equal to the mass amounts of the CO injection, injected at the same pressure, and

introduced during the same injection windows. Since air is primarily composed of N_2, which happens to be the calibration fluid for the gas injector, the injector did not require re-calibration for the new gas flowing through it. Results of a partial burn air injection case are shown in Figure 6.22.

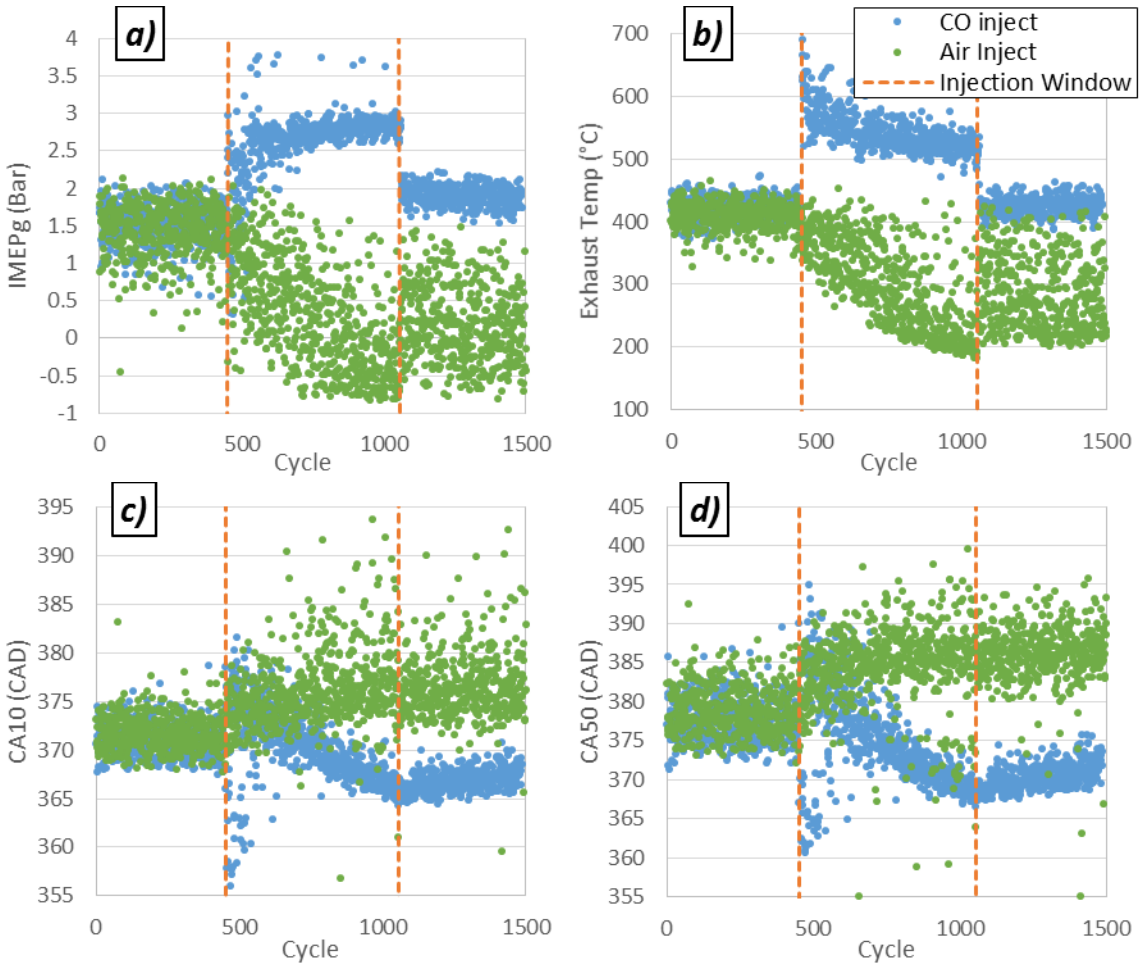

Figure 6.22. Partial burn air injection impact. *a*) IMEPg. *b*) Max exhaust temperatures. *c*) CA10. *d*) CA50.

It can be seen that injections of air in the partial burn regime drive additional instability into the system, an opposite trend to that of the CO injections. COV of IMEP is multiplied tenfold and is driven from an initial partial burn value of 21.5% to a post air injection value that is even less stable of 262%. CA10 and CA50 mean values are also driven toward more retarded, less stable operating conditions, from 371.7 CAD to 376.5 CAD for CA10 and 378.9 CAD to 386.7 CAD for CA50. This goes to show that the act of injecting is not promoting combustion during the CO additions, but rather it seems to suppress and hinder combustion. So, while the CO injection's promoting force is obviously not attributed to the action of introducing a specie, this act of injection is still contributing to some of the cycle-to-cycle dynamics at the transition. And, although the dynamics may be impacted by the suppressive nature of injecting a compressed gas, the chemical impact of the CO still overpowers these effects and drives combustion to the more advanced, stable operation.

It can be noted that the phenomena observable in exhaust temperatures during the CO and air injections of steadily decreasing exhaust temperatures over the injection timeframe likely occurs due to two separate reasons. As noted previously, the CO injection drives a strengthened combustion event with higher max temperatures further from EVO, reducing the temperatures read at the exhaust port. However, the air injection seems to be driving the late combustion events near EVO to less stable, incomplete combustion with weaker, late phased energy release events. That is, the temperatures are simply not reaching the same maximums as the CO injection case.

6.4.2. Air Injection at Steady State. Similar to the CO injection, it is of interest to determine whether the air addition presents a nonlinear impact on HCCI dynamics when injecting at partial burn versus a stable operating point. Therefore, the same air injection sequence was performed at a stable set-point with a 203°C intake temperature, resulting in Figure 6.23.

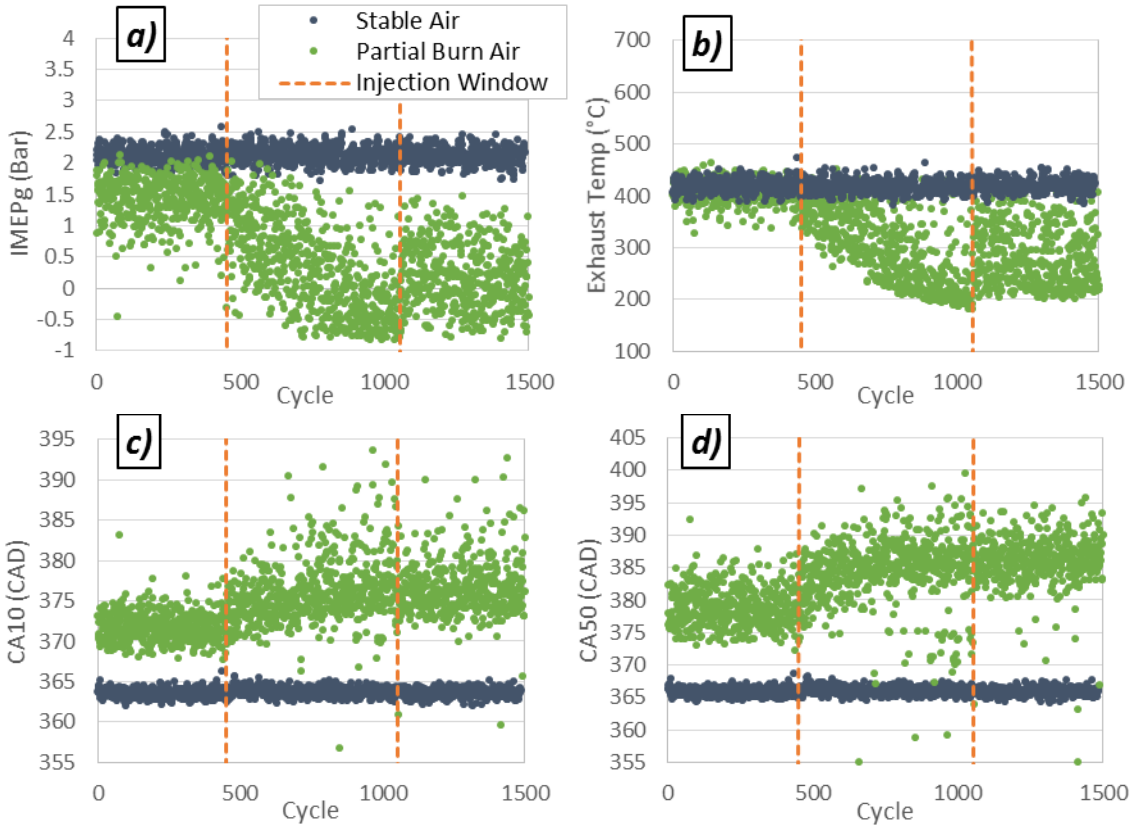

Figure 6.23. Steady state air injection impact. *a*) IMEPg. *b*) Max exhaust temperatures. *c*) CA10. *d*) CA50.

From an initial glance at the results of air injection at a stable operating point, it does not appear that the air injection had any discernable effect on combustion. Even

when looking at mean values of the operating parameters, there is no discernable change across the entire range of stable air addition data collected. Therefore, comparing the two experimental points, the impact of specie injection is substantially amplified in the partial burn regime due to the highly increased sensitivity of the operating region to cycle perturbations.

6.4.3. Air Injection on a Closed Valve. By adding air to the system, the question arises of whether the injection is altering the mixture ratio in a significant manner through dilution. That is, do the perturbations of air result in a significantly leaner equivalence ratio? Injecting on the open intake valve makes it difficult to calculate the full effect with complete confidence. So, to better identify the source behind the air injection's impact, injecting into the cylinder when the cylinder mass is fixed would further isolate the variable of a modified charge fuel/air ratio.

Adding the mass amount of air in a closed valve situation alters the equivalence ratio of the cylinder charge in a manner that can be captured with confidence, although only creating a slightly leaner mixture. Specifically, the 0.0008343g air mass injection was injected at a 199°C partial burn case after IVC, with injections beginning at approximately 55 CAD ABDC and finishing near 80 CAD ABDC. Injections drove the average equivalence ratio of the mixture from 0.3935 to 0.3925. Such a small difference in equivalence ratio set-point is negligible and should not present any notable effect on combustion. Historically speaking, experimental set-points on the Hatz HCCI engine have been shown to fluctuate more than this small scale alteration amount between back-to-back data collections at the same operating set-point without a noticeable

impact on performance. Therefore, the injection's driving impact on combustion is not tied to a change in the fuel/air ratio of the mixture. However, even lacking this justification, a substantial impact of injecting air after IVC can be seen in Figure 6.24.

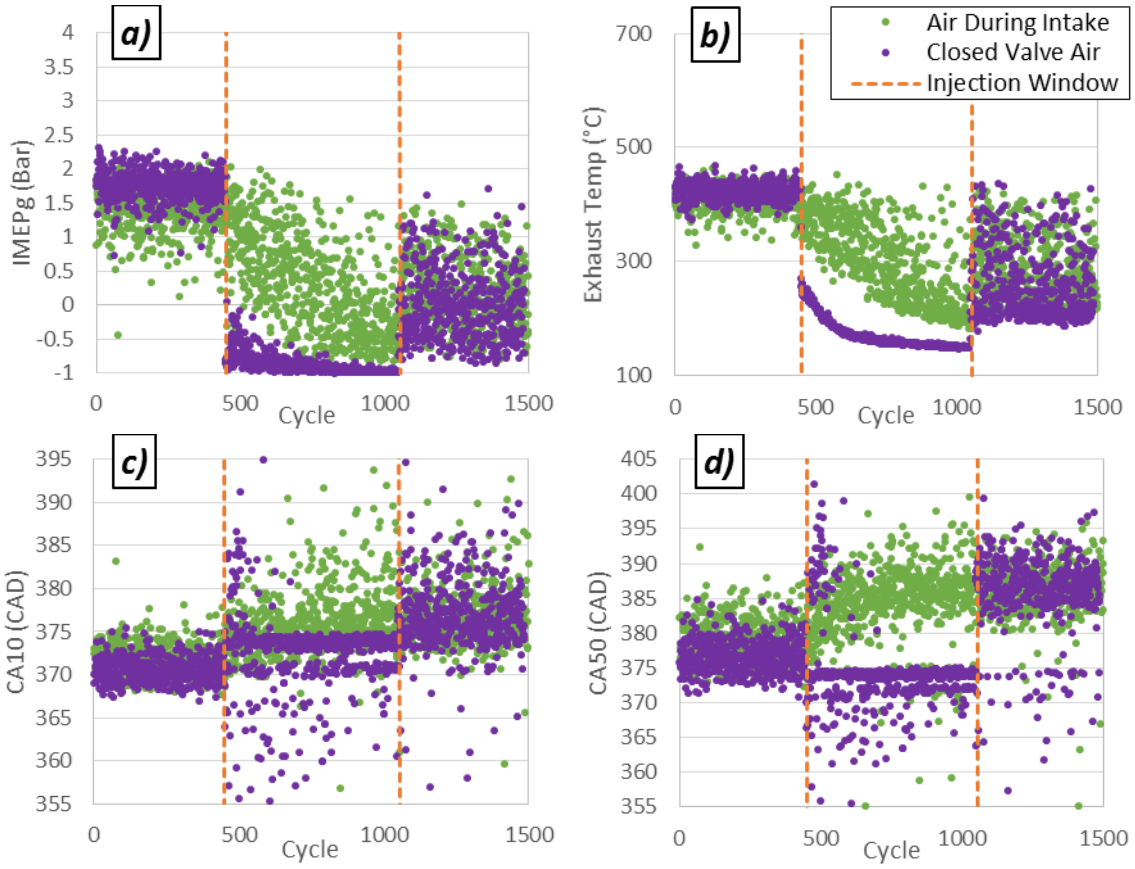

Figure 6.24. Impact of air injection during partial burn in closed valve condition. *a*) IMEPg. *b*) Max exhaust temperatures. *c*) CA10. *d*) CA50.

These closed valve air injections effectively extinguish combustion. Since the impact of the air is not likely a charge composition issue, this leaves the oppressor as being a thermal, mixing, or stratification issue. By pushing the injections later in the

cycle to after IVC, the allowable time for mixing of the charge before combustion occurs is decreased. So, there is likely increased motion, mixing, or induced stratification of the charge composition through the air addition at this late injection period.

Also, since the injections began after IVC, the compression stroke has started when this injection is taking place. As a result, the cylinder pressures and temperatures would have already begun to rise, meaning that the injection's impact on charge temperature would be even less than previously calculated in Section 6.2.3. Therefore, when compared to the initial air injection case, this smaller change in charge temperature would not result in such a drastic increase in effect if this were tied to the small thermal impact of the injection. This leads to the conclusion that the inhibiting effect of specie injection is tied to an increased charge mixing, motion, or induced stratification in the cylinder that is limiting combustion. With this being the case, the phasing of these injections to a later introduction CAD is additional testament to the high sensitivity of HCCI to variable perturbations.

By adding an active species, CO, to the fuel/air mixture, there is an associated chemical energy being added to the system, apart from any role in chemical kinetics that may be introduced. So, to further investigate the impact of the CO as the result of purely energy addition, that is removing the kinetic effects that go hand-in-hand with the CO's energy, an equal energy fueling rate was explored.

6.5. EQUAL ENERGY SET-POINT COMPARISON

To explore the difference in the impact that solely energy addition has on HCCI combustion as opposed to any chemical kinetic driver in the CO, an equal energy set-

point was run containing a higher fueling rate, but no CO addition. To do this, the amount of chemical energy added to the system through the original CO addition was equated to a set-point with a higher fueling rate containing equivalent available energy content.

Utilizing the lower heating values of the fuel and CO, as displayed in Table 6.3, the rate of energy addition within the cyclic 0.0008343 g CO mass additions was calculated to be 7.593 KJ/min. Relating this back to a fueling rate leads to an additional 0.17 gpm of additional fuel that would need added to the system in order achieve an equal energy condition. Adding this fuel rate to the previous operating case results in a fueling rate of approximately 7.7 gpm as an equal energy comparison set-point.

Table 6.3. Lower heating values of CO and PRF96.

	(kJ/kg)	***(J/g)***
CO	10,112	10,112
PRF96*	44,437	44,437

**PRF96 LHV value calculated based off of Iso-Octane and n-Heptane standard values*

6.5.1. Equal Energy Comparison. The engine was run for 1000 cycles at the equal energy instance of 7.7 gpm fueling rate, and the same intake temperature of the partial burn cases, 199°C. Figure 6.25 displays this contrasted with 1000 cycles of the original CO partial burn injection case.

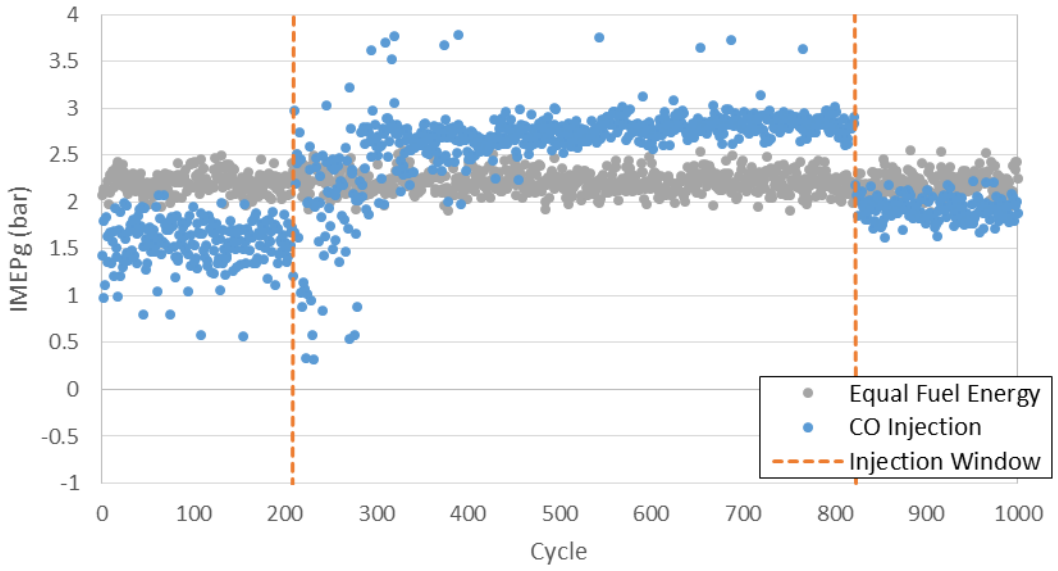

Figure 6.25. IMEPg comparison of partial burn CO injection to equal energy 7.7 gpm fueling rate at 199°C intake temperature.

From these results, it seems that there is something more complex at play than the effects of solely adding available combustion energy to the system. The two conditions shown contain equal amounts of energy during the CO injection window, and are run at the same intake temperatures. However, even with this, the CO addition case still falls substantially above the IMEPg of the increased fueling rate instance. Figure 6.25 demonstrates that there are variables at play in the CO addition that stem beyond a simple case of additional available energy within the engine that may be the result of CO impacting chemical kinetics. The average IMEPg value of the 7.7 gpm fueling rate was 2.21 bar, yet the average IMEPg once the cycle-to-cycle dynamics stabilize in the second half of the CO injection window were 2.82 bar, a difference of 0.61 bar. This then, indicates an improved efficiency in the utilization of the available energy. Looking

at the fuel conversion efficiency, the average efficiency of the 7.7 gpm case is 30.5%. Fuel conversion efficiency of the CO addition set-point, when considering both the fuel energy and the CO energy, is an increased 38.9%. From these numbers, it can be seen that the CO is promoting a significantly more efficient use of the available energy. Looking deeper, Figure 6.26 represents the CA10 and CA50 timing results.

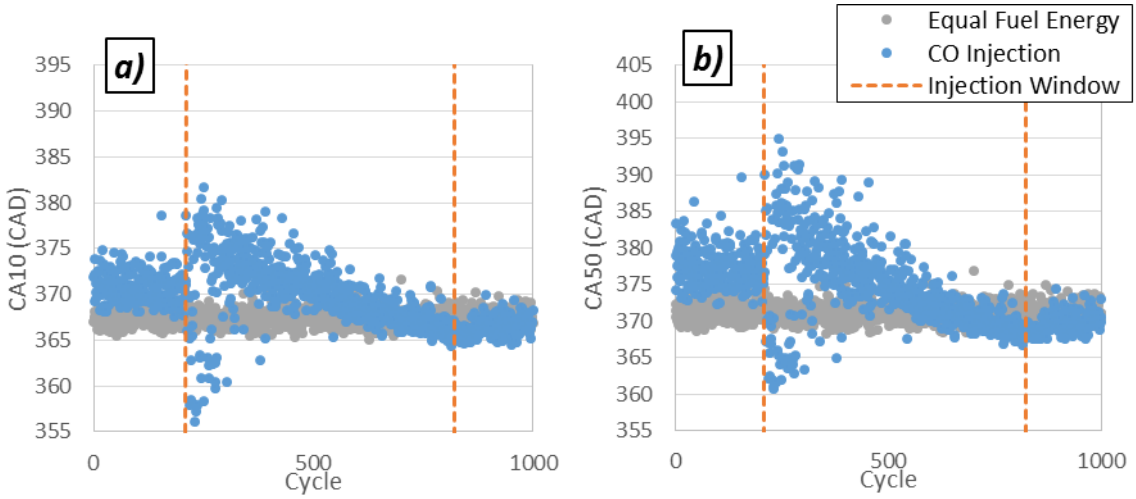

Figure 6.26. Equal energy set-point comparison at intake temp of 199°C. *a*) CA10. *b*) CA50.

CA10 values at end of injection were advanced beyond those of the equal energy counterpart, to a timing of 366 CAD. Likewise, CA50 values at end of injection were as well, to a point of 368 CAD. The difference is quantified when comparing these to the average equal energy CA10 and CA50 values of 367 CAD and 371 CAD respectively. While these differences are not drastic, it could be extrapolated that the gap would continue to grow. This is based on the fact that the CA10 and CA50 values during the

CO injection case are still on a downward trend when injections stop, making it appear that these parameters would advance slightly further if CO injections were continued beyond 600 cycles. This would create an even larger discrepancy against the equal energy instance. Such differences at equal energy, equal inlet temperature set-points are supportive of a deeper CO chemical kinetic effect taking hold on combustion, promoting more efficient energy utilization, and advancing the combustion event in time. A full breakdown of engine performance characteristics at the equal energy set-point can be seen in Table 6.4. Additional breakdown of all data from set-points run can be found in Appendix C.

Table 6.4. Equal energy performance comparison.

	IMEPg (bar)	***Peak Pressure Rise Rate (bar/deg)***	***Max Heat Release (kJ)***	***CA10 (CAD)***	***CA50 (CAD)***	***Burn Duration (degrees)***	***Max Cyclic Exhaust Temp (°C)***
Equal Energy	2.21	1.22	0.161	367.46	371.17	9.3	421.83

6.5.2. Equal Energy Comparison with Air Injection. The equal energy set-point can be taken a step further and injections of air can be made while running at this equal energy fueling rate. In this manner, the cylinder charge would have the same injection disturbance as the CO injection case and the same amount of chemical energy available, but in the form of fuel rather than CO. As such, the only discrepancy is the removal of the kinetic impact that the CO may be providing. Based on previous set-points, it was

not expected that the equal energy air addition would resemble the CO addition case, but nonetheless, it was still an interesting set-point to consider. These equal energy air addition results are shown in Figures 6.27 and 6.28 below.

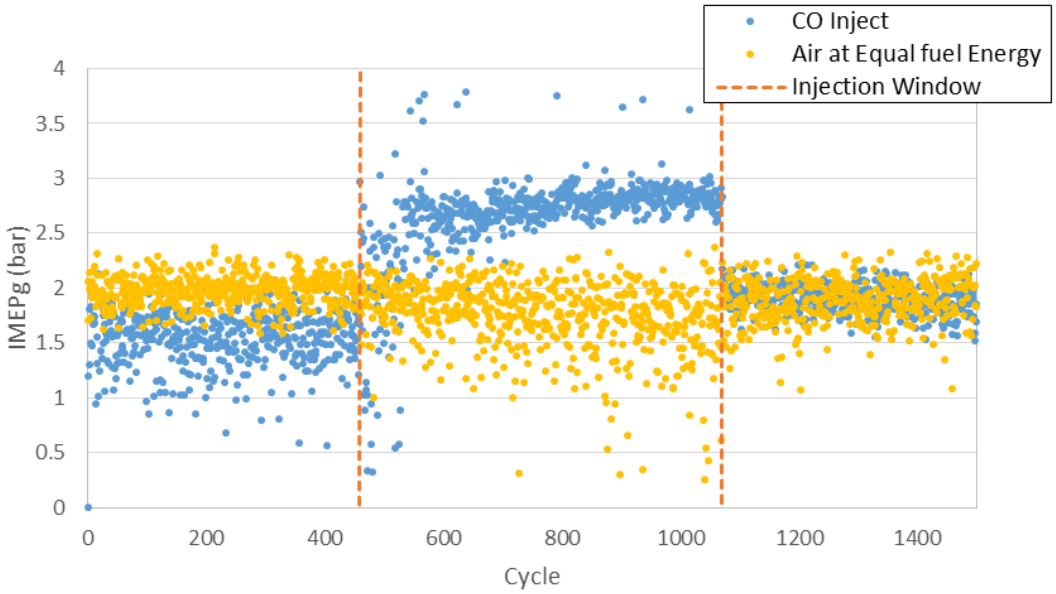

Figure 6.27. Air addition impact on IMEPg at an equal energy fuel rate of 7.7 gpm with intake temperature of 199°C.

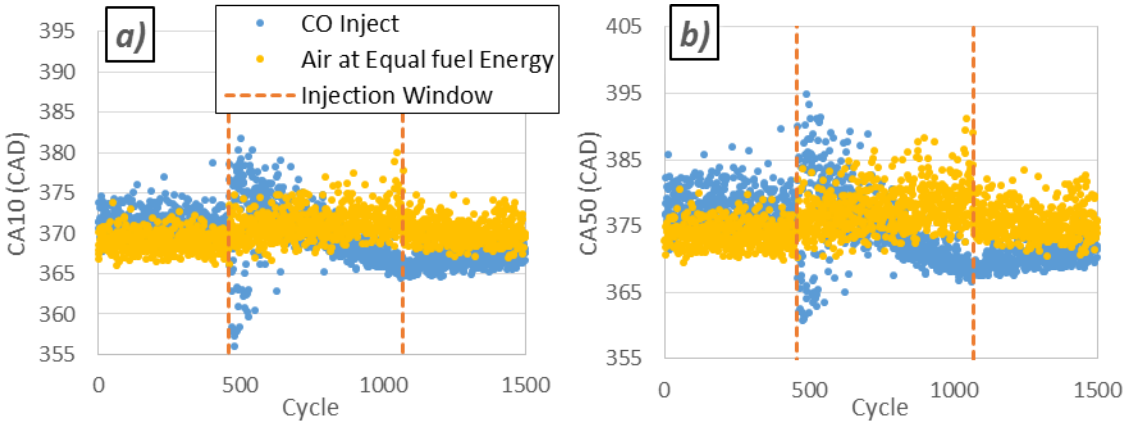

Figure 6.28. Impact of air addition at an equal energy fuel rate of 7.7 gpm and intake temperature of 199°C. *a*) CA10. *b*) CA50.

As could be expected, the equal energy set-point resembles a slightly more stable operating point than that of the 7.5 gpm partial burn CO addition. Therefore, in line with what could be expected, the air injections do destabilize combustion somewhat, which is not surprising when considering the previous air injection cases. From a combustion stability standpoint, it appears that the operation of the 7.7gpm fuel rate at this inlet temperature provides an instance that is more stable than the 7.5 gpm partial burn case, but possibly less stable than the 7.5 gpm steady state condition. Therefore, the response to the air injection is as expected. That is, an increased response to the air addition exists compared to the stable 7.5 gpm air injection case, but not as severe of an inhibiting response as the partial burn 7.5 air injections. The injections here seem to demonstrate a slight thermal cooling of the charge as air is injected. This is observable in the slow retardation of combustion phasing, CA50.

From these results, it can be inferred that the CO not only adds energy to the system, but also has a driving impact on the chemical kinetics that allow for more efficient utilization of energy already present. Additionally, the initial impact on CA10 and CA50 phasing is a retarding effect, which is partially the influence of increased charge motion and stratification that were shown to significantly inhibit combustion during closed valve air injections, but also likely tied to chemical kinetics to a degree. As CO injections continue during long injection sequences, there seems to be a slow thermal buildup resulting from the improved energy release that develops. This chemically promoted thermal growth then begins to push combustion to more advanced SOC and combustion phasing. Along with this, the cycle-to-cycle dynamics

seem to receive initial amplification in line with the general retardation of the heat release events. These dynamics then settle out as injections continue and the thermal impact stabilize combustion. This supports the idea that CO may be playing a chemical kinetic role in HCCI partial burn dynamics. In the end, it seems that there are a variety of factors contributing to the engine's response to the CO injections.

6.6. SENSITIVITY TO A SINUSOIDAL INPUT MASS

As HCCI engines slip from stable operation into the partial burn regime, their deterministic behavior tends to become magnified under the conditions. It is curious to not only determine whether the species carryover of CO has an impact on next cycle combustion, but to gain a greater understanding through an investigation of the engine's sensitivity to perturbations in CO mass amounts

By providing a known input CO mass that fluctuates from cycle-to-cycle, a more detailed look at the engine's response to CO injections can be made. When injecting this variable mass amount in the partial burn regime, it is expected that a nonlinear response of the engine would result as the mass fluctuates. In doing this, the results provide some additional insight in determining the sensitivity of the cycle-to-cycle dynamics to changes in the CO input mass.

6.6.1. Sinusoidal Injection Procedure. The sinusoidal injection amount was chosen to maintain a mean injection mass that relates to 100% of the maximum predicted CO carryover at the given equivalence ratio set-point. A sinusoidal variation in injection mass was introduced over a fixed period of 50 cycles. This sinusoidal input possessed an amplitude of 100% of the CO injection mass so that at its peak, a mass of

twice the simulated CO production was added and at its trough, no CO was added. In this manner, the mean energy addition to the system is the same as the energy available in the 600 cycle CO addition and in the 7.7 gpm fueling rate previously analyzed. Also, at the low point of CO addition, the energy content is equal to the original 7.5 gpm fueling rate. The energy content during injection, related to a fueling rate, is displayed in Figure 6.29 below.

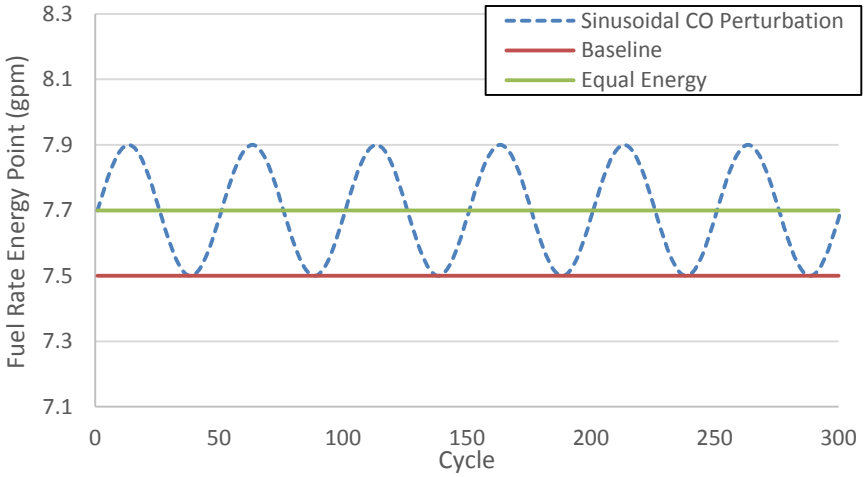

Figure 6.29. Equivalent energy fueling set-point for sinusoidal CO injection.

To analyze the results from this, a Fast Fourier Transform (FFT) was performed on the processed heat release and engine performance data to investigate the output frequencies of the engine performance. The power content of the FFT at each frequency interval is then calculated to characterize the magnitude of the engine's response. A strong response to the input signal frequency of CO mass would be

characterized by a dominant peak in engine output at the same frequencies. Therefore, for the test cases in this work, the output signal of an engine response sensitive to the CO mass amount input would produce power content peaks at the frequency corresponding to a period of 50 cycles. A full investigation of the engine's sensitivity to CO mass amount would involve incremental sweeps of altering the injected mass amplitude and monitoring the engine's response at each interval. Such experiments would be desirable to perform if generating a more precise relationship for control algorithms, but the current work is only attempting to isolate the source and general impact of CO.

6.6.2. Sinusoidal Injection Results. Sinusoidal injections of CO were performed at a fueling rate of 7.5 gpm, with the injection signal consisting of a mean injection mass of 0.0008343g CO, an injection amplitude of 0.0008343g CO, and an injection frequency period of 50 cycle. The data was collected for 200 cycles before injection, followed by 800 cycles of the sinusoidal mass injection. Figures 6.30 and 6.31 display the resulting engine response at partial burn case of 199°C intake temperature, and a steady state case of 203°C intake temperature, respectively.

It is obvious from the IMEPg cycle resolved data that sinusoidal injections strongly drive the system dynamics in both the steady state and the partial burn zones. However, one interesting aspect about the output is the time scale on which the engine's response is realized. When looking back at the constant CO injections, the engine dynamics were more slowly pulled from the partial burn behavior to a fully stable driven response. However, here, it appears that there is a near seamless

transition from the initial partial burn cycle-to-cycle dynamics displayed in IMEPg to the sinusoidal driven response.

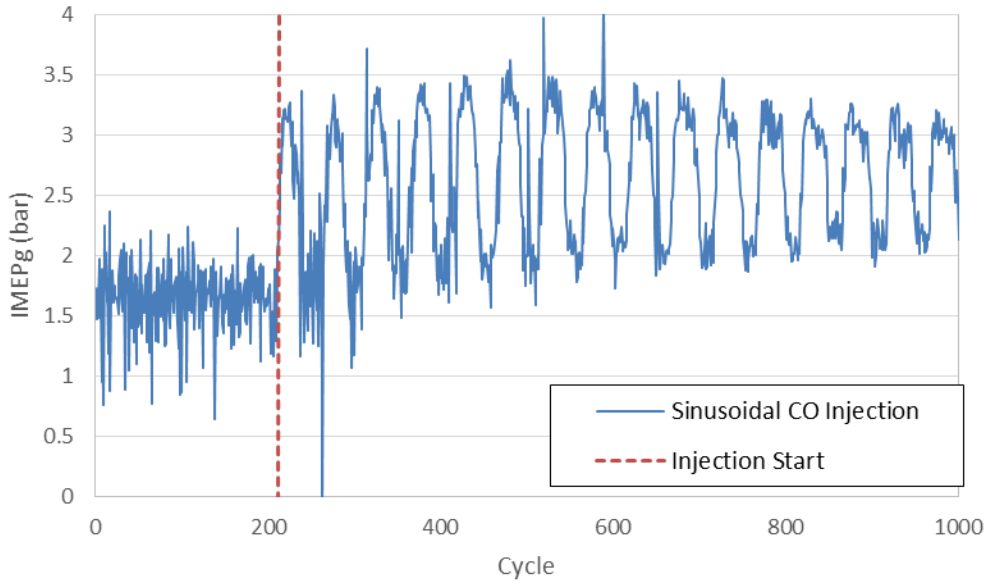

Figure 6.30. IMEPg of CO sinusoidal mass injection at partial burn, Tin = 199°C.

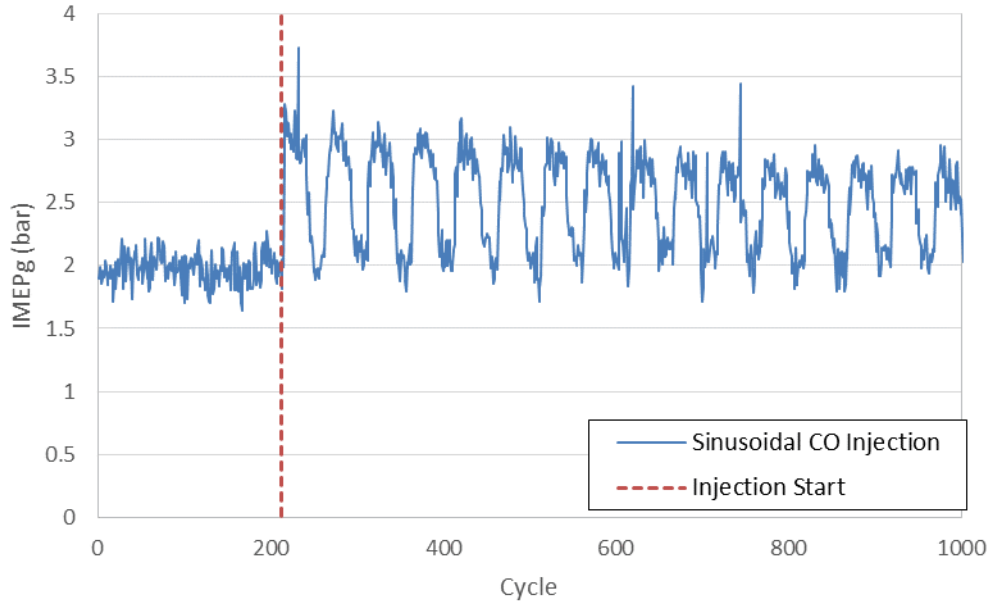

Figure 6.31. IMEPg of CO sinusoidal mass injection at steady state, Tin = 203°C.

Additionally, there still seems to be an amplification of the engine's dynamics initially after injections begin in partial burn introduction. The magnification of the initial dynamics during injections are harnessed in a manner that amplify the engine's IMEPg response before it settles toward more stable driven output. This is seen in the initial large amplitude of the IMEP response to the CO that settles toward a lower, constant amplitude toward the end of the injections. Interestingly, even with the input mass being a fluctuating quantity, the lack of amplification when injecting at a stable operating point is still observable in the fixed IMEP output pattern.

Looking more quantitatively at the engine's performance data, all 800 cycles of sinusoidal CO injection data was run through an FFT analysis to identify the power content of the response. With this, the engine's strong dominating response at the 50 cycle injection frequency is verified, as seen in Figure 6.32.

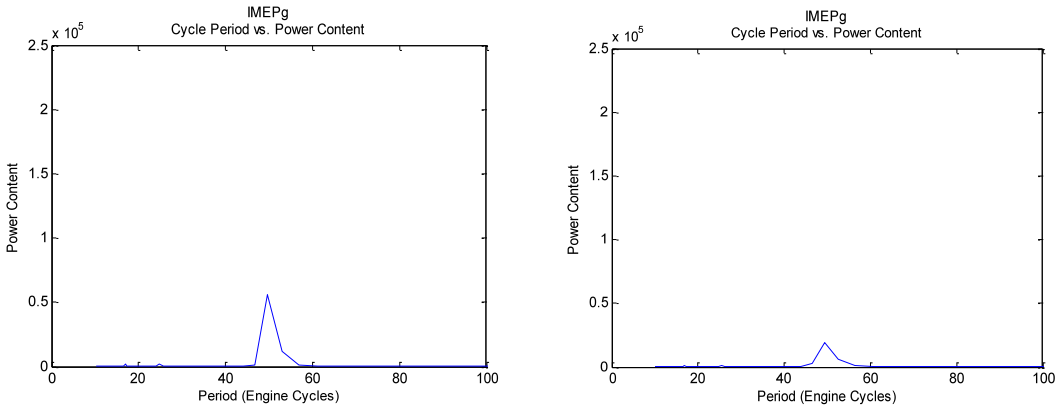

Figure 6.32. FFT power content for sinusoidal injection IMEPg data.
a) Partial burn. *b*) Steady state.

There is a heavily dominant peak in the frequency at a period corresponding to the 50 cycle. In fact, this grossly dominates any noise in the data, supporting combustion's increased sensitivity to the CO presence at partial burn.

It should be noted again that the peak in CO energy addition here is twice that of the originally predicted CO feed forward amount that was the focal of the study. As such, some of the driven behavior may be due to a nonlinear amplification of the engine's response with respect to injected CO mass.

Also interesting is that it seems some behavior may still be tied to a slight thermal influence building over time. This data still presents an observable small thermal influence seen over the sinusoidal injection. When looking across the minimums in the CO injection, there is a minor trend pulling up these dips for the first 400-500c cycles. Specifically, this forms minimums near 1.25 bar during initial injections up to minimums near 2.0 bar at the later series events. Looking at CA10 and CA50 response, these heat release properties also fall into a similar response, though not as immediately. These are depicted in Figures 6.33 and 6.34.

Through these heat release responses to sinusoidal CO injections, it is again shown that there is an initial amplification of cyclic variability of heat release when introducing CO at partial burn before falling into a stable response, even with fluctuating mass amounts. This was similar to the response originally seen in baseline CO injections. It appears that, if used early enough in an instance of combustion drift and in the appropriate sequences, CO addition could be utilized as a means of driving HCCI combustion back to a stable operating point.

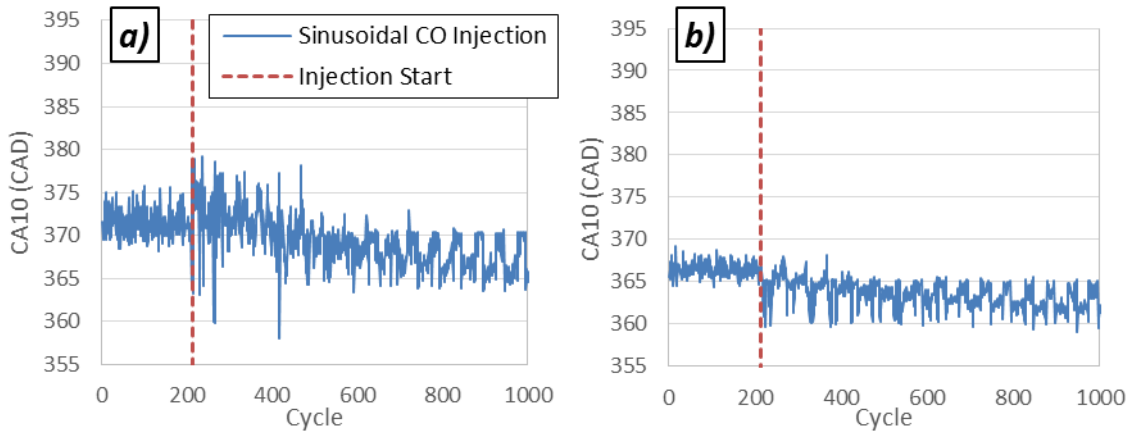

Figure 6.33. CA10 of CO sinusoidal mass injection. *a*) Partial burn. *b*) Steady state.

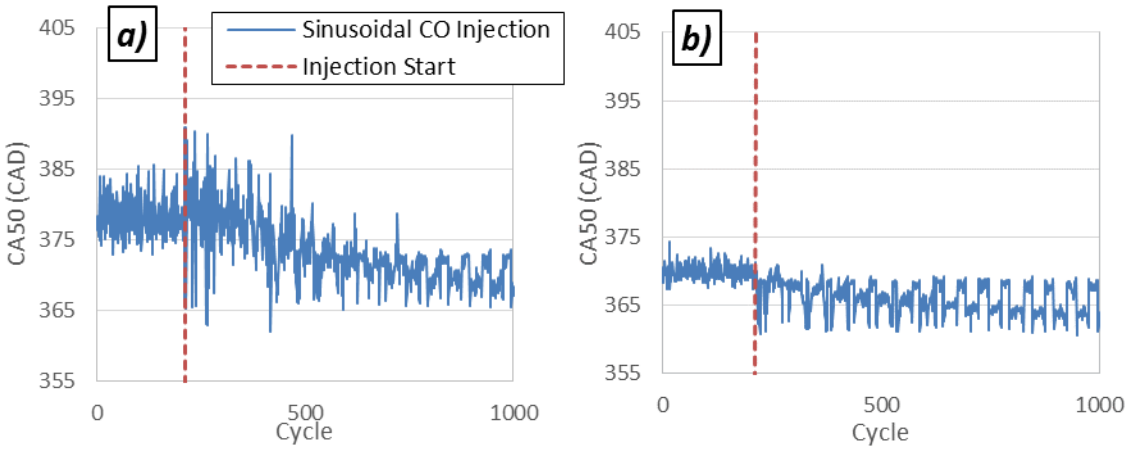

Figure 6.34. CA50 of CO sinusoidal mass injection. *a*) Partial burn. *b*) Steady state.

Turning again to FFT power content, Figure 6.35 and Figure 6.36 are presented. Interestingly, the power content of the CA10 response shows little difference at the 50 cycle frequency period between steady state and partial burn. The primary difference in the CA10 analysis is the magnitude of other frequencies that represent the amplified dynamics of the CO injections in partial burn.

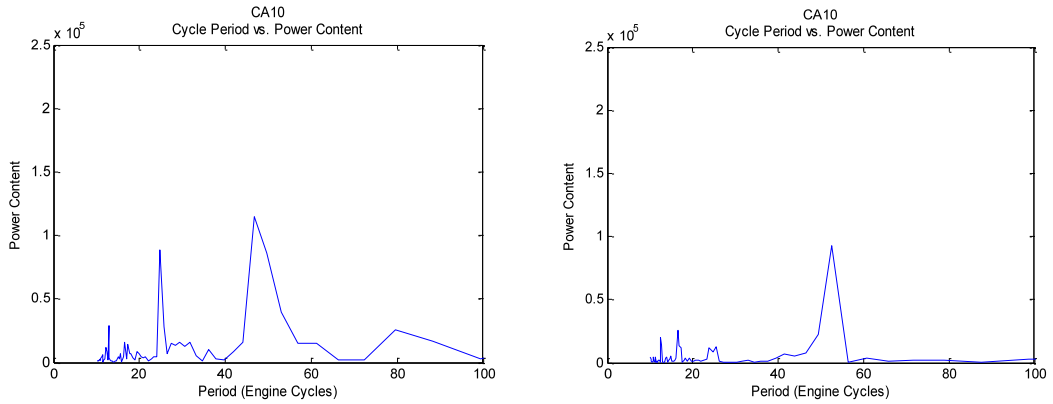

Figure 6.35. FFT power content for CA10 data. *a*) Partial burn. *b*) Steady state.

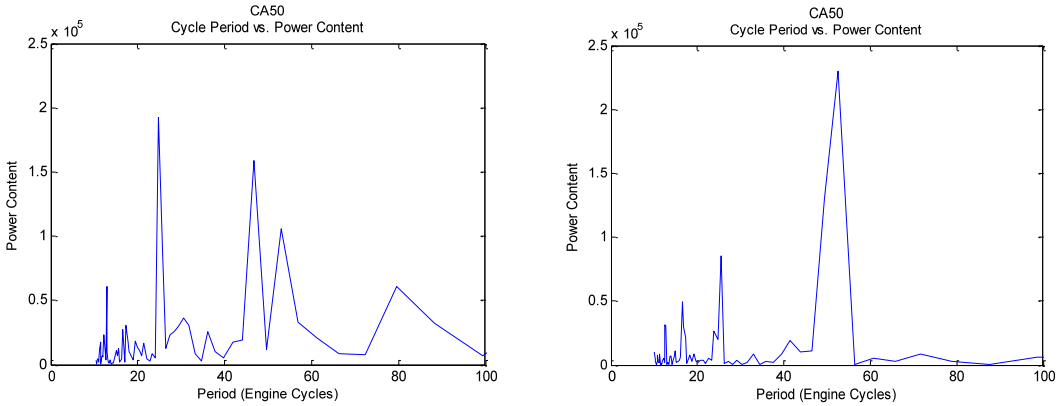

Figure 6.36. FFT power content for CA50 data. *a*) Partial burn. *b*) Steady state.

The especially curious item in Figure 6.36 is that when comparing power content, it is shown that the steady state operating regime's response at the 50 cycle frequency period is stronger than that of partial burn. This is likely due to the fact that the steady state set-point does not have overcome initially present large dynamics in order to be

the dominant tendency. This explanation could also speak to why the other engine parameters do not display greater difference between the two engine set-points.

With this, it could be proposed to develop robust control methodologies using CO to drive combustion. It is supported by these sinusoidal injections that control sequences could likely be developed with CO additions to strongly influence the combustion process during a partial burn set-point, and could potentially be used at steady state as well to provide a more immediate shift in engine set-point changes than a base inlet temperature adjustment. While it is not expected that an individual cycle injection of CO would possess enough influence to drive combustion to a new state, after seeing the response to a sinusoidal mass input, it would seem that pointed, carefully crafted injection sequences could be used to effectively drive combustion through the partial burn regime.

Any control approaches utilizing CO would have to take into account the thermal losses that occur after injection ceases and allow combustion to slip back toward its original operating point. So, these injections could be used for temporary set-point corrections and stability inducement, but a greater, slower change in operating parameters such as intake temperature modification would have to coincide with the CO injection such that the slower operating point shift could take over as primary influencer once the effects of the fast CO set-point manipulation fades.

7. CONCLUSIONS AND FUTURE WORK

7.1. CONCLUSIONS

Although littered with potential benefits, HCCI's largest hurdle in seeing widespread implementation stems from its inherent zones of unsustainable combustion, and the lack of effective control methods for navigating these regions. Carbon monoxide was chosen as the focal specie of this HCCI investigation due to its likely natural presence during the incomplete combustion occurring in the partial burn regime, its ability to be produced through on-board partial reforming of a hydrocarbon fuel, and its potential for nonlinear impact on the chemical kinetics of HCCI combustion. As such, it was investigated as a potential source as a driver of the engine dynamics in the partial burn regime and as a possible control mechanism for pushing HCCI combustion out of undesirable operating envelopes.

To investigate, a constant volume chemical kinetics simulation that utilized Tsurushima's reduced skeletal PRF mechanism was developed for prediction of CO and other species' evolution under incomplete combustion conditions. Maximum potential CO production amounts were predicted for experimentally based simulation set-points when operating on a 96 octane primary reference fuel. The resulting predicted feed-forward CO mass amounts were the basis for injection masses of CO in an investigation on the Hatz HCCI experimental engine at Missouri S&T.

Direct in-cylinder injection of CO was performed at the partial burn limit in mass amounts dictated by the simulation results. Through these experiments, it was shown that CO injections had a significant impact on HCCI combustion through the response

noticed in IMEPg, CA10, and CA50, among other parameters. Return maps and symbol sequencing methods were utilized in order to show how the specie injections drove the dynamics of the engine from unstable, deterministic behavior of partial burn, through a short period of amplified dynamics, and into a more stable, stochastic operating point. Through a series of additional CO injections, air injections, and equal energy set-point experiments, the source of CO's substantial impact was sorted out between the complexities of chemical kinetics, energy addition, thermal influence, and charge turbulence and stratification.

From these results, it can be inferred that the CO not only adds chemical energy to the system, but also has a driving impact on the chemical kinetics that allow for more efficient utilization of the energy present, as shown through the equal energy set-point comparisons. Additionally, the initial impact on CA10 and CA50 phasing is a retarding effect, likely the partial influence of increased charge motion and stratification, but also tied to chemical kinetics to a degree. An immediate jump in IMEPg is experienced, which is the result of the chemical energy and chemical kinetic combustion promotion. As CO injections continue, there is a small thermal buildup resulting from the improved energy release that develops, helping to push combustion to more advanced SOC and combustion phasing. Along with this, the cycle-to-cycle dynamics are initially amplified during early CO injection cycles. These dynamics then settle out as injections continue and the thermal and chemical effects help stabilize combustion. In the end, the impact of CO addition to HCCI combustion is a complex entity that is composed of many factors, but begins from the chemical kinetic and energy sources. From these results, it can be

safely assumed that the likely presence of CO during partial burn operation is a contributor to the significant cycle-to-cycle dynamics seen in this regime.

Additionally, sinusoidal injections of CO were performed on the HCCI engine with a resulting effect of strongly guided engine response. This response was immediately captured in IMEPg but still saw additional amplification, similar to the amplified cyclic dynamics of the original CO injections. CA10 and CA50 response to these injections also followed suit, although not nearly as quickly. This supports the idea that injection control strategies guided by CO injection sequences of 100-200 cycle sequences could be used for HCCI engine control given additional development and definition of the precise impact of CO amounts at other engine set-points. Such use would aid in guiding engine mode transitions, quickly altering operating set-points, and expanding the limits of stable HCI operation.

Overall, the results of these experiments give testament to the amplified hyper sensitivity of the partial burn regime to small charge perturbations. This highlights the necessity of robust control methodologies for HCCI and characterizes the primary hurdle in the mainstream application of HCCI technology.

7.2. FUTURE WORK

Moving forward in the pursuit of HCCI implementation, there are expansions of the current work that could lead to additional insight into this engine mode. The work at hand has validated the existence of a complex impact that the presence of injected CO has on next-cycle combustion. It would be noteworthy to explore other species' impact on HCCI combustion, or more precisely, other specie mixtures. When delving

into the use of CO as a combustion control mechanism, it must be realized that on-board partial reformers generating syn-gas tend to output mixtures of CO and H_2. While, per the literature, H_2 is not expected to possess the same level of kinetic effects, in order to develop fully applicable control schemes for HCCI, it becomes essential to explore producible mixtures of syn-gas compositions and understand the sensitivity of the engine to their presence through cyclically resolved injections. In hand with an experimental investigation of such gas mixture impacts would be the improvement of current HCCI thermodynamic models to incorporate full syn-gas utilization. Improving the 5-state thermodynamic model to capture syn-gas effects would allow for development of neural network based control approaches [29]. However, in order to couple the constant volume simulation code to such a model, a new mechanism would be required due to the lack of H_2 representation in the Tsurushima mechanism. Ideally, if swapping out to a new mechanism, improvements can also be added to the constant volume simulation to tie in an effective heat transfer model to better capture combustion development and exhaust species production when accounting for energy losses at partial burn. Overall, this could provide an extremely thorough look into the syn-gas impact on HCCI control.

Also, for delving deeper into the fundamental understanding of partial burn combustion, it would be beneficial to install additional thermocouples on the experimental Hatz HCCI engine that would allow for more in-depth monitoring of engine block temperatures and thermal influences. With this, the thermal impact of boundary conditions could be captured and used to develop additional understanding of the

chemical-thermal relationship at play, and its deeper impact on cyclic dynamics present on the fringe of partial burn. Taking things even one step further, there is also exciting potential in configuring a water cooled engine to run in HCCI mode and exploring actual mode transitions while possessing the more stable thermal data of a water cooled engine. Such efforts would provide more control over thermal set-points and additional confidence in data associated.

APPENDIX A.

RGI CALIBRATION DATA

Injector Calibration (08/27/16) - 1800 rpm, 1000 psi					
Duration (ms)	Measured Flow Rate (ln/min)	Actual Flow Rate (L/min)	Mass Flow (grams/min)	Mass Injected (grams/cycle)	% of Charge Mass
6.0	0.062	0.066526	0.07750279	0	0
6.5	4.455	4.780215	5.568950475	4.64079E-05	0.011190006
7.0	6.617	7.100041	8.271547765	0.000137859	0.033240973
7.5	10.084	10.820132	12.60545378	0.000315136	0.075986542
8.0	12.603	13.523019	15.75431714	0.000525144	0.126624143
8.5	14.816	15.897568	18.52066672	0.000771694	0.186073088
9.0	16.408	17.605784	20.51073836	0.001025537	0.247280283
9.5	18.541	19.894493	23.17708435	0.001351997	0.325997137
10.0	20.45	21.94285	25.56342025	0.001704228	0.410928148
10.5	22.13	23.74549	27.66349585	0.002074762	0.500272367
11.0	23.477	25.190821	29.34730647	0.002445609	0.58969194
11.5	25.416	27.271368	31.77114372	0.002912355	0.702235012
12.0	26.777	28.731721	33.47245497	0.003347245	0.807097043
12.5	28.347	30.416331	35.43502562	0.003838794	0.925620677
13.0	30.108	32.305884	37.63635486	0.004390908	1.058747834
13.5	31.462	33.758726	39.32891579	0.004916114	1.185387047
14.0	34.314	36.818922	42.89404413	0.005719206	1.379030658
15.0	37.164	39.876972	46.45667238	0.006968501	1.680264099
16.0	39.906	42.819138	49.88429577	0.008314049	2.00470644
17.0	42.844	45.971612	53.55692798	0.00981877	2.367528868
18.0	45.801	49.144473	57.25331105	0.011450662	2.761015175

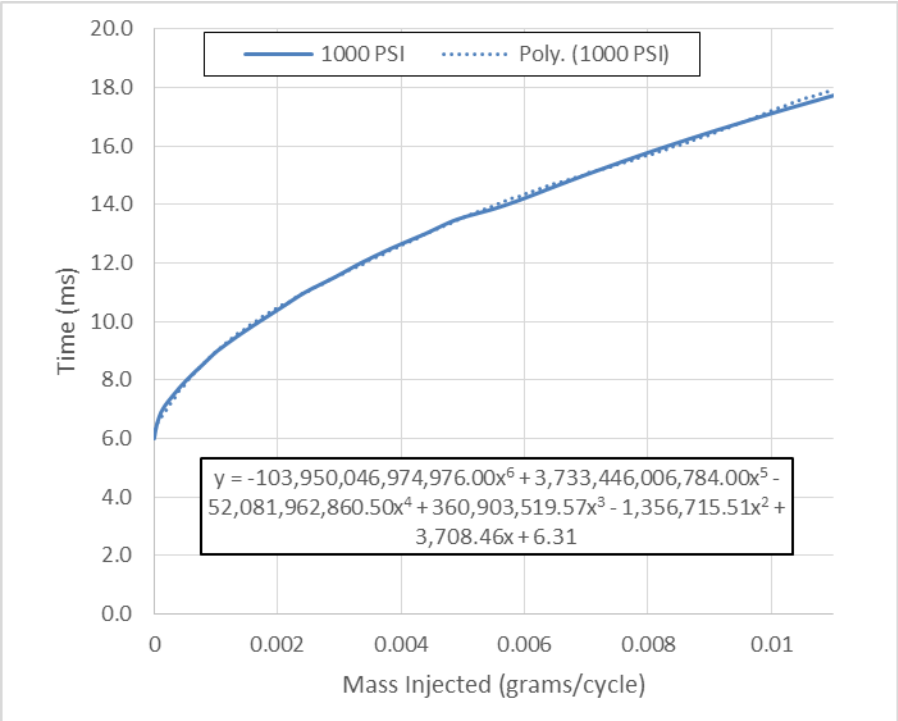

APPENDIX B.

CONSTANT VOLUME SIMULATION CODE

```
PROGRAM CV_PRF_2_1
      ! Constant Volume Combustion Simulation
      ! Allen Ernst - Missouri University of Science and Technology
      ! 7-1-2013
      ! Version 2.1 -Contains Carryover for ALL species in Tsurushima mechanism

      !  This code was designed to work with CHEMKIN to simulate constant volume combustion.
      ! It is configured to operate with Primary Reference Fuel Blends (PRF) of Isooctane and
nHeptane, by Volume.
      ! The current mechanism that it is configured for is that of Tsurushima with species and
...reactioins.  Changing mechanisms would require
      ! the modification of the reference values corresponding to the species, and possibly the
work array sizes
      ! (WORK,IWORK,RWORK1,IWORK1) (for details on the work array size requirements, see CHEMKIN
and dlsode codes).

          ! This code will require use in conjunction with the following files in order to
successfully execute:
          !-dcklib.f   - Chemkin Subroutine Library
          !-dinterp.f  - Interpreter file - Interprets the Thermo and Reaction Description Files
          !-dlsode.f   - Stiff Differential Equation Solver
          !-lin        - Chemical Mechanism  (Tsurushima)
          !-lthrm      - Thermo tables
          !-CKDATA.DAT - Initial Conditions Defining Simulation  (Edit this file for defining
simulation set-points)

! Additional Assumptions
! Adibatic process (Q=0)
! Isentropic compression, but compression can be omitted and skip directly to max compressed state
! Constant ratio of specific heats during compression = 1.4

!       Variables
        IMPLICIT NONE !REAL*8 (A-H,O-Z)  !NONE !
      COMMON /COM1/ RU, WT, IWORK, WORK, QoverV
      EXTERNAL FEX, JAC
        Integer :: Iter, IMFI, NITER, I, J,L,K,IP,MM,KK,II,LENEL,LENSYM,NFIT
        DOUBLE PRECISION PIVC,TIVC,Pinit,Tinit,TTotal,MOLISO,SMOLNHI,MOLNH
        DOUBLE PRECISION Rc,PHI,Gamma
        DOUBLE PRECISION QoverV,RUC,WTAIR,MWtot,MtotFINAL
      INTEGER :: IOPT,IOUT,ISTATE,ITASK,ITOL,LIW,LRW,MF,NEQ,NS,NES  ! from dlsode
      DOUBLE PRECISION ATOL,RWORK,RTOL,T,TOUT,DT,MAIR,N,FuelRate,T2,Qch
      DOUBLE PRECISION RU,PA,ON,HR,PB,PHR,LHV
      DOUBLE PRECISION RWORK1(1484),WORK(1293),Z(35),CC(33),Y(33),ZZ(33)
      INTEGER IWORK(1769), IWORK1(54)               !
      CHARACTER*10 NPATH
      DOUBLE PRECISION MolF,FAstoich,MFUEL,MOLA, NCF(4,33)
      DOUBLE PRECISION M(34),WT(33),YI(33),C(35),CON(33),CVMS(33),MA(33)
!       DIMENSION RWORK1(3194),WORK(2113),IWORK(332F1), IWORK1(72)
!       DIMENSION M(13),WT(13),YI(13),C(15),CON(13)
      CHARACTER*21 :: FILE_SP, FILE_TP, FILE_O, FILE_MP
      DOUBLE PRECISION IsoLHV,HeptLHV,RHOIso,RHOHept,MWIso,MWHept,ISO
      DOUBLE PRECISION nHeptane,CycleFuel,CycleEnergy,C_a,H_b,AFstoich
      DOUBLE PRECISION MoleIso,MoleHept,NormalizedMoleIso,FuelMass
      DOUBLE PRECISION NormalizedMoleHept,SpeciesEnergy,TotalFuelMole
      DOUBLE PRECISION MC7H16,MO2,MN2,MCO2,MC8H18,MCO,MH2O,MOH,MC7Ket          ! Species Carry
Forward Mass amounts
      DOUBLE PRECISION MCH2O,MH3H6,MC2H4,MC7H15,MC5H11CO,MC7H15O2,MC7H14
      DOUBLE PRECISION MC5H11,MH2O2,MC3H7,MC8H17,MC8H17O2,MC6H13CO
      DOUBLE PRECISION MC8H16,MC6H13,MHCO,MHO2,MC2H3,MC7H14OOH
      DOUBLE PRECISION MO2C8H16OOH,MO2C7H14OOH,MC8Ket,MC8H16OOH,MH
! T in Kelvin, P in atm, Tinit is at TDC, Pinit is at TDC
! Rc is compression ratio, Alpha is ratio of specific heats for intake, Phi is equivalence ratio,
Ru is universal gas constant
! AFstoich = stoichiomatric A/F ratio

!**** Open input files
      OPEN (12, FILE= 'CKDATA.dat', STATUS='OLD')
      OPEN (13, FILE='link', FORM='UNFORMATTED', STATUS='OLD')
 !    &ACCESS="STREAM")
```

```
      OPEN (14,FILE='lout',STATUS='OLD')
!**** calling chemkin package ****
      CALL CKINIT(1769, 1293, 13, 14, IWORK, WORK) ! Values here dependent on mechanism
      CALL CKWT(IWORK, WORK, WT)                    ! Returns the Molecular Weights of the species
(GM/Mole)
      CALL CKRP(IWORK, WORK, RU, RUC, PA)           ! outputs RU, the universal Gas Constant
(Ergs/Mole*K), and PA, the pressure of 1 atm (dynes/cm**2)
      CALL CKINDX(IWORK,WORK,MM,KK,II,LENEL,LENSYM,NFIT)
!**** Read inputs from Const_Volume.dat ****
      PRINT *,'MM',MM,'KK',KK,'II',II,'LENEL',LENEL,'LENSYM',LENSYM,NFIT
      PAUSE
      READ (12, 40) NPATH
!      READ (12, 41) IIJ
      READ (12, 41) IMFI
      READ (12, 42) NS
      READ (12, 43) PHI
      READ (12, 43) DT
      READ (12, 43) TTotal
      READ (12, 41) IP
!39    FORMAT (35X,I4)

       Do 54 I=1,NS
          M(I)=0.0D0
54     CONTINUE
40    FORMAT (35X,A)
41    FORMAT (35X,I1)
42    FORMAT (35X,I4)
43    FORMAT (35X,F9.6)     !8.6
      READ (12,44) TIVC
      READ (12,44) PIVC
      READ (12,44) Rc
      READ (12,44) ON
      READ (12,44) FuelRate
      READ (12,44) N
      READ (12,44) PB
      READ (12,44) MC7H16    !Begin Read in of the Carryover masses of Residual Species (Initial
charge composition apart from air/fuel)
      READ (12,44) MO2
      READ (12,44) MN2
      READ (12,44) M(4) !MCO2
      READ (12,44) MC8H18
      READ (12,44) M(6) !MCO
      READ (12,44) M(7) !MH2O
      READ (12,44) M(8) !MOH
      READ (12,44) M(9) !MC7Ket
      READ (12,44) M(10) !MCH2O
      READ (12,44) M(11) !MH3H6
      READ (12,44) M(12) !MC2H4
      READ (12,44) M(13) !MC7H15
      READ (12,44) M(14) !MC5H11CO
      READ (12,44) M(15) !MC7H15O2
      READ (12,44) M(16) !MC7H14
      READ (12,44) M(17) !MC5H11
      READ (12,44) M(18) !MH2O2
      READ (12,44) M(19) !MC3H7
      READ (12,44) M(20) !MC8H17
      READ (12,44) M(21) !MC8H17O2
      READ (12,44) M(22) !MC6H13CO
      READ (12,44) M(23) !MC8H16
      READ (12,44) M(24) !MC6H13
      READ (12,44) M(25) !MHCO
      READ (12,44) M(26) !MHO2
      READ (12,44) M(27) !MC2H3
      READ (12,44) M(28) !MC7H14OOH
      READ (12,44) M(29) !MO2C8H16OOH
      READ (12,44) M(30) !MO2C7H14OOH
      READ (12,44) M(31) !MC8Ket
      READ (12,44) M(32) !MC8H16OOH
      READ (12,44) M(33) !MH
```

```
44    FORMAT (35X,F9.3)

      Print *, NPATH, IMFI, NS, PHI, DT, TTotal, IP, TIVC, PIVC, Rc, ON
      PRINT *, MCO, MOH, MH2O, MCO2,N,PB,Fuelrate
! **** opening output file
      CALL CKNCF (4,IWORK,WORK,NCF)
      Print *, NCF
      FILE_SP=NPATH//'_MoleFR.out'
      FILE_TP=NPATH//'_FC.out'
      FILE_O=NPATH//'_OUT'
      FILE_MP=NPATH//'_MassFR.out'
      OPEN (unit=30, FILE=FILE_SP,  STATUS='UNKNOWN')
      OPEN (unit=40, FILE=FILE_TP, STATUS='UNKNOWN')
      OPEN (unit=45, FILE=FILE_O, STATUS='UNKNOWN')
      OPEN (unit=50, FILE=FILE_MP, STATUS='UNKNOWN')
      WRITE(45,*) '_____Input Values_____'
      WRITE(45,*) 'IMFI: ',IMFI
      WRITE(45,*) '# Species: ',NS
      WRITE(45,*) 'PHI: ',PHI
      WRITE(45,*) 'DT: ',DT
      WRITE(45,*) 'Total Time (s): ',TTotal
      WRITE(45,*) 'Iteration Step at: ',IP
      WRITE(45,*) 'TIVC (K): ',TIVC
      WRITE(45,*) 'PIVC (ATM): ',PIVC
      WRITE(45,*) 'Rc: ',Rc
      WRITE(45,*) 'Octane #: ',ON

! User defined values (Inputs)
       Gamma = 1.4  ! GAMMA will only be a constant for compression.
       QoverV=0    ! Adiabatic Assumption
! Initial Volume before Compression (will need to add in expression for this to be variable to
TDC)
! But, currently fall out of equation, so only is here as a stand in value
!       V=3.68*(10**(-4))  ! m^3
!!_____!!
! This calculates fuel amounts based on PHI and Mass flow rate
! **** initialize variables to zero ****
     Iter = 0   ! initialize iteration count
      Do 55 I=1,NS
!         M(I)=0.0D0
         YI(I)=0.0D0
         C(I) = 0.0D0
         MA(I)=0.0D0
         Y(I)=0.0D0
         CC(I)=0.0D0
         ZZ(I)=0.0D0
55      CONTINUE
       C(NS+1)=0.0D0   !!????
       C(NS+2)=0.0D0   !!???
       SpeciesEnergy = 0.0D0
       Qch = 0.0D0
       CycleEnergy = 0.0D0
!       C(NS+3)=0.0D0
        PRINT *, NS
! This segment of Code calculates the stoichiometric F/A ratio, LHV for a Primary Reference Fuel,
! the mass amounts of C7H16, and C8H18 based on PHI, fuel rate, and engine speed
!!! _____This section only applies to PRF fuels!!_____ !!!

! These fuel property values were taken from Turns' Introduction to Combustion (2nd Edition):
     IsoLHV =  44791      ! kJ/kg
     HeptLHV =  44926     ! kJ/kg
     RHOIso =  703        ! kg/m^3 @20C
     RHOHept = 684        ! kg/m^3 @20C
     MWIso = 114.23       ! g/mole
     MWHept = 100.203     ! g/mole

!Begin Calculating Stoichiometry and mass amounts of fuel
     CycleFuel = FuelRate/(N/2)    ! g/cycle
     ISO = CycleFuel*(((ON/100)*RHOIso)/(((ON/100)*RHOIso)+((100-ON)
```

```
     &/100*RHOHept)))            ! Cycle Mass of Iso
      nHeptane = CycleFuel*(((100-ON)/100*RHOHept)/(((ON/100)*RHOIso)+
     &((100-ON)/100*RHOHept)))  ! Cycle Mass of Heptane
      FuelMass = ISO + nHeptane
      CycleEnergy = (ISO*IsoLHV+nHeptane*HeptLHV)/1000       ! Total fuel energy in the engine
cylinder for this one cycle KJ
      LHV = (CycleEnergy/2)*N*1000/FuelRate                  ! Lower heating value of the PRF
blend fuel.   kJ/kg
      MoleIso = ISO/MWIso
      MoleHept = nHeptane/MWHept
      TotalFuelMole= MoleIso + MoleHept
      NormalizedMoleIso = MoleIso/(TotalFuelMole)
      NormalizedMoleHept = MoleHept/(TotalFuelMole)
      C_a = 7*NormalizedMoleHept+8*NormalizedMoleIso         ! Carbon subscript for PRF fuel
      H_b = 16*NormalizedMoleHept+18*NormalizedMoleIso       ! Hydrogen subscript for PRF fuel
      AFstoich = (34.56*(4+(H_b/C_a))/(12.011+1.008*(H_b/C_a)))  ! Calculate Stoichiometric A/F
      FAstoich = 1/AFstoich

      ! For testing code with Old Mechanism
      MolF=1    ! Number of moles of Fuel (should stay at 1)
!      LHV = 44.5660  ! Lower heating value of the fuel (KJ/g) - 44310 for Iso, 44566 for n-hept
!       MOLA = 1
!!!! **** initial conditions of species H2,02,NO,N2 respectively ****
!          M(1)=MolF*WT(1)   !(EQR*4.03188D0)/D1
      M(1) = MC7H16+nHeptane     !n-Heptane Mass
      M(5) = MC8H18+ISO          !Isooctane Mass
      PRINT *, M(1), M(5), FAstoich, FuelMass, CycleEnergy, LHV
      PAUSE
!          MOLISO= (ON*0.01)*(0.69191*(10**6)/1000)/WT(703)    !! For PRF ISO Fuel Mass of ON 20
w/density at 20 deg C
!          MOLNH= ((1-ON)*0.01)*(0.68374*(10**6)/1000)/WT(925)  !! For PRF N-Hept Fuel Mass of ON
20
!          SMOLNHI=MOLISO+MOLNH
!          M(703)=(MOLISO/SMOLNHI)*WT(703)*MolF    !! For PRF ISO Fuel Mass of ON 20
!          M(925)=(MOLNH/SMOLNHI)*WT(925)*MolF     !! For PRF NHEPT Fuel Mass of ON 20

          WTAIR=(1*WT(2)+3.76*WT(3))   !@#   O2(2)    N2(3)
!!!        MAIR=1/(PHI*(FAstoich)/M(1))
          MAIR = 1/(PHI*(FAstoich)/(M(1)+M(5)))     !@#  102.7525 is MW of fuel
          MOLA=MAIR/WTAIR

      DO 1111 I=1,25
      PRINT *,WT(I)
1111  continue
      PAUSE
      M(2)= MO2+(1*MOLA)*WT(2) !  !@# Mass of O2
!        M(11)=0.0D0         !
      M(3)= MN2+(3.76*MOLA)*WT(3)   !  !@#  Mass of N2

      PRINT *,M(2)
        PRINT *, M(3)
      PRINT *,MOLA,WTAIR,MAIR,WT(1),WT(2),M(1),M(2),M(3)
      PAUSE
      MWtot=0.0D0
      Do 11 I=1,NS  ! Make sure this only goes to the end of the species
          MWtot=MWtot+M(I)
11    CONTINUE

      DO 12 I=1,NS       ! Calculate Initial Mass Fractions
          YI(I)=M(I)/MWtot
12    CONTINUE
      Qch = CycleEnergy !+ SpeciesEnergy ! Calculates total fuel energy fed into the system   __
!!!! possibly add energy from other species added!!!!

      Print *,MWtot, YI,Qch
      PAUSE
       WRITE(45,*) 'Total Charge Mass: ',MWtot
!_____________________________
      Print *,MWtot, YI,Qch
```

```
      PAUSE
! ____________________________________________________________________________
! ____________________________Start Calculations______________________________
!_____________________________________________________________________________
! If User has supplied IVC as initial values and are assuming isentropic compression,
! then uncomment the next two lines!
!
!       Tinit=TIVC*(Rc)**(Gamma-1)
!       Pinit=PIVC*(Rc)**(Gamma)
!_____________________________________________________________
! Otherwise, the supplied initial values are assumed to be the values at TDC
      Tinit=TIVC
      Pinit=PIVC
      Pinit=Pinit*PA    ! Converts P to dyne/cm^2 for use with CHEMKIN
      print *, tinit, pinit, RC

! Initializations for DLSODE, the diffeential equation solver (refer to the solver code for
details of each parameter assigned)
      NEQ = NS+1      ! # Equations = # of species + 1 (for Temp Equation)
      ITOL=1
      RTOL=1.0D-8     ! Relative Tolerance
      ATOL=1.0D-12    ! Absolute Tolerence
      !IMFI = 1       ! Put this in input .dat file
      T = 0.D0        ! Starting Time
      ITASK = 1
      ISTATE = 1
      IOPT = 0        !  was 1
      LRW =1484       ! Length of Real Work Array for Solver       ! Vary with mechanism
      LIW =54         ! Length of Integer Work Array for Solver    ! Vary with mechanism
      MF = 21         ! Dictates solving method of DLSODE.  Use 21 or 22 for stiff equation solver
(The equations in this code are stiff)
                      ! MF: 22 utilizes user supplied jacobian (calculated below), and 21 utilizes
a generated jacobian by the DLSODE code
      TOUT = DT
      HR = 0.0D0      ! Initialize heat release to 0

      PAUSE
      CALL CKYTCP(Pinit,Tinit,YI,IWORK,WORK,CON)   ! Input P,T, Mass Fraction and Returns Molar
Concentrations (mole/cm**3)
!      CALL CKCTX(CON,IWORK,WORK,ZZ)
      DO 3 I=1,NS
          C(I)=CON(I)
3     CONTINUE
      C(NEQ)=Tinit
      C(NEQ+1)=Pinit
      PAUSE
        print *, 'C', C
      PAUSE
! Write initial Data to output
      CALL CKCTX(CON,IWORK,WORK,ZZ)      ! Returns the mole fractions given molar concentrations
      DO 77 I=1,NS
           Z(I)=ZZ(I)
77    CONTINUE
      Z(NEQ)=C(NEQ)
      Z(NEQ+1)=C(NEQ+1)/PA
! These Column Titles apply to the current Tsurushima mechanism used.  Other mechanisms will have
different specieas and in will be in a different order.
      WRITE(30,36) 'Time (s)','c7h16','o2','n2','co2','c8h18','co',
     &'h2o','oh','c7ket','ch2o','c3h6','c2h4','c7h15','c5h11co',
     &'c7h15o2','c7h14','c5h11','h2o2','c3h7','c8h17','c8h17o2',
     &'c6h13co','c8h16','c6h13','hco','ho2','c2h3','c7h14ooh',
     &'o2c8h16ooh','o2c7h14ooh','c8ket','c8h16ooh','h' ! Writes Init Time & species mole fraction
      WRITE(50,36) 'Time (s)','c7h16','o2','n2','co2','c8h18','co',
     &'h2o','oh','c7ket','ch2o','c3h6','c2h4','c7h15','c5h11co',
     &'c7h15o2','c7h14','c5h11','h2o2','c3h7','c8h17','c8h17o2',
     &'c6h13co','c8h16','c6h13','hco','ho2','c2h3','c7h14ooh',
     &'o2c8h16ooh','o2c7h14ooh','c8ket','c8h16ooh','h' ! Writes Init Time & species Mass fraction
      WRITE (40,35) 'Time (s)','Temperature (K)','Pressure (atm)',
     &'Heat Release (kJ)','% Energy Released'     ! Writes Initial Time, Temp, and Pressure
```

```
      WRITE(30,33) T,Z(1),Z(2),Z(3),Z(4),Z(5),Z(6),Z(7),Z(8),Z(9),Z(10),
     &Z(11),Z(12),Z(13),Z(14),Z(15),Z(16),Z(17),Z(18),Z(19),Z(20),Z(21),
     &Z(22),Z(23),Z(24),Z(25),Z(26),Z(27),Z(28),Z(29),Z(30),Z(31),Z(32),
     &Z(33)                              ! Writes Initial Time and species mole fraction
      WRITE(50,33) T, YI                 ! Writes Initial Time and species Mass fraction
      WRITE (40,34) T,Z(NEQ),Z(NEQ+1),0.0D0,0.0D0    ! Writes Initial Time, Temp, and Pressure
!_____________________________________________________________________________________
!_____________________________*********Begin Main Loop*********_____________________________
!_____________________________________________________________________________________
! Calculate Number of Time Steps
        Niter = (TTotal-0)/Dt
        Do I=2,Niter        ! Begin Main Program Loop
        Iter = Iter+1
      T2=C(NEQ)           ! Previous step temperature
        CALL DLSODE(FEX,[NEQ],C,T,TOUT,ITOL,[RTOL],[ATOL],ITASK,ISTATE,
     &IOPT,RWORK1,LRW,IWORK1,LIW,JAC,MF)                                  ! Added [] to three
variables during debugging
!Chaged rwork and iwork to rwork1 and iwork1 for the dlsode integrating.  the originals will be
reserved for chemkin calls

!!!!  Here is where any checks would be put in place to ensure temps and presures are progrssing
in realistic direction!!! (See ex)
!      PRINT *, 'OK'
      IF (ISTATE .LT. 0) GO TO 80                    ! This line is needed to check the success
of lsode
      IF (C(NEQ) .LE.0.0D0) GO TO 90                 ! Checks the Temp to verify it is positive
! This calculates the new pressure and adds it to the C Matrix
       C(NEQ+1)=(Pinit/Tinit)*C(NEQ)

        TOUT = TOUT+DT
 !       print *, Iter, Y(1), Y(2), Y(3), Y(4), Y(5), TOUT

        DO 155 L=1,NS       ! This checks that all concentrations are positive values
          IF (C(L) .LT. 0) THEN
!          WRITE(...,) I
          C(L)=0.00D0
      PRINT *, 'Negative Concentration Corrected to 0 for Species #: ',L
      PRINT *, 'At Time: ',T
!         GOTO 70
          ENDIF
155     CONTINUE

!      PRINT *, 'OK2', NS
!        DO 32 K=1,NEQ-1    ! writes calculated values of C(I) to output for each iteration
          Z=C
!          IF (C(I) .LT. 0.0D0) THEN
!          Z(I)=0.0000D0
!          ENDIF
!32      CONTINUE
!        Z(NEQ)=C(NEQ)
        Z(NEQ+1)=C(NEQ+1)/PA
          !print *, Iter, Y(1), Y(2), Y(3), Y(4), Y(5), TOUTk
       DO 119 L=1,NS
           CC(L)= C(L)
119    CONTINUE

!  Calculates percent heat released based on change in sensible energy
      CALL CKCTY(CC,IWORK,WORK,Y)           ! Returns mass fractions given molar concentrations
      CALL CKCVMS(C(NEQ),IWORK,WORK,CVMS)   ! Returns the specific heats at constant volume in
mass units (ergs/Gm*K)      ! Note: 1 erg = 0.0000000001 kilojoule [kJ]
      DO 121 L=1,NS
          MA(L)=Y(L)*MWtot
          HR=HR+MA(L)*CVMS(L)*(C(NEQ)-T2)*0.0000000001
121   CONTINUE

          PHR=(HR/Qch)*100
      CALL CKCTX(CC,IWORK,WORK,ZZ)          ! Returns the mole fractions given molar
concentrations
```

```
         PRINT *, PHR

!  From lsode example:
 !!     WRITE(30,33) T,Z(1),Z(2),Z(3),Z(4),Z(6),Z(7),Z(5),Z(8),Z(9),Z(12)  ! Writes Time, o2, co,
h2, iso, nhept concentrations, and Temp
      WRITE(30,33) T,ZZ                                  ! Writes Time, and mole fraction
ofspecies
      WRITE(50,33) T,Y                                   ! Writes Time, and Mass Fraction of
species
      WRITE (40,34) T,Z(NEQ),Z(NEQ+1),HR,PHR             ! Writes Time, Temp, Pressure, Heat
Release, and Percent Total Fuel Energy Released
33    FORMAT (F,F,F,F,F,F,F,F,F,F,F,F,F,F,F,F,F,F,F,F,F,F,F,F,F,F,F,F,F,F,F,F,F,F,F,
     &F,F,F,F,F)
34    FORMAT (F,F,F,F,F)
35    FORMAT (A25,A25,A25,A25,A25)
36    FORMAT (A25,A25,A25,A25,A25,A25,A25,A25,A25,A25,A25,A25,A25,A25,A25,
     &A25,A25,A25,A25,A25,A25,A25,A25,A25,A25,A25,A25,A25,A25,A25,A25,A25,
     &A25,A25,A25,A25)
!20    FORMAT(7H AT T =,E12.4,6H   Y =,3E15.7)

!      IF (PHR .GT. PB) THEN      !  Stops program at desired if Heat Release Value is met
!       STOP
!      ENDIF

      ENDDO
!_____________________________________________________________________________________________
!_____________________________**********End Loop*************_____________________________
!_____________________________________________________________________________________________
!  _______________Formatting_____________

100   Format (F,F)
      WRITE (45,*) '_____U-N-I-T-S_____'
      WRITE (45,*) 'R = DYNE-CM/GRAM-K'
      WRITE (45,*) 'T = K'
      WRITE (45,*) 'RHO = GRAM/CM^3'
      WRITE (45,*) ' P = ATM'
      WRITE (45,*) '# OF LINES/STEPS = ',NIter
      STOP

80    WRITE(45,89)ISTATE
89    FORMAT(///22H ERROR HALT.. ISTATE =,I3)
      STOP
90    WRITE (45,99) C(NEQ)
99    FORMAT (//24H ERROR HALT.. Y(NEQ-1) =,E12.5)
      STOP
      END
!_____________________________________________________________________________________________
!_____________________________________________________________________________________________
!!!!!!!!!!!!!!!!!!!!!!!!!!!!!!!!!!!!!!!!!! End Main Program!!!!!!!!!!!!!!!!!!!!!!!!!!!!!!!!!!!!
!_____________________________________________________________________________________________
!_____________________________________________________________________________________________
! This is an attempt to create a CHEMKIN version of the FEX function within the CV Code
! It is similar to that from the Shock4 code from Isaac
! FEX Calculates the ODE's that require solving by DLSODE
      SUBROUTINE FEX(NEQ, T, C, CDOT)
        IMPLICIT REAL*8 (A-H,O-Z)
        DOUBLE PRECISION C(35),ZC(33),CDOT(34),WDOT(33),CPML(33)
        DOUBLE PRECISION WT(33),WORK(1293),X(33),HML(33),CVML(33)
        DOUBLE PRECISION  T, CPBML, HWD, SWD, QoverV
        INTEGER IWORK(1769)
!        INTEGER NEQ
!       DIMENSION  C(15),ZC(13),CDOT(14),WDOT(13)
!       DIMENSION T(13),X(13),HML(13)
!       DIMENSION IWORK(3321),WORK(2113)
        COMMON /COM1/ RU, WT, IWORK, WORK, QoverV
        DO 8 I=1,NEQ-1
           ZC(I)=C(I)
8           CONTINUE
        !  convert P to proper Units!!!!!
```

```
!       CKYTCP(Y(NEQ),Y(NEQ-1),Z,IWORK,WORK,C)   ! Input P,T, Mass Fraction and Returns Molar
Concentrations (mole/cm**3)
      CALL CKWC(C(NEQ),ZC,IWORK,WORK,WDOT)   ! input T, Molar concentration, output molar
production rate (mol/cm**3*s)
      CALL CKHML(C(NEQ),IWORK,WORK,HML)      ! Input T, and output Enthalpy of Species (Ergs/Mole)
 !     CALL CKCTX(ZC,IWORK,WORK,X)            ! Inputs Mole Concentration and outputs Mole
Fractions
 !     CALL CKCPBL(C(NEQ),X,IWORK,WORK,CPBML) ! Inputs T, Mole Fraction and outputs Molar weighted
mean specific heat at const P (Ergs/(mol*K))
      CALL CKCPML(C(NEQ),IWORK,WORK,CPML)    ! Inputs T, Mole Fraction and outputs specific heats
at const P in molar units (Ergs/(mol*K))
      CALL CKCVML(C(NEQ),IWORK,WORK,CVML)    ! Inputs T, Mole Fraction and outputs specific heats
at const V in molar units (Ergs/(mol*K))

       DO 10 I=1,NEQ-1
          CDOT(I)=WDOT(I)
10     CONTINUE
                SWD=0.0D0
                HWD=0.0D0
          DENOM=0.0D0
          QoverV=0.0D0
       DO 20 I=1,NEQ-1
                       HWD=HWD+HML(I)*WDOT(I)
                       SWD=SWD+WDOT(I)
 !            DENOM=DENOM+C(I)*(CPML(I)-RU)
             DENOM=DENOM+C(I)*(CVML(I))
20     CONTINUE
!      CDOT(NEQ) = (QoverV-(HWD)+(RU*C(NEQ)*SWD))/((CPBML-RU)*C(NEQ+1)/
!     &(RU*C(NEQ)))    ! T Dot Simplified
      CDOT(NEQ) = (QoverV-(HWD)+(RU*C(NEQ)*SWD))/(DENOM)    ! T Dot
!              CDOT(NEQ+1) = (Y(NEQ+1)/Y(NEQ))*CDOT(NEQ)  ! P Dot  - may need to reference Pinit
and Tinit
      END
!!!_____________________________________________________________________________________________
!!!_____________________________________________________________________________________________
! This Subroutine calculates the Jacobian Matrix for DLSODE
! The use of this jacobian is not essential-DLSODE is capable of calculating the Jacobian
internally.
      SUBROUTINE JAC(NEQ,T,C,ML,MU,PD,NRPD)
       IMPLICIT REAL*8 (A-H,O-Z) !NONE !
       DOUBLE PRECISION C(35),ZC(33),CDOT(34)
       DOUBLE PRECISION WT(33),WORK(1293)
       DOUBLE PRECISION PD(NRPD,34),DWDCT(33,33),DWDTC(33)
       DOUBLE PRECISION, DIMENSION(33) :: DCPTML,DHDTML,X,CPML,HML,CVML
       DOUBLE PRECISION, DIMENSION(33) :: A7,A8,A9,DCDTPX,WDOT,DCVTML
       DOUBLE PRECISION A1, A2, A3, A4, A5, A6, NS
       INTEGER IWORK(1769)
!       DIMENSION DCPTML(13),DHDTML(13),X(13),CPML(13),HML(13),WDOT(13)
!       DIMENSION PD(NRPD,14),DWDCT(13,13),DWDTC(13)
!       DIMENSION A7(13),A8(13),A9(13),DCDTPX(13),C(15),ZC(13),CDOT(14)
!       DIMENSION IWORK(3321),WT(13),WORK(2113)
       COMMON /COM1/ RU, WT, IWORK, WORK, QoverV
      NS=NEQ-1   ! changed from -1 to -2   3/13
      KDIM = 33 !NS  !changed from 1034 for this old Mech  Number of species for CKDWC !@#
        DO 9 I=1,NS
           ZC(I)=C(I)
9       CONTINUE
       A1=0
       A2=0
       A3=0
       A4=0
       A5=0
       A6=0
!          A9=0
      DO 7 I=1,NS
       A7(I)=0
       A8(I)=0
         A9=0
7     CONTINUE
```

```
      CALL CKWC(C(NEQ),ZC,IWORK,WORK,WDOT)   ! input T, Molar concentration, output molar
production rate (mol/cm**3*s)
      CALL CKDWC(C(NEQ),ZC,KDIM,IWORK,WORK,DWDCT)  ! Input T, Mol Concentrations, Dimension of C
matrix, Returns the partial Derivatives of Molar Production rates wrt Molar Concentrations
      CALL CKDTC(C(NEQ),ZC,IWORK,WORK,DWDTC)    ! Inputs T, Mole Concentrations, Returns the
Partial derivative of molar production rates wrt Temp
      CALL CKDCPL(C(NEQ),IWORK,WORK,DCPTML)     ! Input temp, outputs partial derivatives of
specific heat at const P in molar units wrt Temp (Ergs/mol*K**2)
!      CALL CKDCVL(C(NEQ),IWORK,WORK,DCVTML)     ! Input temp, outputs partial derivatives of
specific heat at const V in molar units wrt Temp (Ergs/mol*K**2)
      CALL CKDHML(C(NEQ),IWORK,WORK,DHDTML)     ! Input Temp, Returns Partial Derivative of
enthalpies wrt Temp (Ergs/mol*K)
      CALL CKCPML(C(NEQ),IWORK,WORK,CPML)       ! Inputs T, Mole Fraction and outputs specific
heats at const P in molar units (Ergs/(mol*K))
      CALL CKHML(C(NEQ),IWORK,WORK,HML)         ! Input T, and output Enthalpy of Species
(Ergs/Mole)
         CALL CKCVML(C(NEQ),IWORK,WORK,CVML)    ! Inputs T, Mole Fraction and outputs specific
heats at const V in molar units (Ergs/(mol*K))
       CALL CKDCVL(C(NEQ),IWORK,WORK,DCVTML)     ! Input temp, outputs partial derivatives of
specific heat at const V in molar units wrt Temp (Ergs/mol*K**2)
! Unsure about whether next two calls are necessary!!
      CALL CKCTX(ZC,IWORK,WORK,X)            ! Inputs Mole Concentration and outputs Mole
Fractions
      CALL CKDCTX(C(NEQ+1),C(NEQ),X,IWORK,WORK,DCDTPX)  ! Inputs P, T, and Mole Fractions, and
Returns Partial Derivative of Molar Concentrations wrt Temp (mole/(cm**3*K))
       DO 17 I=1,NS
       DO 27 J=1,NS
          PD(I,J)=DWDCT(I,J)
27     CONTINUE
17     CONTINUE
       DO 37 I=1,NS
                PD(I,NEQ)=DWDTC(I)    !
!               PD(I,NEQ)=DWDRTY(I)    !*!!!!!!!!!!!!!!
37       CONTINUE
! Calculate Partial of DT wrt Temp
      DO 47 I=1,NS
        A1=A1+DHDTML(I)*WDOT(I)+HML(I)*DWDTC(I)
!        A2=A2+C(I)*(CPML(I)-RU)
        A2=A2+C(I)*CVML(I)
        A3=A3+HML(I)*WDOT(I)
!        A4=A4+X(I)*(DHDTML(I)*C(I)-RU*C(I))            !!!!CHECK THIS - should it be d[C]/dT....?
!        A4=A4+(C(I)*DCPTML(I)+CPML(I)*DCDTPX(I)-RU*DCDTPX(I))          !!!!CHECK THIS -possibly
change to Cv - 4/1
        A4=A4+(C(I)*DCVTML(I)+CVML(I)*DCDTPX(I))
        A5=A5+WDOT(I)+C(NEQ)*DWDTC(I)    ! C(NEQ-1)
        A6=A6+WDOT(I)
47    CONTINUE
! If add HT, need to readdress these equations and add to them
! PD(NEQ,NEQ) Calculates partial derivative of TempDOT wrt Temp
               PD(NEQ,NEQ)=-((A1*A2-A3*A4)/(A2**2))+((RU*A5*A2-RU*C(NEQ)*A6*A4)
     &/(A2**2))    ! or is it (NEQ-1, NEQ-1)
      DO 111 I=1,NS
       DO 112 J=1,NS
          A7(I)=A7(I)+HML(J)*DWDCT(J,I)
          A8(I)=A8(I)+DWDCT(J,I)
!!          A9(I)=A9(I)+DWDCT(J,I)*(CPML(J)-RU)
!          A9(I)=A9(I)+DWDCT(J,I)*(CVML(J))
112    CONTINUE
111    CONTINUE
      DO 97 K=1,NS
       PD(NEQ,K)=-((A7(K))/(A2))+((RU*C(NEQ)*A8(K))/(A2))
97    CONTINUE
      END
```

APPENDIX C.

EXPERIMENTAL MEAN VALUE DATA

	Mean Data and Variance for Experimental Setpoints, Before, During, After Injections										
			IMEPn (bar)	IMEPg (bar)	Peak Pressure Rise Rate (bar/deg)	Max Heat Release (kJ)	Max Heat Release Rate (kJ/deg)	CA10 CAD	CA50 CAD	Burn Duration (CAD)	Max Exh Cyclic Temp (°C)
Baseline Partial Burn, 196°C		Mean	1.378431	1.629601	0.20916	0.133886	0.014329	370.8143	377.3007	20.0276	417.0001
		COV	20.99964	17.80165	93.90654	16.27825	26.36335	0.444544	0.745247	21.13985	4.111229
Baseline Steady State, 203°C		Mean	1.85903	2.112141	2.619045	0.154314	0.04179	364.2076	366.7124	5.48916	420.3745
		COV	4.578828	4.016715	11.88064	6.690749	8.725797	0.13819	0.159918	6.328598	2.165886
CO Injections at partial burn	Before	Mean	1.303951	1.550662	0.21088	0.128982	0.013942	371.0275	377.6305	23.21479	421.833
		COV	19.14889	16.15403	91.41161	14.45262	25.22931	0.452122	0.74257	17.06922	3.848005
	During	Mean	2.411834	2.652711	1.483995	0.207518	0.034571	369.9786	374.3628	11.89816	546.0284
		COV	17.01293	15.48806	82.58817	37.30741	50.60532	1.027258	1.553065	66.49692	7.322411
	After	Mean	1.653175	1.899502	1.194595	0.135297	0.026469	366.8772	370.4203	9.914039	425.7301
		COV	7.649539	6.726502	31.9902	9.159461	16.60175	0.313073	0.443214	33.91179	3.30622
CO injections at steady state	Before	Mean	1.744102	1.995669	1.449527	0.145109	0.02963	366.1632	369.4093	7.691824	417.6684
		COV	7.051572	6.193275	19.74805	8.603546	11.74618	0.215173	0.269019	13.09365	3.040905
	During	Mean	2.539552	2.787096	6.200911	0.234979	0.086214	363.1828	365.0271	3.75015	491.3505
		COV	5.385325	4.901995	32.82926	6.900315	26.51033	0.523941	0.627225	33.16821	3.67902
	After	Mean	1.83183	2.084782	3.247564	0.158973	0.047816	363.2533	365.4442	4.758431	420.5805
		COV	7.359998	6.473919	16.8832	8.862463	13.46269	0.192081	0.222975	8.477731	3.042207
Air Injection at Partial Burn	Before	Mean	1.179522	1.433603	0.125046	0.122739	0.012013	371.7046	378.8895	22.14461	410.3871
		COV	0.299459	0.251119	1.275576	0.239896	0.292495	0.004839	0.007856	0.183983	0.050667
	During	Mean	0.036363	0.297049	-0.00114	0.023671	0.00475	375.9997	384.6284	25.1725	297.4778
		COV	19.3467	2.33975	-104.506	2.842559	0.698656	0.010865	0.013083	0.335372	0.234677
	After	Mean	-0.08094	0.187969	-0.01853	0.015945	0.004015	376.4855	386.1334	28.1597	284.015
		COV	-6.16474	2.617276	-5.90999	3.052665	0.488574	0.009384	0.010062	0.240844	0.202617
Air Injection at Staedy State	Before	Mean	1.880173	2.132439	3.050464	0.161204	0.0462	363.6042	365.909	4.997177	419.832
		COV	6.583572	5.79807	11.5856	8.171472	9.775243	0.142807	0.156057	5.798053	2.885962
	During	Mean	1.891457	2.138732	3.041069	0.159426	0.046453	363.798	366.1106	4.992334	417.7812
		COV	6.745298	5.945033	11.92038	8.531139	10.14766	0.145092	0.157052	5.956825	2.845193
	After	Mean	1.87942	2.13123	3.041005	0.15985	0.046047	363.6124	365.9266	5.017799	420.5128
		COV	6.858349	6.034608	11.9723	8.411071	10.2549	0.145062	0.158358	6.241268	2.861459
Closed Valve Air Injection	Before	Mean	1.505555	1.750096	0.274683	0.141393	0.015785	370.5669	376.6975	19.8938	423.0266
		COV	14.65083	12.64008	78.17312	11.9549	22.3333	0.385426	0.633308	19.0252	3.550981
	During	Mean	-1.16014	-0.87834	-0.04781	-0.11337	-0.0001	372.6935	374.1177	3.527249	171.7709
		COV	-18.4575	-23.9749	-70.1508	-19.5917	-1059.26	1.202872	1.469085	187.6728	16.8834
	After	Mean	-0.28259	-0.01832	-0.03981	-0.00512	0.003152	376.8353	385.8506	25.31389	258.9141
		COV	-185.192	-2814.93	-198.273	-1047.66	65.6365	1.099667	1.464163	38.16556	23.52367
Equal Energy Setpoint, 199°C		Mean	1.964516	2.212146	1.226892	0.161881	0.028707	367.4629	371.1713	9.308421	#DIV/0!
		COV	0.057661	0.051479	0.242066	0.071432	0.120416	0.002348	0.003199	0.172333	#DIV/0!
Air Injection at Equal Energy	Before	Mean	1.729587	1.978324	0.622377	0.15473	0.021268	369.0495	373.7796	13.65514	432.1519
		COV	0.080257	0.070666	0.437187	0.076938	0.163822	0.003317	0.004919	0.215607	0.032385
	During	Mean	1.512373	1.755141	0.261862	0.1454	0.015675	371.1482	377.5558	19.64471	426.2003
		COV	0.206859	0.178857	0.925724	0.158577	0.284996	0.004918	0.008539	0.243237	0.040796
	After	Mean	1.643589	1.892003	0.406383	0.151244	0.018358	370.099	375.648	17.31125	434.6302
		COV	0.12286	0.107313	0.665209	0.098704	0.221664	0.003822	0.006311	0.22542	0.036693

APPENDIX D.

MATLAB SYMBOL SEQUENCING AND FFT ANALYSIS CODE

```
% This is a symbol sequence analysis code for post processed Hatz Data.
% It is currently configured to perform sequence analysis on the Hatz
% cycle average data for a single injection sequence.  Multiple injection
% sequences in a dataset will require modifications to this code. Similar
% code was used to perform symbol sequencing on baseline data, without any injections.
% Allen Ernst - 2016

% Define Sequencing parameters
numbins = 2; % Number of bins to seperate data into
lseq = 6;    % Sequence length
% Input Data
%Input base file name for post processed data from Hatz experiments
filename = ['Critical_Pts_100416'];
% Input file number from Hatz data that is desired for processing
filenumber = ['1'];
colnum = 3; % what data column to perform SS on - Determines engine parameter analyzed
%_____________________________________________________________________________________
_______%
datafilein = [filename '_FPGACAD_' filenumber '.txtCycleData.csv'];  % for the Engine
Cycle Data
[Datafilein] = importdata(datafilein,',',1);
datafilein2 = [filename '_FPGATIME_' filenumber '.txtMaximum_Temperatures.csv'];  % For
the engine exhaust data
[Datafilein2] = importdata(datafilein2,',',1);

% Identify location of injections.
inj_signal=[filename '_FPGATime_' filenumber...
    '.txtMaximum_Temperatures.csv'];
[Inj_signal] = importdata(inj_signal,',',1);
Size = size(Inj_signal.data,1)
if length(Datafilein.data) == length(Inj_signal.data)
   cycles = size(Inj_signal.data,1);
else
    cycles = size(Inj_signal.data,1)-1;
end
threshold = 500;  %threshold set to arbitrary value large enough that an
                %accidental trigger for injection was not recognized in the data
%identifies exact number of cycles injected
numbercycl_inj = sum(Inj_signal.data(:,2)>threshold);
numdiffseq=numbins^(lseq);

% Identify first cycle of injection
j = 0;  %j is value of current cycle evaluated inj signal value
k=0;    %k is cycle tracker for number of injection cycles
for i=1:cycles
    signal=Inj_signal.data(i,2);
    Datafilein.data(i,24) = Inj_signal.data(i,1);  %Adds Max Exhaust Temp Data to
Datafilein
    Datafilein.data(i,25) = 0;    % Adds column for injection (binary format) to
Datafilein
    if signal>threshold
        k=k+1;   % Was first injection at k=0 or k=1?
        if Datafilein.data(i-1,25)==0
            start_inj = i;
        end
        Datafilein.data(i,25)=1;
    elseif signal<threshold
        if i>1     % this is only here to prevent error of reading array spot '0'
            if Datafilein.data(i-1,25)==1
                end_inj = i;
            end
        end
    end
end
% Define the three analysis windows - Pre injection, During injection, Post Injection
preinj = Datafilein.data(1:start_inj,1:25);
duringinj = Datafilein.data(start_inj+1:end_inj,1:25);
postinj =  Datafilein.data(end_inj+1:cycles,1:25);
cutoff = zeros(numbins+1,23);
nseq = zeros(1,3);
```

```
% Perform Symbol Sequencing
for aa = 1:3  % perform for before, during, after injection
    if aa ==1
        data = preinj;
    elseif aa==2
        data = duringinj;
    elseif aa==3
        data = postinj;
    end
dataout = zeros((numdiffseq),24);  % Is this correct? - Verify
sorted = zeros(size(data));
Seq = zeros();
numcycles = length(data);
nseq(1,aa) = length(data)-lseq+1;
for i = 1: 25       %number columns in cycledata
 % Define the partition locations
    cyclesperbin = numcycles/numbins;
    sequential = sort(data);
    cutoff(1,i) = sequential(1,i)-1;
    cutoff(numbins+1,i) = sequential(numcycles,i)+1;
    for j=1:numbins-1
        lowercut = floor(cyclesperbin*j);
        cutoff(j+1,i) = (sequential(lowercut,i)+sequential(lowercut+1,i))/2;
    end
    % Sorts into bins
    for ii=1:numcycles
        for jj=1:numbins
            if cutoff(jj,i)<data(ii,i) && data(ii,i)<=cutoff(jj+1,i)
                sorted(ii,i) = jj-1;
            end
        end
    end
    %Sort into sequences - Converts sequences to numeric values for sorting
    sortstring = transpose(sorted(1:numcycles,i));
    sequence2=zeros(1,nseq(1,aa));
    for q = 1:nseq(1,aa)
        Index = 0;
        for u = 0:lseq-1
            power = lseq-1-u;
            Index = Index+sortstring(1,q+u)*(numbins)^power;
        end
        sequence2(1,q) = Index;
    end
    sortstring2=0:(numdiffseq-1);  % or should this go to 64 (remove the -1)?
    for v=0:(numdiffseq-1)
        stringloc2 =  strfind(sequence2,[v]);
        Seq2(v+1,i)= length(stringloc2);
    end
    dataout(1:numdiffseq,i) = Seq2(1:numdiffseq,i);
    if aa ==1
        dataout1 = dataout;
    elseif aa==2
        dataout2 = dataout;
    elseif aa==3
        dataout3 = dataout;
    end
    Fb (aa,i) =   (1/numbins)^(lseq); % baseline frequency
Hs(aa,i)=0;
sum=0;
for k = 1:numdiffseq
    if Seq2(k,i)==0
        Pk(k,i)=1;
    else
        Pk(k,i) = Seq2(k,i)/(nseq(1,aa));
    end
    sum=sum+Pk(k,i)*log(Pk(k,i));
end
    Hs(aa,i) =  - (1/log(nseq(1,aa)))*sum;
end
end
```

```
TotSequences1=nseq(1,1);  %sum(Seq,1)
TotSequences2=nseq(1,2);
TotSequences3=nseq(1,3);
Dataout1=dataout1./TotSequences1;
Dataout2=dataout2./TotSequences2;
Dataout3=dataout3./TotSequences3;

 Colheader = cellstr(['Start_Sample ';'IMEPn         ';'IMEPg         ';...
    'PMEP         ';'PeakP        ';'PeakPLoc     ';'AvgPRR       ';...
    'PeakPRR      ';'PeakPRRLoc   ';'SOC_CAD      ';'EOC_CAD      ';...
    'Max HR       ';'MaxHR_Loc    ';'Max HRR      ';'Ma_HRR_Loc   ';...
    'CA01         ';'CA05         ';'CA10         ';'CA50         ';...
    'CA90         ';'Burn Duration';'combstart    ';'combend      ';...
    'Exh Temp     ';'Input Mass   ']);

colheader = Colheader(colnum,1);
xax=1:(numbins^(lseq))
```

```
% This code performs data analysis on data from sinusoidal CO mass
% injections on the Hatz HCCI engine.  It performs an FFT and determines
% the power content at each engine cycle frequency interval.
% Allen Ernst
% 2016

%Inputs
%Input base file name for post processed data from Hatz experiments
filename = ['Air_Inject_092416'];
% Input file number from Hatz data that is desired for processing
filenumber = ['0'];
datafilein = [filename '_FPGACAD_' filenumber '.txtCycleData.csv'];
[Datafilein] = importdata(datafilein,',',1);

%pause
period = 50;  % A period of 50 cycles was used for current study
mean = 0.00062573 %Input mean mass that was injected for this run(g)-only used to
generate input signal as reference
amplitude= 0.00026817  %Input CO mass amplitude injected for this run(g)-only used to
generate input signal as reference
colnum = 18; % Specify column of data from Hatz pressure reduction routine to
plot/analyze

% Define Data Table Headers
Colheader = cellstr(['Start_Sample ';'IMEPn         ';'IMEPg         ';...
    'PMEP         ';'PeakP        ';'PeakPLoc     ';'AvgPRR       ';...
    'PeakPRR      ';'PeakPRRLoc   ';'SOC_CAD      ';'EOC_CAD      ';...
    'Max_HR_Kj    ';'MaxHR_Loc    ';'Max_HRR      ';'Ma_HRR_Loc   ';...
    'CA01         ';'CA05         ';'CA10         ';'CA50         ';...
    'CA90         ';'Burn Duration';'combstart    ';'combend      ';...
    'Input Mass   ']);

colheader = Colheader(colnum,1);
%Need to generate input signal for Mass CO injected into the Hatz
%make sure to relate start of input to the correct location
inj_signal=[filename '_FPGATime_' filenumber...
    '.txtMaximum_Temperatures.csv'];
[Inj_signal] = importdata(inj_signal,',',1);
cycles = size(Inj_signal.data,1)

threshold = 500;  %threshold set to arbitrary value large enough that an
%accidental trigger for injection was not recognized in the data

%identifies exact number of cycles injected
numbercycl_inj = sum(Inj_signal.data(:,2)>threshold);
% Identify first cycle of injection
j = 0;  %j is value of current cycle evaluated inj signal value
k=0;    %k is cycle tracker for number of injection cycles
l=0;
```

```
Datafile1 = zeros(numbercycl_inj,(size(Datafilein.data,2))+1);
Datafile2 = zeros(size(Datafile1));
Datafile3 = zeros(size(Datafile1));

for i=1:cycles
    j=Inj_signal.data(i,2);
    Datafilein.data(i,24) = 0;
    if j>threshold
        k=k+1;   % Was first injection at k=0 or k=1?
        if Datafilein.data(i-1,24)==0
            start_inj = i;
        end
         Datafile1(k,:) = Datafilein.data(i,:);
         Datafile1(k,24) = mean+amplitude*sin(2*pi()*(k)/period);
         Datafilein.data(i,24) = Datafile1(k,24);
    elseif j<threshold
        if k>0
            l=l+1;
            Baseline(l,:) = Datafilein.data(i,:);
        end
    end
end

% FFT analysis
m = numbercycl_inj;  %size(Inj_signal.data,1);
Fs = 15;            % Sampling frequency
L = numbercycl_inj;             % Length of signal

for p=1:24
    w=fft(Datafile1(1:m,p));
    Datafile2(1:m,p)=w;
    Datafile2(1,p)=[0];

    n=length(w);
    power(:,p)=abs(w(1:n/2)).^2;   %is ther a way to guarantee n/2 is an integer - Round
possibly?
end

nyquist = 1/2;
freq = Fs*(0:(L/2))/L;
freq = transpose(freq);
period = 1./freq;
cyclperiod=period.*15;   %for 1800rpm, ther are 15 cycles/s
```

BIBLIOGRAPHY

[1] Yao, M., Zheng, Z., and Liu, H. "Progress and Recent Trends in Homogeneous Charge Compression Ignition (HCCI) Engines," Progress in Energy and Combustion Science 35 (2009): 398-437, 2009.

[2] Chiang, C., Stefanopoulou, A. "Stability Analysis in Homogeneous Charge Compression Ignition (HCCI) Engines with High Dilution," IEEE Transactions on Control Systems Technology, Vol. 15, NO. 2, 2007.

[3] Aceves, S., Flowers, D., Espinosa-Loza, F., Martinez-Frias, J., Dec, J., Sjöberg, M., Dibble, R., and Hessel, R. "Spatial Analysis of Emissions Sources for HCCI Combustion at Low Loads Using a Multi-Zone Model," SAE Paper, 2004-01-1910, 2004.

[4] Hosseini, V., and Checkel, M.D. "Effect of Reformer Gas on HCCI Combustion – Part 1: High Octane Fuels," SAE Paper, 2007-01-0208, 2007.

[5] Hosseini, V., and Checkel, M.D. "Effect of Reformer Gas on HCCI Combustion – Part 2: Low Octane Fuels," SAE Paper, 2007-01-0206, 2007.

[6] Subramanian, G., Pires Da Cruz, A., Bounaceur, R., and Verisch, L. "Chemical Impact of CO and H2 Addition on the Auto-Ignition Delay of Homogeneous n-Heptane/Air Mixtures," Combustion Science and Technology, 179 (9), 1937-1962, 2007.

[7] Anderlohr, J.M., Piperel, A., Pires da Cruz, A., Bounaceur, R., Battin-Leclerc, F., Dagaut, P., and Montagne, X. "Influence of EGR Compounds on the Oxidation of an HCCI Surrogate," The Combustion Institute, 32, 2851-2859, 2009.

[8] Guo, H., Hosseini, V., Neill, W.S., Chippior, W.L., and Dumitrescu, C.E. "An Experimental Study on the effect of Hydrogen Enrichment on Diesel Fueled HCCI Combustion," International Journal of Hydrogen Energy, 36 (21) pp. 13820-13830, 2011.

[9] Hosseini, V., and Checkel, M.D. "Reformer Gas Composition Effect on HCCI Combustion of n-Heptane, iso-Octane, and Natural Gas," SAE Paper, 2008-01-0049, 2008.

[10] Eng, J.A., Leppard, W.R., and Stone, T.M. "The Effect of POx on the Autoignition Chemistry of n-Heptane and Isooctane in an HCCI Engine," SAE Paper 2002-01-2861, 2002.

[11] Chen, T., Zhao, H., Xie, H., and He, B. “Analysis of Cyclic Variations During Mode Switching Between Spark Ignition and Controlled Auto-Ignition Combustion Operation,” International Journal of Engine Research, Volume 16, Issue 3, 27 April 2015, pp. 356-365, 2015.

[12] Jungkunz, A., Ravi, N., Liao, H., Erlie, S., and Gerdes, J.C. “An Analytical Method for Reducing Combustion Instability in Homogeneous Charge Compression Ignition Engines Through Cycle-To-Cycle Control,” International Journal of Engine Research, Volume 16, Issue 3, 27 April 2015, pp. 485-500, 2015.

[13] Shahakhti, M. and Koch, C.R. “Characterizing the Cyclic Variability of Ignition Timing in a Homogeneous Charge Compression Ignition Engine Fueled with N-Heptane/Iso-Octane Blend Fuels,” International Journal of Engine Research 9: 361 – 397, 2008.

[14] Argarwal, A.K. “Experimental Investigations on Intake Air Temperature and Air-Fuel Ratio Dependence of Random and Deterministic Cyclic Variability in a Homogeneous Charge Compression Ignition Engine,” SAE Paper 2011-01-1183, 2011.

[15] Attebery, A. “Investigating the Effects of Internally Trapped Residuals on the Performance of a Homogeneous Charge Compression Ignition Engine,” Thesis. Missouri University of Science and Technology, 2012.

[16] Daw, C.S., Edwards, K.D., Wagner, R.M., and Green Jr., J.B. “Modeling Cyclic Variability in Spark-Assisted HCCI,” Journal of Engineering for Gas Turbines and Power 130 (2008): 052801 1-6, 2008.

[17] Turns, S. “An Introduction to Combustion: Concepts and Applications,” Second Edition. McGraw-Hill, 2000.

[18] Lu, X., Chen, W., Hou, Y., and Huang, Z. “Study on the Ignition, Combustion and Emissions of HCCI Combustion Engines Fueled with Primary Reference Fuels,” SAE Paper, 2005-01-0155, 2005.

[19] Bhave, A., Kraft, M., Mauss, F., Oakley, A., and Zhao, H. “Evaluating the EGR-AFR Operating Range of a HCCI Engine,” SAE Paper, 2005-01-0161, 2005.

[20] Sjöberg, M., and Dec, J. “An Investigation into the Lowest Acceptable Combustion Temperatures for Hydrocarbon Fuels in HCCI Engines,” Proceedings of the Combustion Institute, 30, 2719-2726, 2005.

[21] Jamal, Y., and Wyszynski, M. L. “On-board Generation of Hydrogen-Rich Gaseous Fuels – A review,” International Journal of Hydrogen Energy, 19 (7), 557-572, 1994.

[22] Houseman, J., and Cerini, D.J. “On-Board Hydrogen Generator for a Partial Hydrogen Injection Internal Combustion Engine,” SAE Paper 740600, 1974.

[23] Bromberg, L., Cohn, D., Rabinovich, A., Surma, J., and Virden, J. “Compact Plasmatron-boosted Hydrogen Generation Technology for Vehicular Applications,” International Journal of Hydrogen Energy, v 24, n 4, 341-350, 1999.

[24] He, X., Donovan, M., Zigler, B., Palmer, T., Walton, S., Wooldridge, M., and Atreya, A. “An Experimental and Modeling Study of Iso-octane Ignition Delay Times under Homogeneous Charge Compression Ignition Conditions,” Combustion and Flame, 142, 266-275, 2005.

[25] Curran, H.J., Gaffuri, P., Pitz, W.J., and Westbrook, C.K. “A Comprehensive Modeling Study of Iso-Octane Oxidation,” Combust. Flame, 129, 253, 2002.

[26] Dubreuil, A., Foucher, F., and Mounaim-Rousselle, C. “Effect of EGR Chemical Components and Intake Temperature on HCCI Combustion Development,” SAE Paper, 2006-32-0044, 2006.

[27] Dubreuil, A., Foucher, F., Mounaim-Rousselle, C., Dayma, G., and Dagaut, P. “HCCI Combustion: Effect of NO in EGR,” Proceedings of the Combustion Institute,31, 2879-2886, 2007.

[28] Heywood, J.B. “Internal Combustion Engine Fundamentals,” McGraw-Hill, 1988.

[29] Bettis, Josh B. “Thermodynamic Modeling for Nonlinear Control of Combustion Phasing in HCCI Engines,” Thesis. Missouri University of Science and Technology, 2010.

[30] Sjöberg, M., and Dec, J.E. “Comparing Late Cycle Autoignition Stability for Single- and Two-Stage Ignition Fuels in HCCI Engines,” Proceedings of the Combustion Institute, 31 (2) (2007), pp. 2895–290, 2007.

[31] Wagner, R.M., Edwards, K.D., Daw, C.S, Green Jr., J.B., and Bunting, B.G. “On the Nature of Cyclic Dispersion in Spark Assisted HCCI Combustion,” SAE Paper 2006-01-0418, 2006.

[32] Bunting, B., Eaton, S., Naik, C., Puduppakkam, K. et al., "A Comparison of HCCI Ignition Characteristics of Gasoline Fuels Using a Single-Zone Kinetic Model with a Five Component Surrogate Fuel," SAE Technical Paper 2008-01-2399, 2008.

[33] Riseberg, P., Kalghatgi, G., and Angstrom, H. "Auto-Ignition Quality of Gasoline-Like Fuels in HCCI Engines," SAE Paper 2003-01-3215, 2003.

[34] Kee, R.J., Miller, J.A., and Jefferson, T.H. "CHEMKIN: A General-Purpose, Problem-Independent, Transportable, FORTRAN Chemical Kinetics Code Package," Sandia National Laboratories, March 1980.

[35] Tsurushima, T., "A New Skeletal PRF Kinetic Model For HCCI Combustion," Proceedings of the Combustion Institute, 32, 2835-2841, 2009.

[36] Westbrook, C. K. Personal Communication. 2013.

[37] 'Primary Reference Fuels (PRF): iso-Octane/ n-Heptane Mixtures.' Lawrence Livermore National Laboratory. 2013. <https://combustion.llnl.gov/archived-mechanisms/surrogates/prf-isooctane-n-heptane-mixture>

[38] Fox, J., Cheng, W., and Heywood, J. "A Model for Predicting Residual Gas Fraction in Spark-Ignition Engines," SAE Technical Paper 931025, 1993.

[39] Kaul, B. C. "Addressing Nonlinear Combustion Instabilities in Highly Dilute Spark Ignition Engine Operation," Dissertation. Missouri University of Science and Technology, 2008.

VITA

Allen Charles Ernst was born on January 9, 1989 in Belleville, IL to Ron and Phyllis Ernst. He graduated from Belleville West High School in May of 2007. During the Summer of 2010 he worked as a Summer Co-op with the GEnx Certification and Test Integration Team at GE Aviation in Evendale, OH. While at Missouri S&T he ran as a member of the Missouri S&T Cross Country and Track and Field Teams, where he achieved NCAA DII provisional qualifying marks in the 3000m steeplechase in both 2010 and 2012. In May 2011 he received his B.S. in Mechanical Engineering from Missouri University of Science and Technology.

During the Summer of 2011 Allen worked as an Engineering Intern for LMI Aerospace. From July 2013 through April 2016 he worked as a full time Project Engineer for LMI Aerospace while concurrently completing his Master's research. In December 2016 Allen received his M.S. in Mechanical Engineering from Missouri University of Science and Technology.